JOURNAL OF HYDRO - METEOROLOGY

ISSN 2525 - 2208

VIETNAM METEOROLOGICAL AND HYDROLOGICAL ADMINISTRATION

No 18
03-2024

Publishing licence
No: 166/GP-BTTTT - Ministry of Information and Communication dated 17/04/2018

Editorial office
No 8 Phao Dai Lang, Dong Da, Ha Noi
Tel: 024.39364963
Email: tapchikttv@gmail.com

Engraving and printing
Ha Thanh Thang Long Printing And Trading Joint Stock Company
Tel: 0243.2022639

JOURNAL OF HYDRO-METEOROLOGY
Volume 18 - 3/2024

TABLE OF CONTENT

JOURNAL OF
HYDRO-METEOROLOGY

Research Article

Characteristics of seawater intrusion in Soc Trang province, Vietnam

Trieu Anh Ngoc[1]*, Vu Thi Hoai Thu[2], Can Thu Van[3]

[1] Thuy Loi University, 175 Tay Son, Dong Da, Hanoi, Vietnam; ngocta@tlu.edu.vn
[2] University of Transport Ho Chi Minh City; Hoaithu.vu@ut.edu.vn
[3] Ho Chi Minh University of Natural Resources and Environment; ctvan@hcmunre.edu.vn

*Corresponding author: ngocta@tlu.edu.vn; Tel.: +84–902789267

Received: 18 October 2023; Accepted: 22 November 2023; Published: 25 March 2024

Abstract: Seawater intrusion poses many severe issues in many coastal areas around the world, including the Mekong Delta, Vietnam. For sustainable water management in such regions requires, it is crucial to understand the characteristics of salinization. This study aims to investigate the characteristics of the salinization phenomenon in water systems and its controlling factors based on hydrogeochemical analysis, seawater-freshwater mixing model and End Members Mixing Analysis. The results revealed that seawater intrusion negatively affects strongly on surface water quality with different magnitudes, depending on seasonal variation and tidal regime. It was estimated that surface water mixed with approximately 29.5% and 4.12% of seawater in the dry season and rainy season, respectively. However, it was found that the salinity in groundwater showed less seasonal variation and was distributed heterogeneously following the depth of screened wells and distance to the sea. The mixing ratio between seawater and groundwater varied widely, ranging from less than 10% in deep groundwater up to a maximum of 38% in shallow groundwater. Surface water salinization in the study area is controlled by upstream discharge, tidal regime, and operation of sluice gates. Meanwhile, groundwater salinization might be governed by geological characteristics, original recharge sources, human intervention, and natural variation, especially excessive groundwater exploitation in the Mekong Delta. Therefore, integrated sustainable groundwater and surface water use and management strategies in the Mekong Delta are needed in the context of human-nature intervention.

Keywords: Seawater intrusion; Seawater-Freshwarer Mixing; Soc Trang; Vietnam.

1. Introduction

Seawater intrusion (SWI) is the movement of salt sources into water system caused by natural processes and/or human activities, especially groundwater pumping. It results in high salinity concentration in water resources threating to sustainable water use and management in many coastal regions around the world [1]. In particular, high salinity concentration in water system not only strikes directly to crops and ecosystems [2, 3] but also potentially threats to human health [4–6]. It also causes land degradation via interconnection between salt water and soil layers, resulting in the difficulty to recovering agricultural lands in affected areas [7]. Therefore, understanding characteristics of salinization is key to preventing undesirable effects on agricultural activities and freshwater supply systems in many coastal regions in the world. Over the last several decades, SWI has been reported in different magnitudes from regional to global scales. For example, the earliest report to salinization in all coastal aquifers has been conducted by [8], and afterward, this issue has been intensively

reported by [9, 10]. Salinization has been occurring in the United States since 1960s posing many challenges for water management. Likewise, many coastal regions in Asia have experienced salinization. For instance, coastal areas of China have been facing with salinization due to a rapid expanding saline-affected areas since 2000s [11]. A great efforts have been made by the Chinese government to mitigate and prevent effects of water salinization processes, however, it has still been a severe issue as an increase of groundwater extraction along the coast [12]. Similarly, seawater intrusion is a serious water problem in coastal regions of India [13, 14]. In Africa, groundwater salinization was also found in many coastal regions [15] such as in the Nile Delta [16], in coastal areas of Libya [17], Morocco [18, 19], and Tunisia [20–22]. In addition, seawater intrusion has been well documented in many coastal regions in Europe [1]. In recently, water salinization is predicted to increase risks of water shortage and threat to national and global food security under impacts of climate change and sea level rise. Although numerous studies related to SWI have been intensively done for several decades [23], most of previous studies targeted to separated water resource, either surface water system or aquifer system. Naturally, surface water and groundwater are generally interconnected [24], therefore investigation of seawater intrusion into both water resources is crucial to sustainable water management along the coast.

Seawater intrusion has become the widespread environmental problem in Vietnam, threating to water resources and ecosystem in coastal regions, especially in the Red River Delta and the Vietnamese Mekong Delta [25]. In natural conditions without human intervention, saline boundary in the Vietnamese Mekong Delta (VMD) extends to approximately 30-40 km inland [26]. However, the salinity boundary in recent years has been extremely expanding to inland due to changes of upstream discharge to the VMD [27]. For example, extreme drought and salinization have been occurred in the dry season 2016 caused huge losses of agricultural productions and resulted in severe freshwater shortage in many provinces of the delta including Tien Giang, Ben Tre, Tra Vinh, Soc Trang, Bac Lieu, Ca Mau, and Kien Giang. The salinity boundary has extended to 60-90 km inland [28]. As a result, large areas of agricultural lands, especially paddy fields and shrimp farming were destroyed, causing huge economic losses [29]. Water salinization also puts a high pressure on freshwater supply system due to an increase in salinity concentration in both surface water and groundwater [30]. Therefore, previous studies have been conducted to understand the impacts of seawater intrusion in the Mekong Delta based on different scenarios. For instance, most of researcher used hydraulic model to simulate the salt concentration based under affected by water practices in the upstream of the Mekong River Basin and socio-economic development in the Mekong Delta [26–28] as well as climate change [36–38]. However, the understanding of how much percentage of seawater contributing to surface water and groundwater along the coastal is still limited. Hence, this study aims to investigate characteristics of water salinization for sustainable water resources management in coastal area of the VMD. The main objectives are followed: (i) characterizing the tempo-spatial variation of salinity concentration in both surface and groundwater; (ii) examining the main factors controlling seawater intrusion in water system of the study area.

2. Materials and Methods

2.1. Description of study site

The research is situated in Soc Trang province, within the Mekong Delta of Vietnam, covering an approximate area of 2,300 km^2 with an average population of 1.32 million people (General Statistics Office of Vietnam 2016). The climate in this region is characterized by two distinct seasons - the rainy season and the dry season. The rainy season, influenced by the Southwest Monsoon, occurs from May to October annually and contributes more than 85% of the total annual rainfall of 1,875 mm. In contrast, the dry season, dominated by the

Northeast Monsoon, lasts from November to April, with a minimal contribution of just 15% to the annual rainfall. Despite significant seasonal variations in rainfall, other climate parameters such as temperature, humidity, and evaporation exhibit only minor differences. For instance, the mean monthly air temperature remains quite consistent between the dry and rainy seasons, hovering around 26.7°C, while evaporation averages around 34 mm. Humidity is approximately 85% in the dry season and 87% in the rainy season, with occasional exceptionally high daily air temperatures exceeding 36°C, particularly in the warmest months of April and May.

The hydrological system in the study area is highly intricate due to the interconnectedness of rivers, the sea, and an extensive canal network in relation to upstream discharge, tide regime, and local hydraulic construction operations (Figure 1). The region is traversed by two major rivers, Hau and My Thanh, which converge with the canal system and directly connect to the East Sea (Figure 2). Upstream discharge and interactions between river dynamics and marine influences are the primary factors driving seawater intrusion into the coastal river and canal system [31–34]. The impacts of salinization have expanded recently due to human-induced activities in the Mekong River Basin [35, 36]. Changes in upstream discharge and human activities can strongly influence both the hydrological regime and water quality, posing threats such as seawater intrusion, surface water contamination, and potential risks to groundwater resources in the area [37–39].

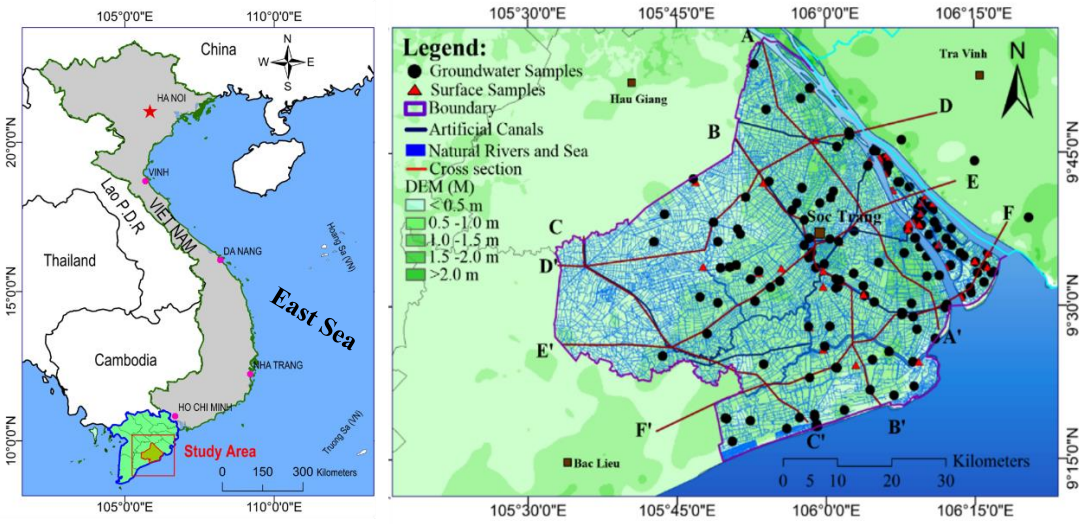

Figure 1. Map of sampling location and the river-canal system in Soc Trang Province, Vietnam.

Similarly, the hydrogeology of the region is intricate, comprising several multi-layered formations. From a management perspective, the aquifer system can be categorized into seven subdivision aquifers: Holocene (qh), Upper Pleistocene (qp3), Upper-Middle Pleistocene (qp23), Lower Pleistocene (qp1), Middle Pliocene (n22), Lower Pliocene (n21), and Upper Miocene (n13) aquifer layers. Generally, each hydrogeological unit consists of upper and lower parts with distinct characteristics. The former comprises low-permeability silt, clay, or silt clay with very low water yield, while the latter is relatively permeable, consisting of fine to coarse sand, gravel, and pebbles [40]. In this study, we group groundwater in seven aquifers into four classes following SGW (aquifer qh); DGW1 (aquifer qp3; DGW2 (qp23); DGW3 (qp1); DGW4 (n22, n21 and n13).

2.2. Methodologies

2.2.1. Hydrogeochemical data analysis

Between 2013 and 2018, a comprehensive set of geochemical analyses was conducted on a total of 278 groundwater samples and 79 surface water samples collected from the study

area. These water samples were meticulously gathered in 100 ml plastic bottles and meticulously prepared for both chemical and stable isotopes analysis. Additionally, field measurements were undertaken to acquire essential physical parameters – namely, temperature (T°C), pH, dissolved oxygen (DO), and electrical conductivity (EC) – utilizing portable instruments from HANNA.

2.2.2. Hydro-geochemical Evaluation Methods

Fresh seawater mixing analysis.

It was presumed that Cl- serves as a conservative tracer primarily originating from seawater. Consequently, the fraction of seawater (f_{sea}) in the water sample can be determined based on chloride concentrations in both seawater and freshwater, as outlined in [41]:

$$f_{sea} = \frac{m_{Cl^-,sample} - m_{Cl^-,fresh}}{m_{Cl^-,sea} - m_{Cl^-,fresh}} \quad (2)$$

where $m_{Cl^-,sample}$, $m_{Cl^-,fresh}$ and $m_{Cl^-,sea}$ represent the concentrations of Cl- in the water sample, freshwater, and seawater, respectively, all expressed in mmol/L. In coastal delta regions, fresh groundwater primarily contains Ca^{2+} and HCO_3^-, resulting from mineral dissolution processes. Consequently, the presence of all other ions in water samples may be attributed to seawater admixture. Under such circumstances, $mi_{fresh} = 0$ for all components except Ca^{2+} and HCO_3^- [1], and the seawater fraction ratio in Equation 2 is modified accordingly:

$$f_{sea} = \frac{m_{Cl^-,sample}}{m_{Cl^-,sea}} = \frac{m_{Cl^-,sample}}{566} \quad (3)$$

The concentration of an ion i (mi) in the blended fresh seawater was determined by applying the mass fraction of seawater (f_{sea}), as outlined in Equation 2, as follows:

$$mi_{mix} = f_{sea} \times mi_{sea} + (1 - f_{sea}) mi_{fresh} \quad (4)$$

where mi_{mix} represents the concentration of ion i in mmol/L in the anticipated mixed fresh-seawater. Subscripts mix, sea, and fresh denote the conservative mixture, seawater end member, and freshwater end member, respectively. The alteration in concentration, $mi_{reaction}$ (Δ_{mi}), due to reactions without mixing is then expressed as:

$$\Delta_{mi} = mi_{sample} - mi_{mix} \quad (5)$$

where mi_{sample} is the measured concentration in the sample, expressed in mmol/L. Deviation in the chemical composition from a fresh-seawater mixture signifies chemical reactions resulting from seawater intrusion. A positive value indicates that the ion has been introduced to the water sample, such as through desorption from the exchange complex, while a negative value may suggest absorption processes.

End members mixing analysis (EMMA)

In this study, the EMMA model was employed to compute the ratio of each water source contributing to the surface water and groundwater within the study area. EMMA, a widely used hydro-geochemical mixing model in hydrogeological studies, has been applied extensively to identify and quantify the contribution ratios of various water sources to both surface water and groundwater [42–45]. The model utilizes the dominant chemical compositions of potential end members within the watershed to determine the percentages of each original parent water contributing to the final mixture [46, 47]. The mixing model relies on four assumptions: (i) surface water/groundwater is a final mixture of different water sources, (ii) the mixing process follows a linear and hydrodynamic mechanism, (iii) the mixed compositions act as conservative tracers, and (iv) the source solutions exhibit dominant concentrations [44]. However, hydrological processes within the watershed can vary in time and space, emphasizing the importance of careful consideration in the selection of end members before applying the EMMA approach [44, 45].

In coastal estuarial regions, water sources typically originate from various contributors, including rainfall, surface water, seawater, and groundwater from different aquifers. To

simplify the complexity of contributors, it was assumed that surface water primarily derived from rainfall, upstream surface water, and seawater, while groundwater originated from rainfall and seawater. The estimation of the contribution ratio for each end member to surface water and groundwater is based on the following equations:

For surface water:

$$f_R + f_{UPW} + f_{SW} = 1 \quad (6)$$

$$f_R \times \delta_R + f_{UPW} \times \delta_{UPW} + f_{SW} \times \delta_{SW} = \delta_S \quad (7)$$

$$f_R \times Cl_R + f_{UPW} \times Cl_{UPW} + f_{SW} \times Cl_{SW} = Cl_S \quad (8)$$

For groundwater:

$$f_R + f_{SW} = 1 \quad (9)$$

$$f_R \times Cl_R + f_{SW} \times Cl_{SW} = Cl_G \quad (10)$$

Where f represents the contribution ratio of each end member to the final mixtures (f_R – local ratio of rainfall, f_{SW} – ratio of seawater, and f_{UPW} – ratio of upstream freshwater). The notation δ and Cl denote the stable isotope of oxygen-18 (‰) and chloride concentration (mg/L), respectively, considered as conservative tracers.

In this study, the selected end members include R for rainwater (with $\delta_{18}O$ = -9.29‰ and Cl = 0.99 mg/L), SW for seawater (with $\delta_{18}O$ = -0.82‰ and Cl = 16020.59 mg/L), both collected during a field survey in 2017, and UPW for average upstream fresh surface water (with $\delta_{18}O$ = -7.20‰ and Cl = 6.75 mg/L).

3. Results and discussion

3.1. Tempo-spatial variation of salinity

The statistical analysis of hydro-geochemistry was presented in Table 1.

Table 1. Statistical summary of hydrochemical parameters of surface water and groundwater in the study area.

Parameters	pH	EC	TDS	Na	K	Ca	Mg	Cl	HCO_3	SO_4	NO_3
Surface water in dry season (N=38)											
Min.	6.32	133.10	86.52	20.43	1.67	9.36	0.66	26.28	67.10	11.45	0.72
Averg.	7.49	9669.27	6285.02	1748.51	60.64	56.00	212.48	3015.84	93.14	838.12	67.14
Max.	8.04	24400.00	15860.00	4877.02	255.06	174.34	625.91	9354.58	186.65	2667.21	234.40
STD	0.44	6718.23	4366.85	1410.23	56.06	40.61	172.97	2462.84	23.55	705.66	81.56
Surface water in rainy season (N=41)											
Min.	6.57	13.48	8.76	1.84	1.34	0.68	0.05	0.99	7.32	0.31	0.34
Averg.	7.34	937.37	609.29	151.10	12.40	17.31	21.49	253.82	76.06	33.61	3.48
Max.	7.77	13320.00	8658.00	2632.92	98.98	111.39	334.46	4642.72	136.07	536.06	54.13
STD	0.27	2189.41	1423.12	429.23	20.68	16.87	53.70	758.53	19.22	86.41	8.98
Groundwater in dry season (N=137)											
Min.	6.27	116.70	75.86	16.88	0.52	1.44	1.28	2.85	14.03	1.83	0.27
Averg.	7.26	1307.59	849.94	178.27	22.06	35.41	33.08	189.62	318.30	76.03	5.65
Max.	8.68	11710.00	7611.50	2407.00	149.35	475.29	455.53	3705.75	779.23	474.30	59.48
STD	0.47	1380.76	897.50	260.64	21.64	43.57	42.66	421.99	156.80	81.96	9.29
Groundwater in rainy season (N=140)											
Min.	6.12	129.80	84.37	33.10	2.38	0.11	0.03	5.27	16.48	0.02	0.11
Averg.	7.32	2216.79	1440.91	459.95	15.79	65.91	69.21	741.18	329.98	178.24	15.59
Max.	8.55	21200.00	13780.00	8535.80	278.81	970.48	1290.06	16970.45	649.25	3239.46	264.18
STD	0.48	3327.06	2162.59	1164.28	30.14	151.53	157.18	2385.36	148.50	405.71	45.11

Note: EC is expressed in µS/cm, all chemical compositions were in mg/L

In general, hydrogeochemical data reveal distinctive characteristics between surface water and groundwater. The pH values for both surface water and groundwater ranged from 6.12 to 8.68, with an average and standard deviation of 7.32±0.45, indicating primarily alkaline nature. Surface water salinity exhibited significant seasonal variation. For example, the electrical conductivity (EC) values of surface water varied widely between the dry season and the rainy season, with averages and standard deviations of 9,669.27±6718.23 µS/cm and 937.37±2,189.41 µS/cm, respectively. Similarly, total dissolved solids (TDS) values in surface water displayed substantial seasonal and spatial fluctuations (Fig. 2), ranging from 8.76 to 15,860 mg/l, with mean values and standard deviations of 1,634.78±2,654.10 mg/l compared to 609.29±1423.12 mg/l in the dry season (Table 1). Low to slightly saline surface water (TDS = 1,000 – 3,000 mg/l) was observed during the rainy season from the coast up to 60 km inland (Figure 2), possibly due to a high rate of freshwater discharge into the coastal estuary. This contrasts with the dry season, where a higher TDS concentration (moderately saline > 3,000 mg/l) is noted due to seawater intrusion.

On the other hand, groundwater exhibited less seasonal variation in hydro-geochemistry but displayed spatial heterogeneity in salinity based on distance to the sea and well depth. Elevated TDS concentrations (ranging from 3,000 to 14,000 mg/l) were observed not only in coastal groundwater wells with depths less than 100m but also in inland areas located more than 10 km from the coastline. In contrast, deep groundwater wells (depths exceeding 100m) showed relatively lower TDS concentrations. The heightened salinity in coastal groundwater may be attributed to the effects of seawater intrusion into the freshwater body through a complex mechanism, involving saline water infiltration, modern seawater intrusion, and aquifer leaks or upwelling. Furthermore, TDS concentrations in groundwater varied widely due to differences in the magnitudes of mineral dissolution and precipitation within heterogeneous aquifers.

3.2. Salinization and freshening processes

Based on a simple fresh-seawater mixing model, the deviation of Na^+ (called $Na_{re\text{-}act}$) for all water samples was estimated to investigate the possibility of salinization and freshening processes. Most of water samples experienced freshening process which has a decrease of the fraction of seawater (f_{sea}) in corresponding to an increase of $Na_{re\text{-}act}$. More noticeably, some surface water samples presented higher fraction ratio (f_{sea}> 0.1) and high positive $Na_{re\text{-}act}$ value indicated that they might be strongly affected by freshening process as an increase upstream freshwater discharge into the VMD in rainy season. Meanwhile, several groundwater samples have significantly experienced freshening process because of fresh groundwater submarine flow to the sea. Conversely, groundwater and surface samples had high fraction ratio (f_{sea}> 0.1) and more negative value of $Na_{re\text{-}act}$ might experience salinization processes.

3.3. Mixing ratios between fresh and seawater

Mixing fresh and seawater strongly effects on chemical characteristics of coastal water resources. The magnitude of mixing between freshwater and seawater depends on local rainfall-runoff process, upstream discharge, and tidal regime. In the study area, surface water showed a seasonal fresh seawater mixing trend. In dry season, for instance, it was found that 29.5% of seawater mixing with freshwater surface water in the study area compared with just only 4.12% in rainy season (Table 2). The mixing ratios also showed wide spatial-temporal variation, depending on the distance to the East Sea and tidal regime. In the high tidal altitude period, the mixing ratios ranged from 50% in the coast to 20% in the inland, approximately 30 km to the sea while in the low tidal peak these ratios were lower than 10% and without mixing, respectively (Figure 2).

The hydraulic connection between river-canal system and the East Sea plays important role in mixing between surface water and seawater. The surface water had high mixing ratios and high chloride concentration along approximately 10 km from Hau River and 30 km to the East Sea. Although some surface water samples were located along the coast, they had very low TDS concentration. It is perhaps due to the operation of sluice gate to prevent seawater intrusion into the canal system along the coast.

Table 2. Ratios (in percentage) of each water sources contribution in surface water samples.

Water Sources	Water sources	Min	Average	Max	STD
Surface Water in Dry Season	Rainwater	0.00	0.08	0.66	0.18
	Upstream Water	0.14	0.62	0.94	0.23
	Seawater	0.03	0.30	0.64	0.19
Surface Water in Rainy Season	Rainwater	0.00	0.28	0.80	0.33
	Upstream Water	0.20	0.68	0.99	0.30
	Seawater	0.00	0.04	0.23	0.06
SGW	Rainwater	0.18	0.83	1.00	0.23
	Seawater	0.00	0.17	0.82	0.23
DGW1	Rainwater	0.79	0.99	1.00	0.03
	Seawater	0.00	0.01	0.21	0.03
DGW2	Rainwater	0.84	0.99	1.00	0.02
	Seawater	0.00	0.01	0.16	0.02
DGW3	Rainwater	0.62	0.67	0.72	0.05
	Seawater	0.28	0.33	0.38	0.05
DGW4	Rainwater	0.95	0.98	1.00	0.01
	Seawater	0.00	0.02	0.05	0.01

The mixing processes of freshwater and seawater in coastal water system might be explained via four steps based on chloride and stable isotopes signatures combined with hydrological system. At the beginning, upstream surface water discharges into the study area entering internal river-canal system and discharges directly into the sea in the low peak of tide. After that, a part of upstream water escapes out of river mouth while the remaining one will return into local canal system in the high tidal peak. The returned water then mixes with evaporated water in the large river system as well as local water from semi-isolated canals, aquaculture ponds and wastewater from residential areas.

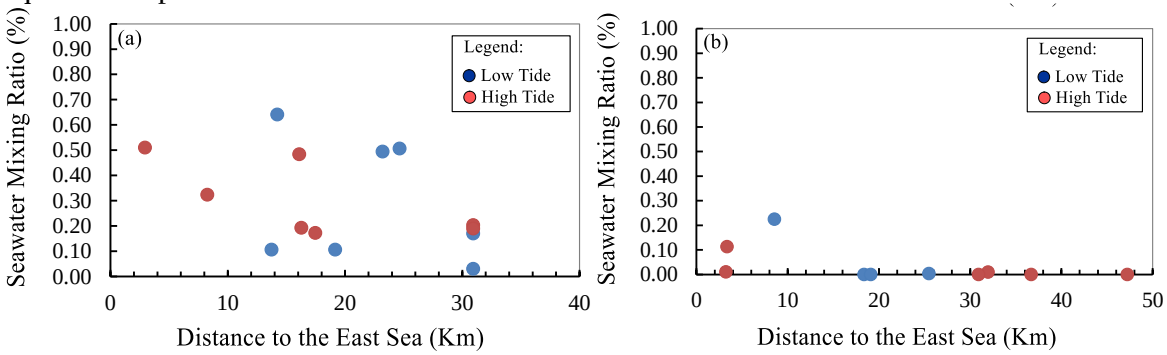

Figure 2. The seawater-mixing ratio with fresh water following distance from the sea and tidal regime in the dry season (a) in the rainy season (b).

Eventually, the mixed water runs into the river mouth and enters the sea afterward before returning to the next circulation. These flow processes establish water circulation in coastal-

estuarial area resulting in complicated mixing processes between upstream water, coastal surface water, local rainfall and seawater. The mixing ratio between groundwater from shallow (SGW) and deep aquifers (DGW1, DGW2 and DGW3) and seawater showed a large variation. For instance, groundwater samples from SGW (qh, qp_3) aquifers consist of from 0% to 82% seawater while DGW3 (n^1_2) aquifer contains from 28% to 38% seawater. More noticeably, the mixing ratio between shallow groundwater and seawater a heterogeneous variety following depth of screened well and distance to the sea (Figure 3). High mixing ratios with seawater was observed up to 30 km inland and until 400 m depth of well, indicating that salt sources might originate from seawater trapped in Holocene period in shallow aquifers and paleo-seawater intrusion in depth aquifers. In contrast, groundwater in remaining aquifers were dominated by freshwater type, indicating the main rainfall recharge source with contribution ratios from 79% to 100%. However, groundwater in some locations contains from 5% to 21% of seawater, reflecting effects of seawater intrusion.

4. Conclusion

This research aims to investigate the dynamics of seawater intrusion in both surface water and groundwater within a coastal tropical area of the Vietnamese Mekong Delta. The inflow of seawater into the coastal surface water system exhibits significant spatial and temporal variations, influenced by the interplay of upstream discharge and tidal-driven flow into the river system. The mixing proportion of seawater is notably higher at 29.5% in the dry season, contrasting with the rainy season's 4.12%. The study highlights the critical role of upstream discharge, contributing 62% and 68% to averting seawater intrusion in the dry and rainy seasons, respectively. Additionally, local rainfall-runoff in the rainy season contributes 28% to coastal surface water.

In contrast, seawater intrusion into the aquifer system demonstrates less seasonal fluctuation but presents a heterogeneous distribution based on well depth and proximity to the sea. The mixing ratio between seawater and groundwater varies widely, ranging from less than 10% in deep groundwater to a maximum of 38% in shallow groundwater. The intricate factors influencing seawater intrusion into the surface water system include upstream discharge, tidal patterns, and sluice gate operations. Conversely, seawater intrusion into the coastal aquifer system is influenced by geological characteristics, original recharge sources, human activities, and natural variations, particularly groundwater pumping and climate change.

While the operation of sluice gates may alleviate the impacts of seawater intrusion, it introduces significant water pollution to the area. Due to limited hydro-geochemical data in this region, the study emphasizes the necessity for further investigations to comprehend the interrelationships between surface and groundwater. Establishing a safe yield for sustainable groundwater use and management is crucial, taking into account factors such as the effects of seawater intrusion, especially considering the potential impacts of climate change.

Author contribution statement: Conceived and designed the experiments; Analyzed and interpreted the data; contributed reagents, materials, analysis tools or data; manuscript editing: T.A.N.; Performed the experiments; contributed reagents, materials, analyzed and interpreted the data, wrote the draft manuscript: T.A.N., V.T.H.T.; Revised and improved the manuscript: C.T.V.

Acknowledgements: The author would like to thank Dr. Tran Dang An for supporting the data and giving useful comments for improving the manuscript.

References

1. Alfarrah, N.; Walraevens, K. Groundwater overexploitation and seawater intrusion in coastal areas of arid and semi-arid regions. *Water* **2018**, *10(2)*, 143.

2. Williams, V.J. The ecological effects of salt water intrusion on the agriculture industry after hurricane Katrina. New York, NY: Springer New York, 2009.
3. Herbert, E.R.; Boon, P.; Burgin, A.J.; Neubauer, S.C.; Franklin, R.B.; Ardón, M.; Hopfensperger, K.N.; Lamers, L.P.M.; Gell, P. A global perspective on wetland salinization: ecological consequences of a growing threat to freshwater wetlands. *Ecosphere* **2015**, *6(10)*, 206.
4. Khan, A.; Ireson, A.; Kovats, S. Drinking water salinity and maternal health in coastal Bangladesh: implications of climate change. *Environ. Health Perspect* **2011**, *119*.
5. Khan, A.E.; et al. Salinity in Drinking Water and the Risk of (Pre)Eclampsia and Gestational Hypertension in Coastal Bangladesh: A Case-Control Study. *PLoS ONE*, **2014**, *9(9)*, e108715.
6. Talukder, M.R.R.; et al. Drinking water salinity and risk of hypertension: A systematic review and meta-analysis. *Arch. Environ. Occup. Health* **2017**, *72(3)*, 126–138.
7. Arslan, H.; Demir, Y. Impacts of seawater intrusion on soil salinity and alkalinity in Bafra Plain, Turkey. *Environ. Monit. Assess*. **2013**, *185(2)*, 1027–1040.
8. Todd, D.K. Salt water intrusion of coastal aquifers in the United States, in Subterranean Water. 1960.
9. Konikow, L.F.; Reilly, T.E. Seawater intrusion in the United States, in seawater intrusion in coastal aquifers – concepts, methods and practices. Bear, J.; et al. Editors. Springer Netherlands: Dordrecht. 1999, pp. 463–506.
10. Barlow, P.M.; Reichard, E.G. Saltwater intrusion in coastal regions of North America. *Hydrogeol. J.* **2010**, *18(1)*, 247–260.
11. Shi, L.; Jiao, J.J. Seawater intrusion and coastal aquifer management in China: a review. *Environ. Earth Sci*. **2014**, *72(8)*, 2811–2819.
12. Han, D.; Currell, M.J. Delineating multiple salinization processes in a coastal plain aquifer, northern China: hydrochemical and isotopic evidence. *Hydrol. Earth Syst. Sci*., **2018**, *22(6)*, 3473–3491.
13. Datta, B.; Vennalakanti, H.; Dhar, A. Modeling and control of saltwater intrusion in a coastal aquifer of Andhra Pradesh, India. *J. Hydro-environ. Res.* **2009**, *3(3)*, 148–159.
14. Kanagaraj, G.; et al. Hydrogeochemical processes and influence of seawater intrusion in coastal aquifers south of Chennai, Tamil Nadu, India. *Environ. Sci. Pollut. Res.* **2018**, *25(9)*, 8989–9011.
15. Steyl, G.; Dennis, I. Review of coastal-area aquifers in Africa. *Hydrogeol. J*. **2010**, *18(1)*, 217–225.
16. Nofal, E.R.; et al. Delineation and modeling of seawater intrusion into the Nile Delta Aquifer: A new perspective. *Water Sci.* **2015**, *29(2)*, 156–166.
17. Sadeg, S.; Karahanoðlu, N. Numerical assessment of seawater intrusion in the Tripoli region, Libya. *Environ. Geol*. **2001**, *40(9)*, 1151–1168.
18. Haddout, S.; Igouzal, M.; Maslouhi, A. Seawater Intrusion in Semi-Closed Convergent Estuaries (Case Study of Moroccan Atlantic Estuaries): Application of Salinity Analytical Models. *Mar. Geod*. **2017**, *40(5)*, 275–296.
19. Himi, M.; et al. Geophysical characterization of saltwater intrusion in a coastal aquifer: The case of Martil-Alila plain (North Morocco). *J. Afr. Earth. Sci.* **2017**, *126*, 136–147.
20. Zghibi, A.; Tarhouni, J.; Zouhri, L. Assessment of seawater intrusion and nitrate contamination on the groundwater quality in the Korba coastal plain of Cap-Bon (North-east of Tunisia). *J. Afr. Earth. Sci*. **2013**, *87*, 1–12.

21. Trabelsi, N.; et al. Aquifer vulnerability and seawater intrusion risk using GALDIT, GQISWI and GIS: case of a coastal aquifer in Tunisia. *Environ. Earth Sci.* **2016**. *75(8)*, 669.
22. Ayed, B.; et al. Assessment of Seawater Intrusion in the Maritime Djeffara Coastal Aquifer (Southeastern Tunisia). in Recent Advances in Environmental Science from the Euro-Mediterranean and Surrounding Regions. Cham: Springer International Publishing, 2018.
23. Badaruddin, S.; Werner, A.D.; Morgan, L.K. Characteristics of active seawater intrusion. *J. Hydrol*. **2017**, *551(C)*, 632–647.
24. Fleckenstein, J.H.; et al. Groundwater-surface water interactions: New methods and models to improve understanding of processes and dynamics. *Adv. Water Resour*. **2010**, *33(11)*, 1291–1295.
25. Trung, N.H.; Tri, V.P.D. Possible impacts of seawater intrusion and strategies for water management in coastal areas in the Vietnamese Mekong Delta in the context of climate change A2 - Thao, Nguyen Danh, in Coastal Disasters and Climate Change in Vietnam, H. Takagi and M. Esteban, Editors. Elsevier: Oxford. 2014, pp. 219–232.
26. Nguyen, A.D.; Savenije, H.H. Salt intrusion in multi-channel estuaries: a case study in the Mekong Delta, Vietnam. *Hydrol. Earth Syst. Sci. Discuss*. **2006**, *10(5)*, 743–754.
27. Vu, D.T.; Yamada, T.; Ishidaira, H. Assessing the impact of sea level rise due to climate change on seawater intrusion in Mekong Delta, Vietnam. *Water Sci. Technol.* **2018**, *77(6)*, 1632–1639.
28. Thanh, N.C. Saltwater Intrusion - An Evident Impact of Climate Change in the MD and Propose Adaptable Solutions. *Am. J. Environ. Resour. Econ.* **2016**, *1(1)*, 1–8.
29. Sebastian, L.; et al. The drought and salinity intrusion in the Mekong River Delta of Vietnam - Assessment report. 2016.
30. An, T.D.; et al. Isotopic and Hydrogeochemical Signatures in Evaluating Groundwater Quality in the Coastal Area of the Mekong Delta, Vietnam, in Advances and Applications in Geospatial Technology and Earth Resources: Proceedings of the International Conference on Geo-Spatial Technologies and Earth Resources 2017, Tien Bui, D. et al. Editors. Springer International Publishing: Cham. 2018, pp. 293–314.
31. Dang, T.D.; et al. Hydrological alterations from water infrastructure development in the Mekong floodplains. *Hydrol. Processes* **2016**, *30(21)*, 3824–3838.
32. Manh, N.V.; et al. Future sediment dynamics in the Mekong Delta floodplains: Impacts of hydropower development, climate change and sea level rise. *Global Planet. Change* **2015**, *127*, 22–33.
33. Hoang, L.P.; et al. Mekong River flow and hydrological extremes under climate change. *Hydrol. Earth Syst. Sci.* **2016**, *20(7)*, 3027–3041.
34. Nhan, N.H. Tidal regime deformation by sea level rise along the coast of the Mekong Delta. Estuarine. *Estuarine Coastal Shelf Sci.* **2016**, *183*, 382–391.
35. Lauri, H.; et al. Future changes in Mekong River hydrology: impact of climate change and reservoir operation on discharge. *Hydrol. Earth Syst. Sci.* **2012**, *16(12)*, 4603–4619.
36. Elena, G.; Dianne, M. Environmental and political implications of Vietnam's water vulnerabilities: A multiscale assessment. *Singapore J. Trop. Geogr.* **2016**, *37(1)*, 59–75.
37. Smajgl, A.; et al. Responding to rising sea levels in the Mekong Delta. *Nat. Clim. Change* **2015**, *5(2)*, 167–174.

38. Shrestha, S.; Bach, T.V.; Pandey, V.P. Climate change impacts on groundwater resources in Mekong Delta under representative concentration pathways (RCPs) scenarios. *Environ. Sci. Policy*. **2016**, *61*, 1–13.
39. Chea, R.; Grenouillet, G.; Lek, S. Evidence of Water Quality Degradation in Lower Mekong Basin Revealed by Self-Organizing Map. *PLOS ONE* **2016**, *11(1)*, e0145527.
40. Wagner, F.; Tran, V.B.; Renaud, F.G. Groundwater Resources in the Mekong Delta: Availability, Utilization and Risks, in The Mekong Delta System: Interdisciplinary Analyses of a River Delta, F.G. Renaud and C. Kuenzer, Editors. Springer Netherlands: Dordrecht. 2012, pp. 201–220.
41. Appelo, C.A.J. Cation and proton exchange, pH variations, and carbonate reactions in a freshening aquifer. *Water Resour. Res*. **1994**, *30(10)*, 2793–2805.
42. Hooper, R.P.; Christophersen, N.; Peters, N.E. Modelling streamwater chemistry as a mixture of soilwater end-members – An application to the Panola Mountain catchment, Georgia, U.S.A. *J. Hydrol*. **1990**, *116(1)*, 321–343.
43. James, A.L.; Roulet, N.T. Investigating the applicability of end-member mixing analysis (EMMA) across scale: A study of eight small, nested catchments in a temperate forested watershed. *Water Resour. Res.* **2006**, *42(8)*, W08434.
44. Barthold, F.K.; et al. How many tracers do we need for end member mixing analysis (EMMA)? A sensitivity analysis. *Water Resour. Res*. **2011**, *47(8)*, W08519.
45. Pelizardi, F.; et al. Identifying geochemical processes using End Member Mixing Analysis to decouple chemical components for mixing ratio calculations. *J. Hydrol*. **2017**, *550*, 144–156.
46. Gracz, M.B.; et al. Analyzing peatland discharge to streams in an Alaskan watershed: An integration of end-member mixing analysis and a water balance approach. *J. Hydrol.* **2015**, *530*, 667–676.
47. Sakakibara, K.; et al. Spatiotemporal variation of the surface water effect on the groundwater recharge in a low-precipitation region: Application of the multi-tracer approach to the Taihang Mountains, North China. *J. Hydrol.* **2017**, *545*, 132–144.

JOURNAL OF
HYDRO-METEOROLOGY

Research Article

Experimental optimization to enhance oil removal efficiency from water using carbonized rambutan peel

Trinh Trong Nguyen[1], Nguyen Dinh Loc[1], Le Huy Ba[2], Thai Van Nam[1]*

[1] HUTECH Institute of Applied Sciences, HUTECH University, Ho Chi Minh City, Vietnam; tt.nguyen@hutech.edu.vn; lochenni@gmail.com; tv.nam@hutech.edu.vn
[2] Faculty of Biology and Environment, Ho Chi Minh City University of Industry and Trade, 140 Le Trong Tan, Ho Chi Minh 700000, Viet Nam; lhuyba@gmail.com

*Corresponding author: tv.nam@hutech.edu.vn; Tel: +84–945007990

Received: 15 October 2023; Accepted: 27 November 2023; Published: 25 March 2024

Abstract: In this study, the objective was to employ experimental design in order to optimize the efficiency of diesel oil removal from water using activated carbon sourced from rambutan peel. A central composite design was utilized to investigate the impact of contact time, adsorbent dosage, initial oil concentration, and pH on both the removal efficiency and oil adsorption capacity across 30 different experimental designs. The analysis of activated carbon properties derived from rambutan peel revealed a BET surface area of 786.014 m2/g, a BJH adsorption cumulative pore volume of 0.054 cm3/g, and an average BJH adsorption pore diameter of 55.243 nm. The quadratic model was employed to estimate the mathematical relationship between the removal efficiency and adsorption capacity of diesel oil in relation to the four key independent variables. The ANOVA analysis demonstrates F-values of 12.36 and 39.92 for the respective models, both exhibiting ρ-values < 0.05. The predicted values closely align with experimental results, showcasing R2 values of 92.02% for removal efficiency and 97.39% for adsorption capacity. The investigation anticipates that, based on the analysis of 87 solutions, optimal conditions of 70.60 minutes of contact time, 0.25 g/g adsorbent dosage, 0.97% v/v initial oil concentration, and a pH of 6.20 will yield a maximum removal efficiency of 72.12% and a maximum adsorption capacity of 5.3570 g/g. This combination of factors achieves a desirability rating of 0.741.

Keywords: Activated carbon; Diesel oil; Materials science; Modeling; Rambutan peel.

1. Introduction

Contaminated water containing oil has a worldwide impact on the quality of water and underwater ecosystems, resulting in serious health repercussions [1]. Techniques for oil elimination in aquatic environments can be sorted into in-situ combustion, chemical approaches (solidification and dispersion), biological methodologies, and physical means (such as skimming and absorbents) [2]. Within these options, oil adsorbents continue to be the favored method for oil cleanup due to their swiftness, simplicity, environmental sustainability [3], and cost-effectiveness. The selection of the adsorbent material is contingent on factors like availability, cost, and safety considerations [4]. Among these categories, adsorbent materials originating from natural organic sources offer notable benefits when compared to others, particularly in regard to their environmental compatibility in marine settings and their lightweight characteristics, which facilitate effortless retrieval and reuse [5].

Activated carbon, produced through carbonization, is employed for the adsorption of a wide range of substances [6]. Activated carbon derived from plant biomass is especially preferred due to its abundant and easily accessible origin, leading to notably reduced manufacturing expenses when compared to commercially available activated carbon [7]. Consequently, numerous distinct activated carbon materials have been manufactured from diverse plant-based sources, including coconut shells [7], coconut coir [8], corn cobs [9], safou seeds [10], oil palm endocarp [11] and rambutan peel [12]. Some activated carbon materials of natural origin have been recently used for oil absorption, such as carbonized pith bagasse [13], carbonized rice husk [14], activated carbon tablets from corncobs [6], mango shell activated carbon [15], and corn cobs activated carbon [9].

Rambutan peel (RP) is considered an agricultural waste with a substantial cellulose content, amounting to 24.28 % [16], rendering it a cost-effective and suitable economical material for the adsorption of oil in water. In this study, the rambutan peel will be chosen as the primary material to produce low-cost and environmentally friendly oil-absorbent substances. The employment of statistical experimental design approaches within the adsorption process has been put into practice to reduce process variability and minimize resource demands [17]. Response Surface Methodology (RSM) is a mathematical and statistical method utilized for experimental design, modeling, assessing the relative importance of independent variables, and determining optimal conditions for desired outcomes [18]. Grounded in Central Composite Design (CCD), RSM has been broadly utilized for determining the best conditions in multivariate systems [19]. More recently, it has been effectively used to optimize parameters in various wastewater treatment processes [20].

Presently, there have been no investigations that have employed Response Surface Methodology (RSM) with Central Composite Design (CCD) to optimize parameters for the removal of oil from water utilizing chemically activated carbon derived from RP. The use of RMS via CCD helps fine-tune the factors influencing the adsorption process to determine optimal values for enhancing the oil adsorption and removal capabilities of RPAC under realistic environmental conditions. The objective of this study will focus on experiment optimization to enhance the efficiency of oil removal from water using carbonized rambutan peel through a surface response method based on CCD.

2. Material and methods

2.1. Materials

Rambutan peel was procured from the primary market located in Ho Chi Minh City, Vietnam. Diesel oil (DO) 0.05 S was acquired from Petrolimex Aviation in Ho Chi Minh City, Vietnam, and it exhibited a specific gravity at 15^{o}C ranging from 820 to 860 kg/m^{3}. Potassium hydroxide, n-Hexane, and sodium sulfate anhydrous were obtained from Xilong Scientific Co., Ltd. in Shenzhen, China. Hydrochloric acid (c(HCl) = 0.1 mol/l or 0.1 N) was supplied by Merck in Germany.

2.2. Preparation of adsorbent

Rambutan peel underwent a series of steps, including rinsing with deionized water, drying at 105^{o}C for 24 hours, grinding to achieve a particle size of 1-2 mm, and subsequent carbonization at 550^{o}C for 2 hours in purified nitrogen (99.99 %). The resultant product was subjected to impregnation with KOH pellets at a 1:2 ratio [21]. These KOH pellets were dissolved in deionized water to form a 1 N KOH solution, and the mixture was soaked for a period of 24 hours. Afterward, it was dried for 24 hours at 105^{o}C to eliminate moisture, followed by activation in a muffle furnace at 550^{o}C for 1 hour. The resulting rambutan peel activated carbon (RPAC) was subsequently cooled, treated with a 0.1 N HCl solution to

eliminate ash content, rinsed with distilled water until achieving a pH range of 6-7, dried at 105^{o}C for 2 hours, crushed, sieved into various particle sizes, and finally stored in a desiccator for future use.

2.3. Characterization of adsorbent

Brunauer-Emmett-Teller (BET) theory is used to measure the surface area of RP and RPAC. The solid sample is cooled under vacuum to cryogenic temperature using liquid nitrogen. Nitrogen gas is incrementally dosed to the sample, allowing equilibration of relative pressure (P/P_0) after each dose. The BET equation involves a linear plot of $1/((P_0/P)-1)$ vs. P/P0, typically within the range of 0.05 to 0.35 for most solids. From this plot, the weight of nitrogen for a monolayer (Wm) is determined, enabling calculation of the total surface area using the BET equation and the nitrogen molecule's known cross-sectional area [22].

$$\frac{1}{W\left(\frac{P_0}{P}-1\right)}=\frac{1}{W_mC}+\left(\frac{C-1}{W_mC}\right)\frac{P}{P_0} \quad (1)$$

The weight of gas adsorbed at a relative pressure of P/P_0 is represented by W, while Wm signifies the weight of the adsorbate forming a monolayer of surface coverage. The term C, known as the BET C constant, correlates with the energy of adsorption within the initial adsorbed layer. Therefore, its value serves as an indicator of the strength of interactions between the adsorbent and adsorbate [22].

To ascertain the pore volume and distribution of pore sizes, the gas pressure is gradually increased until all pores are saturated with nitrogen molecules. Subsequently, the pressure is gradually decreased, causing the condensed nitrogen gas to evaporate from the system. Analyzing the adsorption and desorption isotherms provides insights into both pore volume and the distribution of pore sizes [22]. The RPAC produced under optimal conditions was evaluated for its surface area, pore volume, and average pore diameter using the Micromeritics® TriStar II Plus Version 3.03.

Scanning Electron Microscope (SEM) analysis was conducted using the JSM-IT500 InTouchScope™ Scanning Electron Microscope.

2.4. Approach for assessing the effectiveness of oil adsorption

In each trial, the quantity of oil adsorbed per gram of adsorbent at equilibrium is represented as q_e (g/g), at a given time t is denoted as q_t (g/g), and the adsorption efficiency is calculated using the subsequent equation [21]:

$$q_e=\frac{(C_o-C_e)\times V}{M} \quad (2)$$

$$q_t=\frac{(C_o-C_t)\times V}{M} \quad (3)$$

$$\%\ \text{Effective removal}=\frac{(C_o-C_e)\times 100}{C_o} \quad (4)$$

where C_o stands for the initial oil concentration (mg/L); C_e is the concentration at equilibrium (mg/L); C_t denotes the oil concentration at time t (mg/L); V represents the solution volume (ml); and M is the mass of the adsorbent used.

2.5. Experimental design for optimization

The CCD encompasses 2^n factorial runs, along with 2n axial runs and n_c center runs. The center points serve to evaluate experimental error and data reproducibility, while the axial points ensure rotatability to maintain a constant variance of model predictions equidistant

from the design center [23]. Hence, as per [24], the necessary number of experimental runs can be determined using equation (5).

$$N = 2^n + 2n + n_c = 2^4 + 2 \times 4 + 6 = 30 \quad (5)$$

where N = Total number of experimental runs, n = number of independent variables (factors), and n_c = number of center points. This study considered four independent variables: contact time (A), adsorbent dosage (B), initial oil concentration (C), and pH (D). The dependent parameters or responses were removal efficiency (Y_1) and adsorption capacity (Y_2). The RSM model analysis utilized the CCD from Design-Expert 13. The optimal values (Center) of the factors influencing the oil adsorption process of RPAC will be selected based on the research findings of [12] to incorporate into the optimal experimental design. The ranges of the independent variables are presented in Table 1.

Table 1. Factors and levels tested for experimental design.

	Symbol	Low	Center	High	Unit
Level		-1	0	1	
Contact time	A	50	60	70	min
Adsorbent dosage	B	0.25	0.5	0.75	g
Initial oil concentration	C	0.75	1.0	1.25	% v/v
pH	D	5.0	6.0	7.0	

3. Results and discussion

3.1. Characteristics of the adsorbent

The BET surface area of RPAC was 786.014 m^2/g. The increased BET surface area in RPAC indicated more active sites, enhancing oil uptake [25]. The pore volume is 0.054 cm^3/g, while the pore diameter increased is 55.243 nm. The surface structure of raw RP exhibits uniform fiber-like crystal bonds and small pores, indicative of mineral presence (Figure 1a). This surface primarily consists of a lignocellulose network and a fiber matrix containing lignin, cellulose, volatile organic compounds, and hemicellulose. Following carbonization and alkaline treatment, RPAC's surface displays uneven, rough, and rugged structures with larger, deeper existing pores, accompanied by an increase in their number on the material's surface (Figure 1b). The KOH-C reaction enhances pore development during activation, thereby increasing surface area and adsorption capacity. A nearly heterogeneous pore structure pattern is also observable on the RPAC surface.

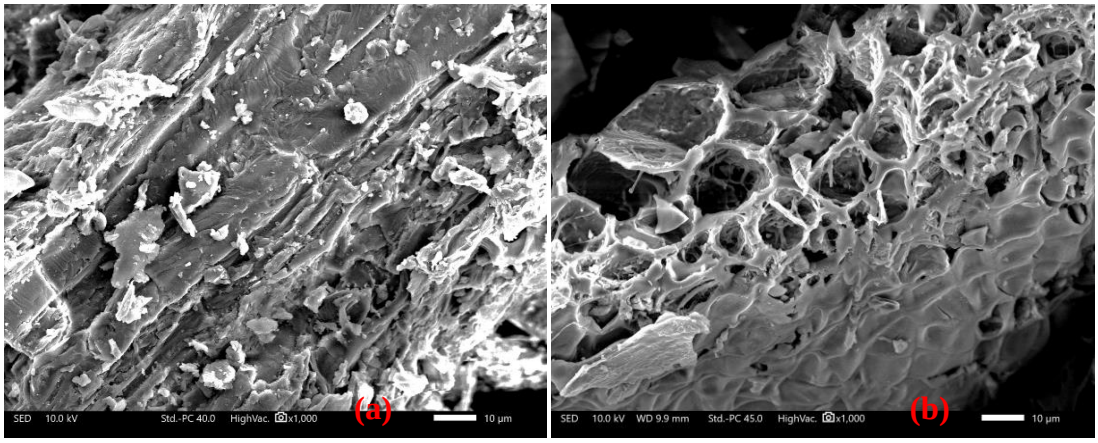

Figure 1. SEM images of raw RP (a) and RPAC (b).

3.2. Experimental design

Table 2 shows that the oil removal efficiency (Y_1) of RPAC ranged from 48.05% to 86.20%, with the highest and lowest values recorded. Similarly, the oil adsorption capacity (Y_2) ranged from 1.1679 g/g to 5.9876 g/g.

Table 2. Experimental design matrix of RPAC.

Run	Factors				Responses			
	Contact time (min)	Adsorbent dosage (g)	Initial oil concentration (% v/v)	pH	Removal efficiency (%)		Adsorption capacity (g/g)	
	(A)	(B)	(C)	(D)	Experimental	Predicted	Experimental	Predicted
1	60	0.5	1	6	74.52	74.65	3.2296	3.2500
2	70	0.75	1.25	5	72.40	71.06	2.6236	2.3400
3	50	0.75	1.25	7	70.20	70.67	2.5372	2.3800
4	70	0.75	0.75	7	72.21	73.47	1.5692	1.5700
5	70	0.25	1.25	7	54.83	54.82	5.9756	5.9500
6	60	0.5	0.5	6	55.21	52.13	1.1926	1.0300
7	60	0.5	1	6	75.38	74.65	3.2788	3.2500
8	70	0.75	0.75	5	61.61	64.78	1.3477	1.4100
9	60	0.5	1	6	73.90	74.65	3.2076	3.2500
10	70	0.25	1.25	5	54.00	55.35	5.8600	5.7900
11	50	0.25	0.75	7	55.23	57.86	3.6416	3.8000
12	50	0.25	1.25	7	55.13	50.63	5.9876	5.6400
13	60	0.5	1.5	6	48.05	51.18	3.2244	3.7900
14	50	0.75	1.25	5	74.01	68.82	2.7064	2.3200
15	70	0.25	0.75	7	65.95	69.81	4.3152	4.4300
16	60	0.5	1	6	75.61	74.65	3.2988	3.2500
17	50	0.75	0.75	5	53.48	54.78	1.1679	1.0700
18	60	0.5	1	4	50.60	52.62	2.2036	2.5000
19	60	0.5	1	8	62.16	60.18	2.7010	2.8000
20	70	0.25	0.75	5	63.28	64.10	4.1532	4.1900
21	40	0.5	1	6	52.15	58.22	2.2680	2.7200
22	50	0.25	0.75	5	56.97	52.75	3.7220	3.5800
23	50	0.75	0.75	7	65.55	62.87	1.4343	1.2200
24	80	0.5	1	6	78.43	72.41	3.4180	3.3700
25	60	0.5	1	6	78.51	74.65	3.4108	3.2500
26	70	0.75	1.25	7	70.62	73.51	2.5565	2.4200
27	60	0.5	1	6	72.95	74.65	3.1728	3.2500
28	60	0.5	1	6	71.65	74.65	3.1284	3.2500
29	60	1	1	6	86.20	86.25	1.8775	2.2800
30	50	0.25	1.25	5	51.72	51.75	5.6204	5.5000

3.3. Analysis of variance (ANOVA)

The selected model equations for removal efficiency (response Y_1) and adsorption capacity (response Y_2) underwent ANOVA analysis to assess the significance and adequacy of the models. The ANOVA results of the quadratic model, presented in Table 3 and Table 4, indicate that the model equations effectively describe the oil removal performance of RPAC under the experimental conditions. The F-values for the two corresponding models are 12.36 and 39.92, and the ρ -values for both models are < 0.05, demonstrating the significance of both models. Regarding removal efficiency, factors A (ρ = 0.0007), B (ρ < 0.0001), D (ρ = 0.0383), BC (ρ = 0.0022, A^2 (ρ = 0.0087), C^2 (ρ < 0.0001), and D^2 (ρ < 0.0001) significantly influence the response (with p-values less than 0.05 and high F-values) (Table 3). Similarly, for adsorption capacity, factors A (ρ = 0.0205), B (ρ < 0.0001), C (ρ < 0.0001), BC (ρ = 0.043), B^2 (ρ < 0.0001), C^2 (ρ = 0.0026), and D^2 (ρ = 0.022) significantly impact the response (with p-values less than 0.05 and high F-values) (Table 4). Factors that do not have a significant influence (ρ > 0.05) will be removed from the regression equation, as presented in equations (6) and (7).

Table 3. Analysis of variance of regression model for removal efficiency of RPAC.

Source	Sum of Squares	df	Mean Square	F-value	ρ -value
Model	2877.06	14	205.5	12.36	< 0.0001*
A	302.25	1	302.25	18.18	0.0007*
B	459.98	1	459.98	27.67	< 0.0001*

Source	Sum of Squares	df	Mean Square	F-value	ρ -value
C	1.35	1	1.35	0.0811	0.7797
D	85.77	1	85.77	5.16	0.0383*
AB	1.83	1	1.83	0.11	0.7447
AC	60.18	1	60.18	3.62	0.0765
AD	0.357	1	0.357	0.0215	0.8854
BC	225.98	1	225.98	13.59	0.0022*
BD	8.87	1	8.87	0.5333	0.4765
CD	38.91	1	38.91	2.34	0.1469
A2	151.18	1	151.18	9.09	0.0087*
B2	1.57	1	1.57	0.0946	0.7626
C2	917.56	1	917.56	55.19	< 0.0001*
D2	577.61	1	577.61	34.74	< 0.0001*
Residual	249.38	15	16.63		
Lack of Fit	220.56	9	24.51	5.10	
Pure Error	28.82	6	4.80		
Cor Total	3126.44	29			

Note: * = Significant; df = Degree of freedom.

Table 4. Analysis of variance of regression model for adsorption capacity of RPAC.

Source	Sum of Squares	df	Mean Square	F-value	ρ -value
Model	52.35	14	3.74	39.92	< 0.0001*
A	0.6284	1	0.6284	6.71	0.0205*
B	39.01	1	39.01	416.46	< 0.0001*
C	11.45	1	11.45	122.27	< 0.0001*
D	0.1366	1	0.1366	1.46	0.2459
AB	0.0731	1	0.0731	0.78	0.3911
AC	0.0985	1	0.0985	1.05	0.3214
AD	0.0001	1	0.0001	0.0015	0.9692
BC	0.458	1	0.458	4.89	0.043*
BD	0.0061	1	0.0061	0.0653	0.8018
CD	0.0065	1	0.0065	0.0696	0.7955
A2	0.0714	1	0.0714	0.7619	0.3965
B2	4.3	1	4.3	45.94	< 0.0001*
C2	1.22	1	1.22	12.99	0.0026*
D2	0.6113	1	0.6113	6.53	0.022*
Residual	1.41	15	0.0937		
Lack of Fit	1.35	9	0.1503	17.36	
Pure Error	0.0520	6	0.0087		
Cor Total	53.75	29			

Note: * = Significant; df = Degree of freedom

For the model presented in equations (6) and (7) of coded factors, the correlation coefficients R^2 and adjusted R^2 exhibit a high degree of correlation, reaching 92.02 % and 84.58 % for Y_1, and 97.39 % and 94.95 % for Y_2, respectively. This indicates that the regression model closely aligns with the experimental data and effectively reveals the relationships between the independent variables and the response. The coefficients associated with single factors represent the influence of that specific factor, while the coefficients related to two factors depict the interaction between those two factors. The negative coefficients preceding the independent and interaction factors in these equations signify that they exert a diminishing effect on the responses. For the individual effects, three factors, A, B and D, exhibit a positive influence on Y_1 in the sequence of B > A > D, while two factors, A and C, positively impact Y_2 and B adversely affects Y_2 with the order of B > C > A. Concerning interacting effects, BC positively affects Y_1 and adversely affects Y_2. In terms of quadratic effects, A^2, C^2, D^2 negatively impact Y_1 in the order of $C^2 > D^2 > A^2$. Conversely, B^2 has a positive effect, while C^2 and D^2 have negative impacts on Y_2 in the order of $B^2 > C^2 > D^2$. Among these factors, C^2 (as quadratic effects) significantly influences Y_1 (with the highest

F-value of 55.19), while B (as an individual factor) notably affects Y_2 (with the highest F-value of 416.46).

$$Y_1\ (\%) = 74.65 + 3.55A + 5.18B + 1.89D + 3.76BC - 2.33A^2 - 5.75C^2 - 4.56D^2 \quad (6)$$

$$Y_2\ (g/g) = 3.25 + 0.1618A - 1.51B + 0.6908C - 0.1692BC + 0.5124\ B^2 - 0.2093C^2 - 0.1484D^2 \quad (7)$$

The comparison between the predicted removal efficiency and adsorption capacity of RPAC and the observed values is illustrated in Figure 2. The model has successfully captured the correlation between independent variables and dependent parameters or responses, as the results indicate a close match between the predicted values and the actual experimental values.

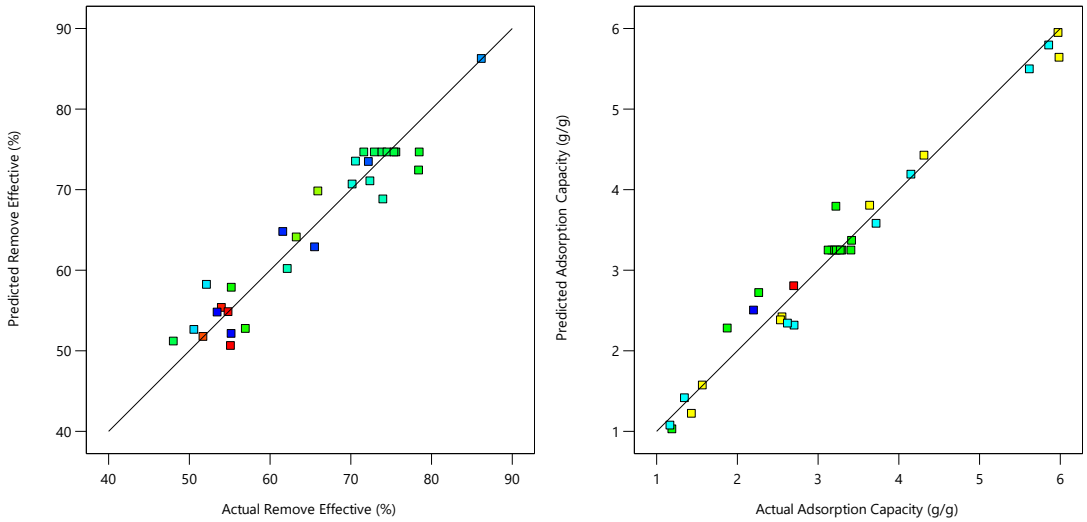

Figure 2. Actual and predicted plot of removal efficiency and adsorption capacity of RPAC.

3.4. Pareto diagram

From the Pareto charts for removal efficiency of RPAC (Figure 3a), it is evident that the adsorbent dosage, contact time, pH of the solution, and the interaction between adsorbent dosage and initial oil concentration are significant and positive standardized effects on RPAC's removal efficiency. Similarly, from the Pareto charts for adsorption capacity of RPAC (Figure 3b), the initial oil concentration, contact time, and pH of the solution significantly positively impact RPAC's adsorption capacity.

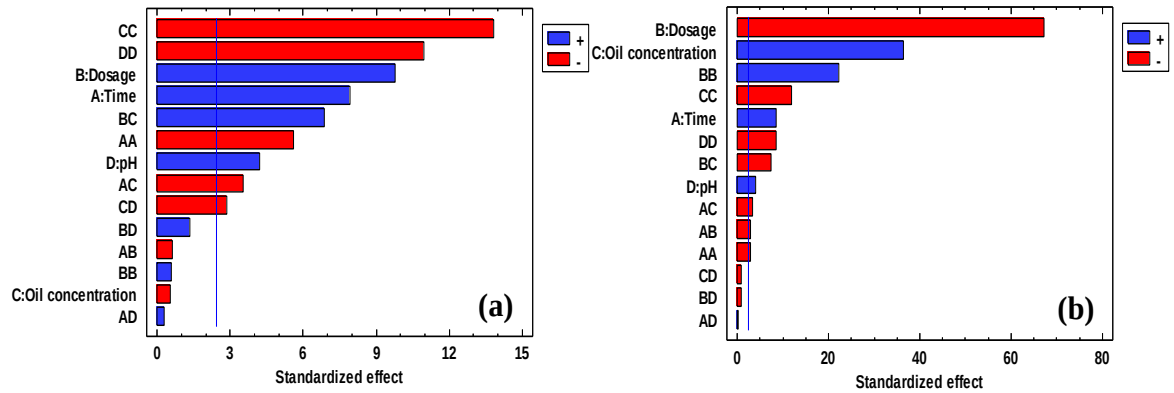

Figure 3. (a) Pareto diagram for removal efficiency of RPAC; (b) Pareto diagram for adsorption capacity of RPAC.

3.5. Response surface analysis

In this segment, the impact of notable interactive effects between the adsorbent quantity (B) and initial oil concentration (C) on the efficiency of elimination and adsorption capability using RPAC is deliberated.

3.5.1. Interaction of adsorbent dosage and initial oil concentration on removal efficiency

Figures 4a,b show contour plots and response surface plots for adsorbent dosage and initial oil concentration on removal efficiency.

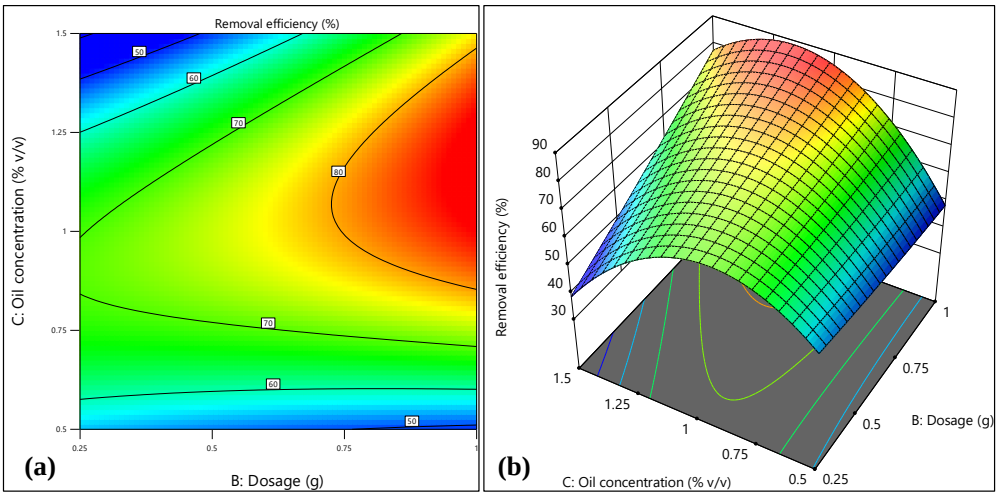

Figure 4. Interaction of adsorbent dosage and initial oil concentration on removal efficiency: (a) Contour plot of adsorbent dosage and initial oil concentration (pH = 6, Contact time = 60 min); (b) Response surface plot of time and dosage (pH = 6, Contact time = 60 min).

As depicted in Figure 4, it is evident that increasing the dosage of the adsorbent does not significantly enhance the removal efficiency when the initial oil concentration is low (0.5% v/v). The RPAC achieves maximum oil removal efficiency of 86.2% at an adsorbent dosage of 1g and an initial oil concentration of 1% v/v. The lowest oil removal efficiency of RPAC (48.5%) occurs at an adsorbent dosage of 0.5g and an initial oil concentration of 1.5% v/v. Increasing the adsorbent dosage from 0.5g to 1g alongside an increase in the initial oil concentration contributes more significantly to the RPAC's removal efficiency. However, with the same adsorbent dosage, excessively high initial oil concentrations lead to a decrease in RPAC's removal efficiency. This can be ascribed to the decrease in the quantity of active sites accessible on the adsorbent's surface responsible for adhering to oil. This discovery corresponds [8] observations, which demonstrated a comparable pattern while employing coconut coir-activated carbon for oil spill remediation.

3.5.2. Interaction of adsorbent dosage and initial oil concentration on adsorption capacity

Figures 5a,b show contour plots and response surface plots for adsorbent dosage and initial oil concentration on adsorption capacity.

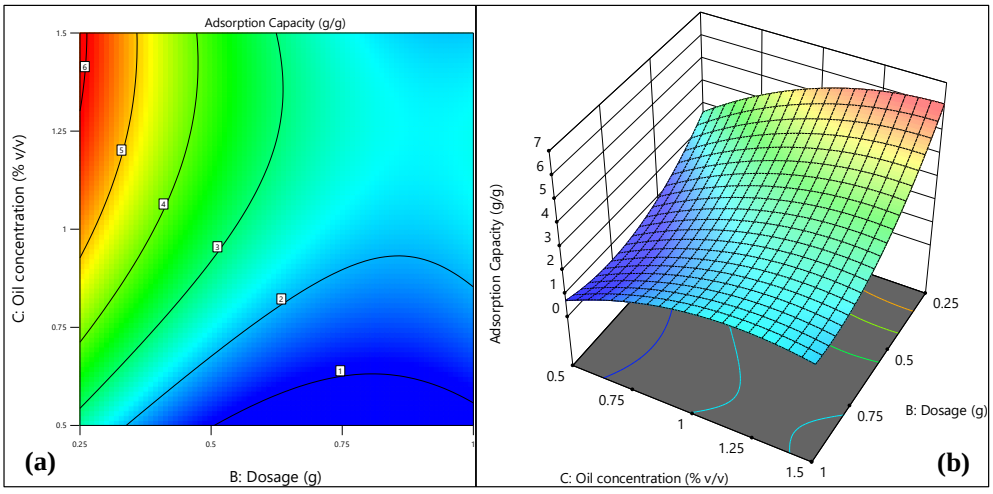

Figure 5. Interaction of adsorbent dosage and initial oil concentration on adsorption capacity: (a) Contour plot of adsorbent dosage and initial oil concentration (pH = 6, Contact time = 60 min); (b) Response surface plot of time and dosage (pH = 6, Contact time = 60 min).

As evident in Figure 5, increasing the adsorbent dosage at the same oil concentration leads to a reduction in RPAC's adsorption capacity. The surplus presence of RPAC in the surroundings might impede the infiltration of oil molecules, restricting their access to active sites on the surface. Consequently, this limitation curtails additional adsorption capacity and hampers the complete elimination of oil. A similar trend was observed in a study by [26], wherein the adsorption capacity initially rose as the adsorbent dosage increased from 0.5 g to 1.5g, but then exhibited a declining pattern. This decline could be attributed to the compression of fibers at higher dosages, potentially impeding the uniform penetration of oil into the fibers. Increasing the initial oil concentration from 0.5% v/v to 1.5% v/v at different dosages consistently demonstrates an elevation in RPAC's oil adsorption capacity, particularly at lower adsorbent dosages. Specifically, the RPAC's oil adsorption capacity peaks when the initial oil concentration is 1.25% v/v, coupled with an adsorbent dosage of 0.25g.

3.6. Optimization of the adsorption process

Optimizing each response will help determine the optimal conditions for the influencing factors in the oil adsorption process of RPAC. Table 5 shows that to maximize the removal efficiency to 88.89 %, the optimal conditions for the factors (i.e., contact time, adsorbent dosage, initial oil concentration, and pH) are 66.45 min, 1 g/g, 1.09% v/v, and 6.33, respectively. To achieve a maximum adsorption capacity of 6.0940 g/g, the optimal conditions for the factors (i.e., contact time, adsorbent dosage, initial oil concentration, and pH) are 63.64 min, 0.25 g/g, 1.36% v/v, and 6.43, respectively.

Table 5. Optimization of the adsorption process to achieve the goal of maximizing removal efficiency and adsorption capacity.

Factor	Low	High	Optimum	
			Maximizing removal efficiency	Maximizing adsorption capacity
- Contact time (min)	40	80	66.45	63.64
- Adsorbent dosage (g)	0.25	1.0	1.0	0.25
- Initial oil concentration (% v/v)	0.5	1.5	1.09	1.36
- pH	4.0	8.0	6.33	6.43
Responses				
- Removal efficiency (%)			88.89	
- Adsorption capacity (g/g)				6.0940

Multiple response optimization aims to find the best combination of factors to maximize both oil removal efficiency and adsorption capacity simultaneously. This is done by finding the highest value of a particular desirability measure. Table 6 displays the factor settings that achieve the highest desirability values within the specified range. After evaluating 87 solutions, the optimal conditions were determined: contact time of 70.60 min, adsorbent dosage of 0.25 g/g, initial oil concentration of 0.97% v/v, and a pH of 6.20. Under these conditions, the optimal oil removal efficiency is 72.12%, and the optimal oil adsorption capacity is 5.3570 g/g.

Table 6. Optimization of the adsorption process to achieve the goal of maximizing removal efficiency and adsorption capacity.

Factor	Low	High	Optimum
- Contact time (min)	40	80	70.60
- Adsorbent dosage (g)	0.25	1.0	0.25
- Initial oil concentration (% v/v)	0.5	1.5	0.97
- pH	4.0	8.0	6.20
Responses			
- Removal efficiency (%)	48.05	86.20	72.12
- Adsorption capacity (g/g)	1.1679	5.9876	5.3570

Based on the results in Table 5 and Table 6, the maximum predicted oil adsorption capacity (RPAC) is 6.0940 g/g, and the target for optimizing multiple responses is 5.3570 g/g. These results are higher than the oil adsorption capacity of pyrolyzed rice husk (5.02 g/g) [27] as well as activated carbon from coconut husk fibers (4,859.5 mg/g) [8]. However, they are lower than the Gas oil adsorption capacity of activated carbon from barley straw [13].

4. Conclusion

Activated carbon derived from rambutan peel demonstrates effective oil removal from water. The main conclusions are as follows: (1) The carbonization and KOH activation processes result in a more porous structure with a BET surface area of 786.014 m^2/g, BJH adsorption cumulative pore volume of 0.054 cm^3/g, and BJH adsorption average pore diameter of 55.243 nm. Raw RP's surface structure shows uniform fiber-like crystal bonds and small pores, indicating mineral presence. After carbonization and alkaline treatment, RPAC's surface exhibits uneven, rough, and rugged structures with larger, deeper pores, accompanied by an increased number of pores on the material's surface. (2) ANOVA analysis indicates F-values of 12.36 and 39.92 for the respective models, both displaying ρ-values < 0.05. The predicted values closely align with experimental results, demonstrating R^2 values of 92.02% for removal efficiency and 97.39% for adsorption capacity. In terms of diesel oil removal efficiency, the significant influential factors follow the sequence of B > A > D for contact time (A), adsorbent dosage (B), and pH (D). Meanwhile, adsorption capacity is influenced by contact time (A), adsorbent dosage (B), and initial oil concentration (C) in the order of B > C > A. (3) The response surface plots, Pareto chart, and variance analysis indicated the most significant antagonistic interaction between adsorbent dosage and initial oil concentration concerning removal efficiency (F-value = 13.59, ρ-value = 0.0022) and adsorption capacity (F-value = 4.89, ρ-value = 0.043). (4) The study predicts a maximum removal efficiency of 72.12% and a maximum adsorption capacity of 5.3570 g/g under specific conditions: 70.60 min of contact time, 0.25 g/g adsorbent dosage, 0.97% v/v initial oil concentration, and a pH of 6.20, with a desirability rating of 0.741 based on the analysis of 87 solutions.

Author contribution statement: Defining and developing the research idea and researchframework: T.V.N., L.H.B.; Collecting data and literature, data analysis and synthesis: T.T.N., N.D.L.; Experimental research: T.T.N., N.D.L.; Drafting the manuscript: T.T.N.; Manuscript editing and revision: T.V.N., L.H.B.

Acknowledgement: This research was fully funded by HUTECH University under grant number 25/HĐ-ĐKC and the AKIHIKO IKAI Family Scholarship Fund.

Competing interest statement: The authors declare that this article was the work of theauthors, has not been published elsewhere, has not been copied from previous research; therewas no conflict of interest within the author group.

Reference

1. Kolokoussis, P.; Karathanassi, V. Oil spill detection and mapping using sentinel 2 imagery. *J. Mar. Sci*. **2018**, *6*, 1–12.
2. Alaa El-Din, G.; Amer, A.A.; Malsh, G.; Hussein, M. Study on the use of banana peels for oil spill removal. *Alex. Eng. J*. **2018**, *57*, 2061–2068.
3. El-Nafaty, U.A.; Muhammad, I.M.; Abdulsalam, S. Biosorption and kinetic studies on oil removal from produced water using banana peel. *Civ. Environ. Res*. **2013**, *3*, 125–136.

4. Idris, J.; Eyu, G.D.; Mansor, A.M.; Ahmad, Z.; Chukwuekezie, C.S. A preliminary study of biodegradable waste as sorbent material for oil-spill cleanup. *Sci. World J.* **2014**, *2014*, 1–5.
5. Banerjee, S.S.; Joshi, M.V.; Jayaram, R.V. Treatment of oil spill by sorption technique using fatty acid grafted sawdust. *Chemosphere* **2006**, *64*, 1026–1031.
6. Maulion, R.V.; Abacan, S.A.; Allorde, G.G.; Umali, M.C.S. Oil spill adsorption capacity of activated carbon tablets from corncobs in simulated oil-water mixture. *Asia Pac. J. Multidiscip. Res.* **2015**, *3*, 146–151.
7. Aljeboree, A.M.; Alshirifi, A.N.; Alkaim, A.F. Kinetics and equilibrium study for the adsorption of textile dyes on coconut shell activated carbon. *Alex. Eng. J.* **2017**, *10*, S3381–S3393.
8. Anwana Abel, U.; Rhoda Habor, G.; Innocent Oseribho, O. Adsorption studies of oil spill clean-up using coconut coir activated carbon (CCAC). *Am. J. Chem. Eng.* **2020**, *8*, 36–47.
9. Igwegbe, C.A.; Umembamalu, C.J.; Osuagwu, E.U.; Oba, S.N.; Emembolu, L.N. Studies on adsorption characteristics of corn cobs activated carbon for the removal of oil and grease from oil refinery desalter effluent in a downflow fixed bed adsorption equipment. *Eur. J. Sustain. Dev. Res.* **2020**, *5*, 1–14.
10. Atemkeng, C.D.; Anagho, G.S.; Tagne, R.F.T.; Amola, L.A.; Bopda, A.; Kamgaing, T. Optimization of 4-nonylphenol adsorption on activated carbons derived from safou seeds using response surface methodology. *Carbon Trends*. **2021**, *4*, 100052.
11. Silgado, K.J.; Marrugo, G.D.; Puello, J. Adsorption of chromium (VI) by activated carbon produced from oil palm endocarp. *Chem. Eng. Trans.* **2014**, *37*, 721–726.
12. Nguyen, T.T.; Loc, N.D.; Ba, L.H.; Nam, T.V. Efficient oil removal from water using carbonized rambutan peel: Isotherm and kinetic studies. *Vietnam Journal of Hydrometeorology*. **2023**, *4*, 1–18.
13. Hussein, M.; Amer, A. A.; Sawsan, I. I. Oil spill sorption using carbonized pith bagasse: 1. Preparation and characterization of carbonized pith bagasse. *J Anal Appl Pyrolysis*. **2008**, *82(2)*, 205–211.
14. Angelova, D.; Uzunov, I.; Uzunova, S.; Gigova, A.; Minchev, L. Kinetics of oil and oil products adsorption by carbonized rice husks. *J. Chem. Eng.* **2011**, *172(1)*, 306–311.
15. Olufemi, B. A.; Otolorin, F. Comparative adsorption of crude oil using mango (Mangnifera indica) shell and mango shell activated carbon. *Environ. Eng. Res.* **2017**, *22(4)*, 384–392.
16. Oliveira, E.; Santos, J.; Goncalves, A.P.; Mattedi, S.; Jose, N. Characterization of the rambutan peel fiber (nephelium lappaceum) as a lignocellulosic material for technological applications. *Chem. Eng. Trans.* **2016**, *50*, 391–396.
17. Khataee, A.R. Optimization of UV-promoted peroxydisulphate oxidation of C.I. Basic blue 3 using response surface methodology. *Environ. Technol.* **2010**, *31*, 73–86.
18. Draper, N.R.; John, J.A. Response-Surface Designs for Quantitative and Qualitative Variables. *Technometrics*. **1988**, *30*, 423–428.
19. Bayuo, J.; Pelig-Ba, K.B.; Abukari, M.A. Optimization of adsorption parameters for effective removal of lead (II) from aqueous solution. *Phys. Chem.: Indian J.* **2019**, *14*, 1–25.
20. Izevbekhai, O.U.; Gitari, W.M.; Tavengwa, N.T.; Ayinde, W.B.; Mudzielwana, R. Response surface optimization of oil removal using synthesized polypyrrole-silica polymer composite. *Molecules* **2020**, *25*, 4628.

21. Ahmad, M.A.; Alrozi, R. Optimization of rambutan peel based activated carbon preparation conditions for remazol brilliant blue R removal. *J. Chem. Eng*. **2011**, *168*, 280–285.
22. Naderi, M. Chapter fourteen - surface area: brunauer–emmett–teller (BET). Progress in Filtration and Separation. **2015**, pp. 585–608.
23. Mourabet, M.; El Rhilassi, A.; El Boujaady, H.; Bennani-Ziatni, M.; Taitai, A. Use of response surface methodology for optimization of fluoride adsorption in an aqueous solution by Brushite. *Arab. J. Chem.* **2017**, *10*, S3292–S3302.
24. Owolabi, R.U.; Usman, M.A.; Kehinde, A.J. Modelling and optimization of process variables for the solution polymerization of styrene using response surface methodology. *J. King Saud Univ. Eng. Sci.* **2018**, *30*, 22–30.
25. Nnamdi Ekwueme, B.; Anthony Ezema, C.; Asadu, C.O.; Elijah Onu, C.; Onah, T.O.; Sunday Ike, I.; Chinonyelum Orga, A. Isotherm modelling and optimization of oil layer removal from surface water by organic acid activated plantain peels fiber. *Arab. J. Chem*. **2023**, *16*, 104443.
26. NwabuezeH, H.O.; Chiaha, P.N.; Ezekannagha, B.C.; Okoani, O.E. Acetylation of corn cobs using iodine catalyst, for oil spills remediation. *Int. J. Eng. Sci*. **2016**, *5(9)*, 53–59.
27. Vlaev, L.; Petkov, P.; Dimitrov, A.; Genieva, S. Cleanup of water polluted with crude oil or diesel fuel using rice husks ash. *J. Taiwan Inst. Chem. Eng.* **2011**, *42(6)*, 957–964.

JOURNAL OF
HYDRO-METEOROLOGY

Rerearch Article

Evaluation of the Can Gio Vegetation Index changes using the Sentinel-2 Datasets from 2015 to 2023

Anh Bui Khanh Van[1]*

[1] Ho Chi Minh City University University of Natural Resources and Environment; bkvanh@hcmunre.edu.vn; bkvanh2020@gmail.com

*Corresponding author: bkvanh2020@gmail.com; Tel.: +84–908836115

Received: 27 October 2023; Accepted: 4 December 2023; Published: 25 March 2024

Abstract: Can Gio Mangrove Biosphere Reserve provide many ecosystem services, such as provisioning, regulating, cultural, and supporting services for the urban areas as well as wildlife of suburban areas in Ho Chi Minh City and the nearby ecosystems. Therefore, it is important to monitor and evaluate the change of mangrove forest cover in the long term. In this study, the Normalized Difference Vegetation Index - NDVI at 10 m resolution from 2015 to 2023 of Can Gio was obtained from the Copernicus Sentinel-2 database using Google Earth Engine - GEE. Subsequently, NDVIs statistic were computed by R to assess the slope of NDVI change with p-value significance in Can Gio. The results indicated that NDVI values typically range from -0.4 to +0.8 and vary annually. It is evident that NDVIs values from 2015 to 2020 are marginally higher than those recorded between 2021 and 2023. The degradation in average NDVI from 2015 to 2023 was rationally deducible either from the downsizing of mangrove forest areas or the degradation of the mangrove forest. However, the annual NDVI statistic revealed there were areas with an acceleration of NDVI in comparison with the destruction of NDVI areas from 2015 to 2023. Linear regression effectively models continuous processes like deposition or erosion. However, to evaluate other factors such as discrete human-made or sporadic impacts, alternative statistical models should be considered.

Keywords: Normalized Difference Vegetation Index - NDVI; The Copernicus Sentinel-2 database; Can Gio; Spatial and temporal pattern.

1. Introduction

Can Gio is an important ecosystem in Ho Chi Minh City, not only for historical meaning but also the future development. In the past, a large area of Can Gio was destroyed by herbicides using from 1965 to 1969 and by anthropogenic of local people from 1970 to 1980 [1]. From 1990 to 2000, many projects to reforestation were conducted. After being declared as the first Mangrove Biosphere Reserve (MBR) in Viet Nam in 2000, the studies of Can Gio has been increased and Can Gio has become an important research site [2].

Can Gio Mangrove Biosphere Reserve has provided many ecosystem services, such as provisioning, regulating, cultural, and supporting services for the urban areas as well as wildlife of suburban areas in Ho Chi Minh City and the nearby ecosystem[1]. The mangrove ecosystem in Can Gio serves as a crucial habitat for a diverse range of flora and fauna. Also, mangrove forest act as a natural barrier, protecting the coastline from erosion and minimizing the impact of storm surges. Besides, mangrove trees are highly effective at sequestering carbon dioxide from the atmosphere [2]. The root systems of mangrove filter pollutants and sediment from the water, improving water quality. Among other functions, the role of Can Gio requires a quantitative and complementary assessment.

Can Gio is currently confronted with a combination of human-induced and natural impacts [1,3]. Consequently, monitoring the ongoing changes in Can Gio is crucial for both present management and future development. Previous studies have delineated three primary processes characterizing the water-soil-plant dynamics in Can Gio, including (1) bank erosion stemming from both river systems and seawater; (2) seasonal fluctuations within the mangrove forests; and (3) anthropogenic influences encompassing preservation efforts or induced alterations [4–6].

For instance, Ly Nhon, the largest commune in Can Gio, experiences significant effects from the dynamics of the Dong Tranh River, notably in its near-shore areas. Studies indicate that the riverbank along Dong Tranh experiences considerable deposition, whereas areas draining into the East Sea endure severe erosion processes [4]. Situated between Cape of Dong Tranh and the East Sea borders, Long Hoa faces substantial impacts from waves, coastal storms, and typhoons, causing severe erosion along the commune's borders. Similarly, significant erosion points are observed in Can Thanh, yet constructed infrastructures such as concrete groins and rock dikes have mitigated shoreline erosion. In contrast, Thanh An experiences minimal erosion within Can Gio, although some bank river erosion has been reported [4].

Various studies utilized vegetation indices, such as the Normalized Difference Vegetation Index (NDVI), to gauge the quality of vegetation [2, 7–10]. Nevertheless, the emphasis in most of these studies has been on delineating spatial distribution rather than exploring ongoing temporal fluctuations over a yearly timescale. As such, there is a need to shift focus towards examining the temporal dynamics of vegetation to better understand the evolving conditions in mangrove forests, specifically in Can Gio over time.

Therefore, this study objective is to assess Can Gio vegetation index's variation across a continuous time series spanning from 2015 to 2023. This analysis infers significance as it employs statistical linear regression method to highlight areas demonstrating noteworthy annual fluctuations, illustrating either substantial increase or decrease in NDVI values at yearly timescale.

2. Materials and Methods

2.1. Study area

Located in the southeastern region of Ho Chi Minh City, Can Gio spans an estimated area of approximately 70,000 hectares, predominantly comprising an expansive mangrove

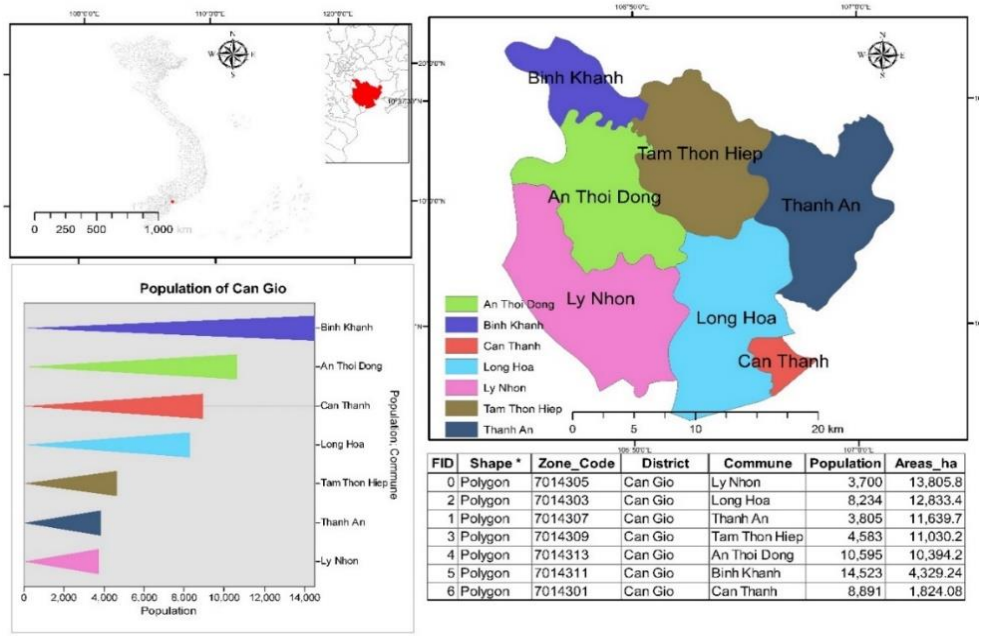

FID	Shape *	Zone_Code	District	Commune	Population	Areas_ha
0	Polygon	7014305	Can Gio	Ly Nhon	3,700	13,805.8
2	Polygon	7014303	Can Gio	Long Hoa	8,234	12,833.4
1	Polygon	7014307	Can Gio	Thanh An	3,805	11,639.7
3	Polygon	7014309	Can Gio	Tam Thon Hiep	4,583	11,030.2
4	Polygon	7014313	Can Gio	An Thoi Dong	10,595	10,394.2
5	Polygon	7014311	Can Gio	Binh Khanh	14,523	4,329.24
6	Polygon	7014301	Can Gio	Can Thanh	8,891	1,824.08

Figure 1. Study area of Can Gio.

forest that is integral to Ho Chi Minh City. This district is intersected by four major rivers Soai Rap, Dong Tranh, Nga Bay (Long Tau), and Thi Vai which course through the Can Gio mangroves before reaching the East Sea. The water bodies cover roughly 22,000 hectares of Can Gio, amounting to approximately 20 percent of its total area [6].

Can Gio encompasses one township, Can Thanh, and is further divided into six communes: Binh Khanh, An Thoi Dong, Ly Nhon, Tam Thon Hiep, Long Hoa, and Thanh An. Notably, Binh Khanh and An Thoi Dong are the two most populous communes, each with populations exceeding 10,000 inhabitants. Can Thanh and Long Hoa have populations exceeding 8,000, while Ly Nhon, Thanh An, and Tam Thon Hiep have the lowest populations, ranging from 3,700 to 4,500 residents (Figure 1).

2.2. Methods

The Copernicus program is a large Earth Observation by the European Union, and it encompasses various satellites, instruments, data services, and applications. The number of satellites in the program may change over time as new satellites are launched and integrated into the system. Some satellites of this program are Sentinel-1A and Sentinel -1B, Sentinel-2A and Sentinel-2B, Sentinel-3A and Sentinel-3B, and many others. In this study, Sentinel-2A and Sentinel-2B were applied to calculate NDVI. Sentinel-2 satellites includes two identical satellites which were respectively launched in 2015 and 2017 at a mean altitude of 786 km. These two satellites operate and provide high-resolution optical imagery for Earth observation and environmental monitoring, including the monitoring of vegetation, soil and water cover, as well as observation of inland waterways and coastal areas [8]. Sentinel-2 offers extensive coverage of vegetation across coastal areas, boasting a superior spatial resolution of 10 meters and frequent revisits every five days. Notably, this satellite service is cost-free, making it a valuable data resource for studying the spatial and temporal dynamics of mangrove forests. Its benefits are particularly significant in developing nations with constrained budgets for such research endeavors [11].

Google Earth Engine is a cloud-based platform designed for global-scale data analysis. It combines a variety of satellite imagery and other geospatial datasets with analysis capabilities by Google's computational infrastructure. In Google Earth Engine, there are multiple datasets of Sentinel-2 such as Sentinel-2 MSI, harmonized Sentinel – 2 MSI. In this study, Sentinel-2 Multi-Spectral Instrument, Level-1C was employed. Each Sentinel-2 product in .zip archive may contain multiple granules. Each granule becomes a separate Earth Engine asset. Earth Engine asset IDs for Sentinel-2 have the following format: COPERNICUS/S2/20230211T030849_20230211T031915_T48PYS. Here the first numeric part represents the sensing date and time which was February 11th, 2023, the second numeric part represents the product generation date and time which was from 03:08:49 to 03:19:15 of the same day, and the final 6-character string is a unique granule identifier indicating its UTM grid reference of Can Gio at T48PYS.

In this study, clouds degree was removed by using Earth Engine code which is ".filterMetadata ("CLOUDY_PIXEL_PERCENTAGE", "less_than", 10)". FilterMetadata is a method used in GEE to filter a collection based on metadata properties. The term "CLOUDY_PIXEL_PERCENTAGE" is the metadata property being used for filtering. It refers to the percentage of cloudy pixels in satellite imagery. The term "less_than" is a comparison operator specifying the filtering condition and 10 is the threshold value of the cloudy pixel percentage.

NDVI stands for Normalized Difference Vegetation Index, it is a fraction of the differences between the reflectance in the near-infrared -NIR and the reflectance in the visible red - RED of the electromagnetic spectrum. NDVI is calculated as in the following formula (1):

$$\mathrm{NDVI} = \frac{(\mathrm{NIR}-\mathrm{RED})}{(\mathrm{NIR}+\mathrm{RED})} \quad (1)$$

NDVI ranges from -1 to +1, in which NDVI values near -1 typically represent water bodies. NDVI values are near 0 representing barren areas, rocks, or built-up urban areas. NDVI values between 0 to 1 indicate varying levels of vegetation density, with higher values suggesting healthier and more dense vegetation [7,12]. NDVIs of Can Gio from 2015 to 2023 were calculated directly on GEE from Sentinel-2 MSI.

The accuracy of NDVI representing land-use types is normally evaluated by Cohen's Kappa which is a statistical measure that assessed the level of agreement between the interpreted raster and observed raster. In this study, the interpreted raster is the NDVI in 2021 and observed raster is the updated observation in Google Earth.

To calculate the observed agreement and the expected agreement, a confusion matrix was produced with columns and rows. Each row and column respectively represent the classification for raster interpretation. The rows are the classification algorithm, while the columns represent the validation [13, 14].

Then, Kappa efficiency is computed in the formula (2):

$$\kappa = \frac{Po - Pe}{1 - Pe} \quad (2)$$

where P_o is the observed agreement between rasters, Pe is the expected agreement, which represents the probability of agreement occurring by chance. κ values of 1 indicates perfect agreement; the closer κ values are to 1, the higher consistency between the data [15].

The research method is summarized in the following flow diagram:

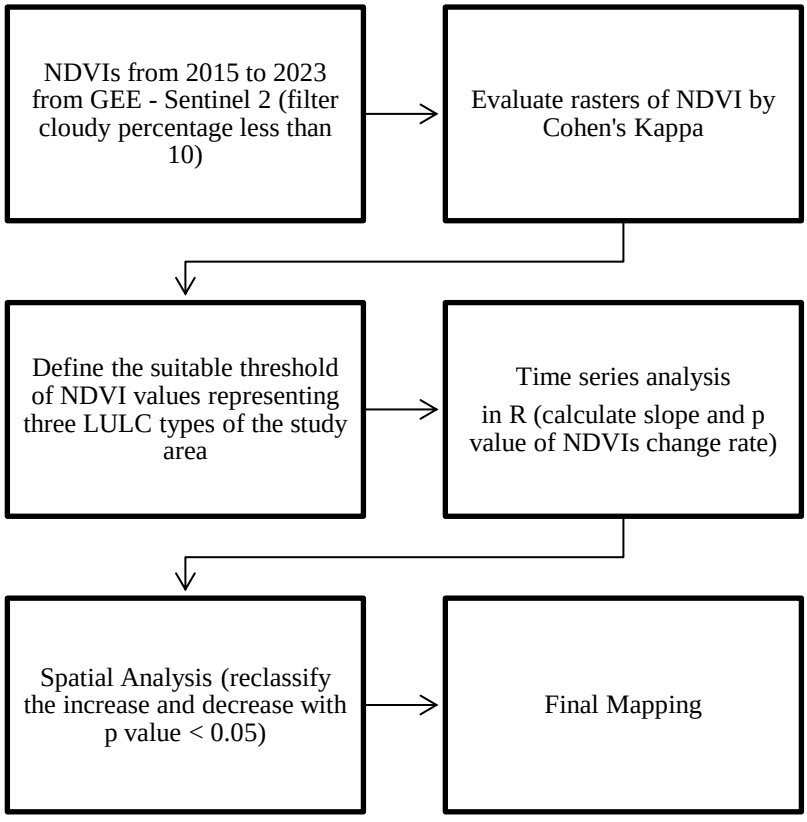

Figure 2. Flow diagram of methodology.

NDVI data spanning from 2015 to 2023 were gathered using GGE's cloud storage tool, specifically filtering the Sentinel-2 dataset to include only data with a cloud cover rate below 10%. This selection predominantly represents NDVI values observed during the dry season. Subsequently, the project adopted an NDVI value index exceeding 0.377 to delineate mangrove forests. It is crucial to assess the accuracy of this interpretation utilizing the Kappa coefficient.

In conducting statistical analysis on the temporal changes in NDVI values for every pixel annually, each pixel comprises 9 NDVI values across consecutive years from 2015 to 2023. The

'raster' package in the R statistical analysis software was employed to compute the slope values representing the upward or downward trends of NDVI for each pixel over the 9-year period, spanning from 2015 to 2023. Due to the extensive dataset, the computation process is time-consuming, given the approximately 7,000,000 pixels for each raster file in each year. Following the computation, a raster map delineating the slope values derived from the analysis model is generated. In addition, the statistical significance assessment - p - value of each slope value for every pixel is also extracted from the statistical model results.

Upon integrating both slope values and the associated p-values for each pixel, the generated map highlights pixels exhibiting significant trends in NDVI. Consequently, the final map delineates areas where NDVI values have consistently risen over 9 consecutive years and those where a consistent decline is simulated. This representation of the raising or reducing trends in NDVI holds paramount importance in identifying specific areas demonstrating sustained growth or decline in NDVI through time.

3. Results and discussion

3.1. NDVIs from 2015 to 2023

NDVIs for Can Gio were calculated as the difference between Band 8 and Band 4, representing the reflectance of near-infrared and visible red light in the electromagnetic spectrum, respectively. NDVI values typically range from -0.4 to +0.8 and vary annually, as in Figure 3a.

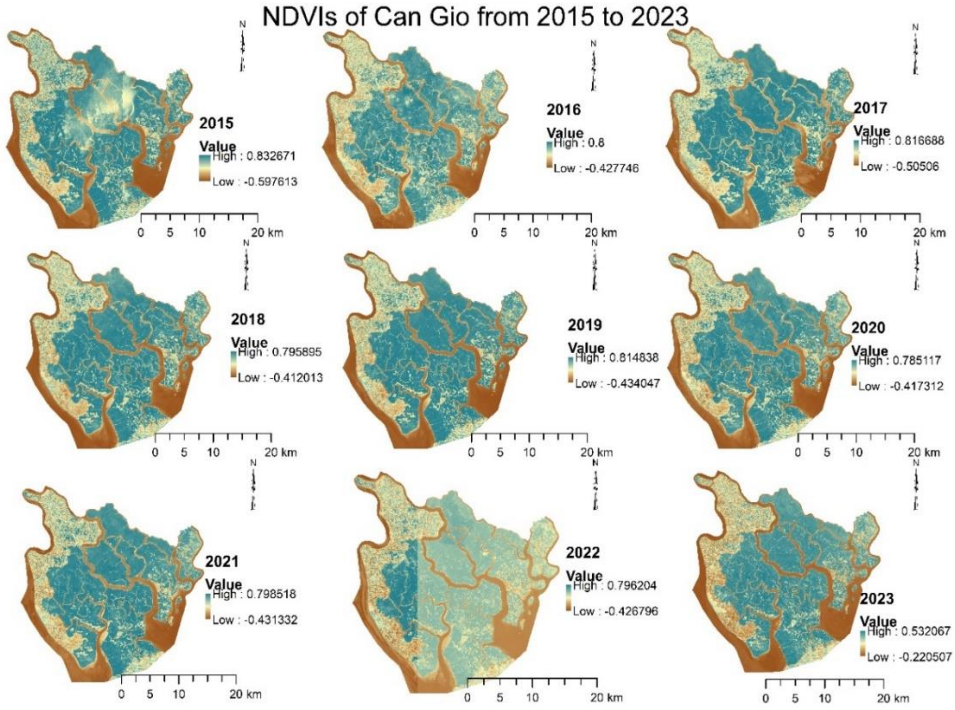

Figure 3a. Annual NDVIs for Can Gio from 2015 to 2023.

The maximum NDVI values for 2015, 2016, 2017, and 2019 exceeded 0.8, whereas those for 2018, 2020, 2021, and 2023 were below 0.8. Specifically, the maximum NDVI in 2023 was recorded at 0.53. These variations highlight the significant impact of annual maximum NDVI values on the overall NDVI average. Regarding the minimum NDVI values, 2015 and 2017, both fell below -0.5, while for 2016, 2018, 2019, 2020, 2021, and 2022, the values were above -0.4. Notably, in 2023, the minimum NDVI reached its highest value of -0.22.

The line graph in Figure 3b illustrates the average yearly NDVI values spanning from 2015 to 2023. It is evident that NDVIs values from 2015 to 2020 are marginally higher than those recorded between 2021 and 2023.

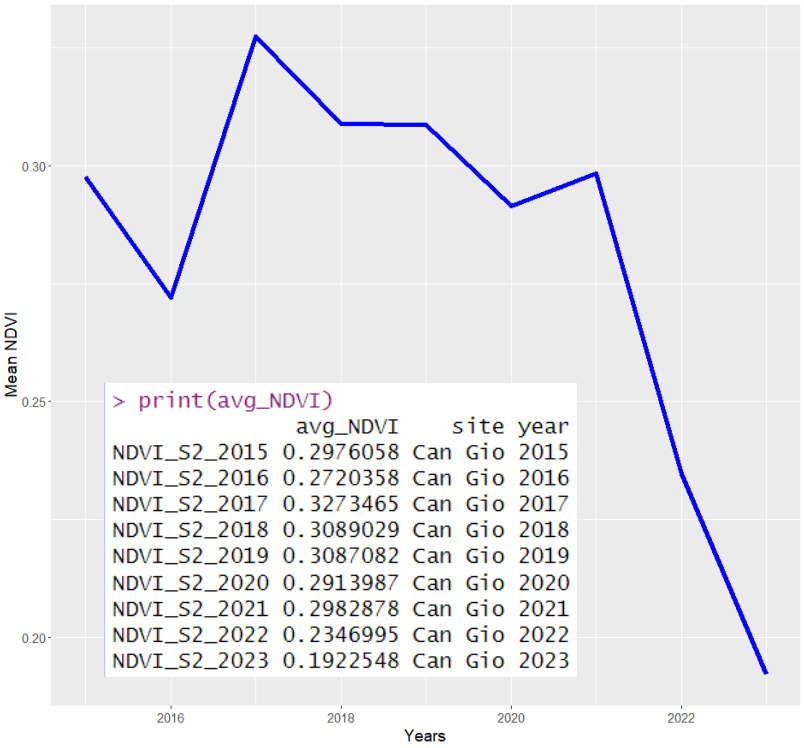

Figure 3b. Average NDVIs for Can Gio from 2015 to 2023.

Typically, NDVIs fluctuated between 0.298 and 0.291 over the 6-year period, while the values of NDVIs considerably diminished from 0.298 in 2021 to 0.192 in 2023. Specifically, the NVDI for 2023 falls within the lowest range. This could be attributed to the fact that the NDVIs for 2023 were collected during the dry season, while the NDVIs for other years reflected values for the entire of year. Similarly, the annual average NDVIs for Can Gio from 2015 to 2023 illustrated a reduction over this period.

3.2. Defining the suitable threshold of NDVI values representing three LULC types

NDVI, widely utilized in studies assessing plant growth, plays a crucial role in vegetation cover classification through various value thresholds. Recently, there have been many studies applying satellite data to identify the vegetation cover. These study have proposed various methods to determine NDVI threshold values to interpret the land-use types for Can Gio. In the estimation conducted by Sugara et al., distinct NDVI thresholds were established for mangroves across three ranges: 0.11 to 0.35 indicating very low vegetation coverage, 0.35 to 0.5 representing medium coverage, and 0.5 to 0.67 signifying high levels of coverage [7].

Among other studies, the NDVI values in the Can Gio mangrove forest area have been classified on a scale ranging from -1 to +0.1999, where values below zero to +0.1999 indicate non-vegetative cover, from +0.2 to +0.2999 signify low vegetation coverage, from +0.3 to +0.3999 represent moderate coverage, and values above +0.4 denote high coverage [11], [16]. Additionally, the author concludes in this study that NDVI values exceeding 0.3 indicate error categorizing areas, partly within the buffer zone [11]. In a separate study, a composite of NDVI and other metrics was employed to assess alterations in mangrove forests. The study categorized NDVI values accordingly: values below 0 indicated bare land, while those between 0 and 0.2 represented low land cover. Ranges of 0.2 to 0.3 indicated shrub and grassland, and higher values, specifically between 0.4 and 0.9, signified dense vegetation coverage [17].

A recent study utilized GEE data from Landsat satellite images to combine the NDVI index with other vegetation assessment indices every five years between 1990 and 2022, aiming to determine vegetation cover. In this study, NDVI threshold adopted the results which were defined in [9] and indicated that majority of vegetation pixels had an NDVI greater than 0.377.

Additionally, other studies indicated that water areas typically exhibit an NDVI less than 0 [4, 9].

To sum up, previous studies focusing on mangrove vegetation and the NDVI index have frequently proposed thresholds around 0.4 to delineate high mangrove forest coverage. Hence, in this particular study, the classification of NDVI values aligns with those determined in prior research, serving as a basis for assessment. Therefore, NDVI values were categorized into three groups: the first group represents water areas with NDVIs less than 0; the second group corresponds to built areas with NDVIs ranging from 0 to 0.377; the third group encompasses mangrove forest areas with NDVIs greater than 0.377.

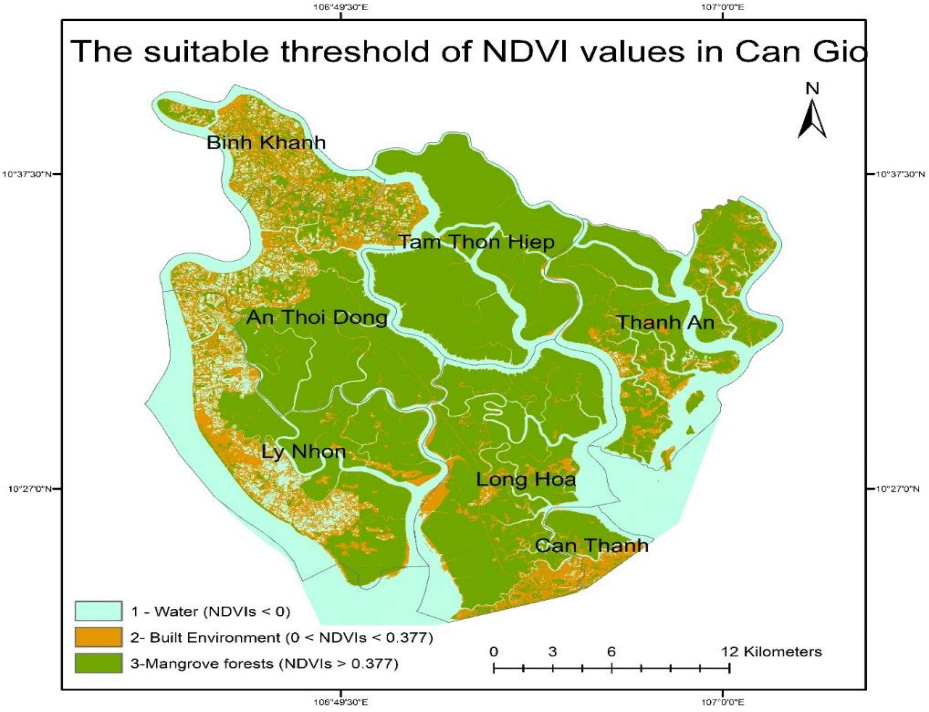

Figure 4. The suitable threshold of NDVI values in Can Gio.

Accordingly, regions with extensive mangrove forest cover predominantly span across Tam Thon Hiep, Thanh An, Long Hoa, and An Thoi Dong communes. Conversely, areas like Binh Khanh, Ly Nhon, and Can Thanh primarily consist of man-made environment. The distributed water surface area corresponds to the primary waterways in the Can Gio area, including Soai Rap, Dong Tranh, Nga Bay (Long Tau), and Thi Vai.

Certain studies utilizing the NDVI index to assess vegetation dynamics in Can Gio have selected random points for accuracy assessment between the simulated land cover results with observed land cover. These studies have proposed varying observation points, ranging from less than 100 points [18] to 300 points [11, 19] or 500 points [9] and over 1,000 [20] sampling points. Some research has computed the number of random points based on a statistically more reliable equation [9].

To evaluate the accuracy for the classification algorithm, 300 random points as in Figure 4 were generated using the segmentation and classification tool in GIS. Subsequently, the point shapefile was converted to a .KML file for potential viewing on Google Earth. Following this, the table of point shapefile was manually edited and compared to the Google Earth Imagery from 2021.

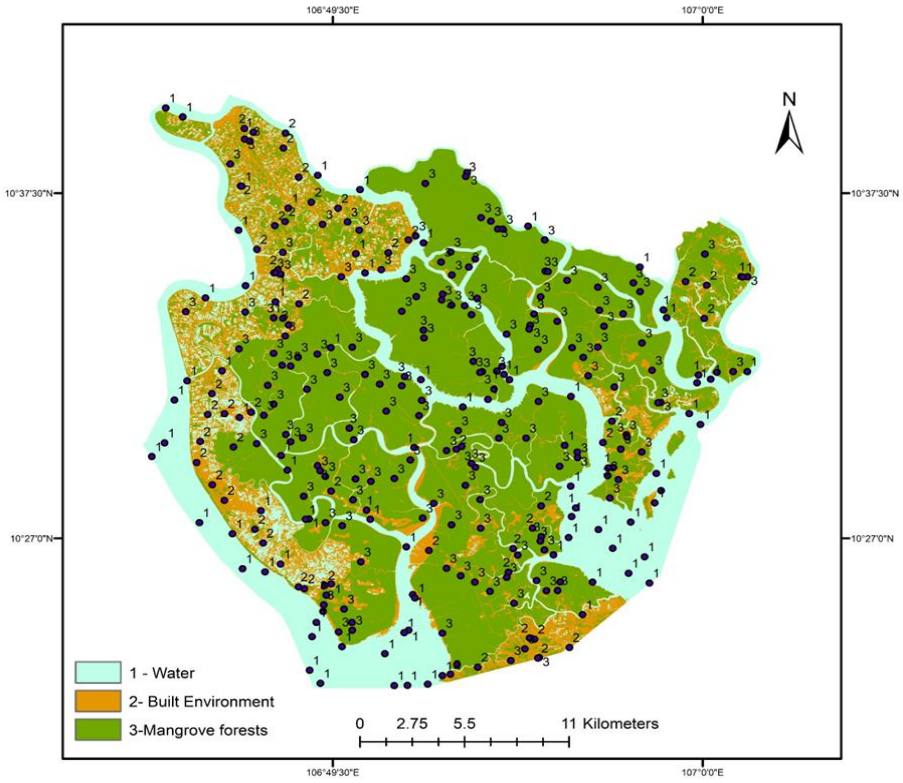

Figure 5. 300 random points for accuracy assessment.

Table 1 shows the confusion matrix result, comparing the results of NDVI classification to Google Earth imagery in 2021 for assessing the accuracy of the proposed classification. The User's Accuracy (U_Accuracy) reveals that 85% of water, 83% of built areas, and 88% of mangrove forest were correctly classified. Notably, the Producer's Accuracy (P_Accuracy) for built areas was 57%, significantly lower than that for water areas and mangrove forests, indicating a lower level of correctness in classifying pixels for the built areas. Despite this, the Kappa coefficient was 0.78, suggesting substantial agreement beyond chance.

Table 1. Confusion matrix for NDVI in 2021.

OID	ClassValue	1 – Water	2 – Built Areas	3 – Mangrove Forests	Total	U_Accuracy	Kappa
0	1 – Water	76.00	13.00	0.00	89.00	0.85	0.00
1	2 – Built Environment	3.00	39.00	5.00	47.00	0.83	0.00
2	3 – Mangrove Forests	2.00	17.00	145.00	164.00	0.88	0.00
3	Total	81.00	69.00	150.00	300	0.00	0.00
4	P_Accuracy	0.94	0.57	0.97	0.00	0.87	0.00
5	Kappa	0.00	0.00	0.00	0.00	0.00	0.78

3.3. Slope and p-value of NDVIs changing rate from 2015 to 2023

NDVIs from 2015 to 2023 were analyzed through a time series to monitor changes in vegetation over time. Raster data spanning from 2015 to 2023 were stacked into a time series dataset. The slope of the linear regression of NDVI against yearly time was calculated for each pixel, providing valuable insights into the temporal trends. Distribution of slope values and p-values is illustrated in Figure 6. The frequency distribution of slope values less than 0 dominants over that of slope values greater than 0. Distribution of p-values is also depicted, ranging from 0 to 1, where p-values below 0.05 indicate the statistically significant meaning.

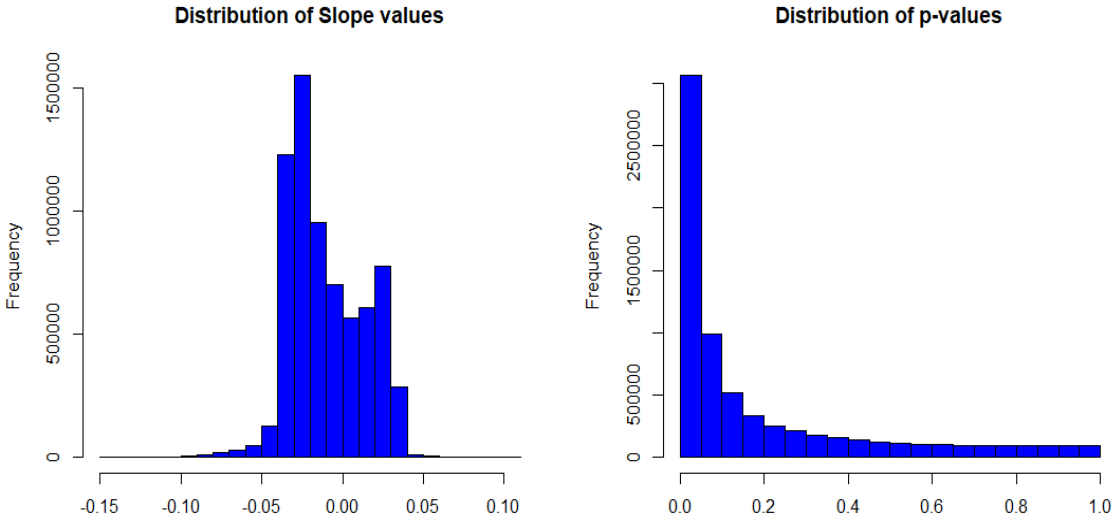

Figure 6. Distribution of slope values and p-values.

However, the p-values of the linear regression for each pixel (Figure 7) were not statistically significant ($p > 0.05$) across a large area, including Binh Khanh, Tam Thon Hiep, An Thoi Dong, and Ly Nhon. In these regions, the observed changed in NDVI over time were not found to be statistically different from zero.

Conversely, statistically significant p - values ($p < 0.05$) were observed at the upper portion of Tam Thon Hiep, Thanh An, Long Hoa, and in most water areas. In these locations, the linear regression analysis provided evidence of a significant trend in NDVI over the study period.

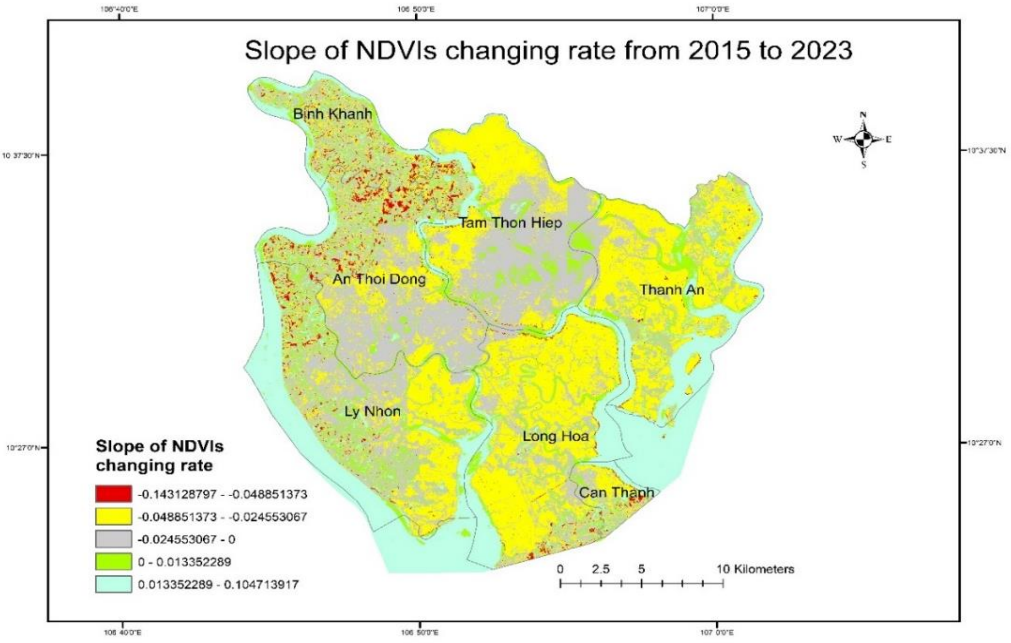

Figure 7a. Slope values of NDVIs changing rate from 2015 to 2023.

The slope raster in Figure 7 was classified into five groups based on specific criteria. Negative slope values indicate a decrease in NDVI, while positive slope values represent an increase. As a result, highly decreases were observed in Binh Khanh, An Thoi Dong, and Can Thanh. Moderately decreases were notable in the buffer zones such as Long Hoa, Thanh An, and the upper of Tam Thon Hiep. On the other hand, the strongly increases were predominately observed in most of water areas and some in Ly Nhon and Tam Thon Hiep.

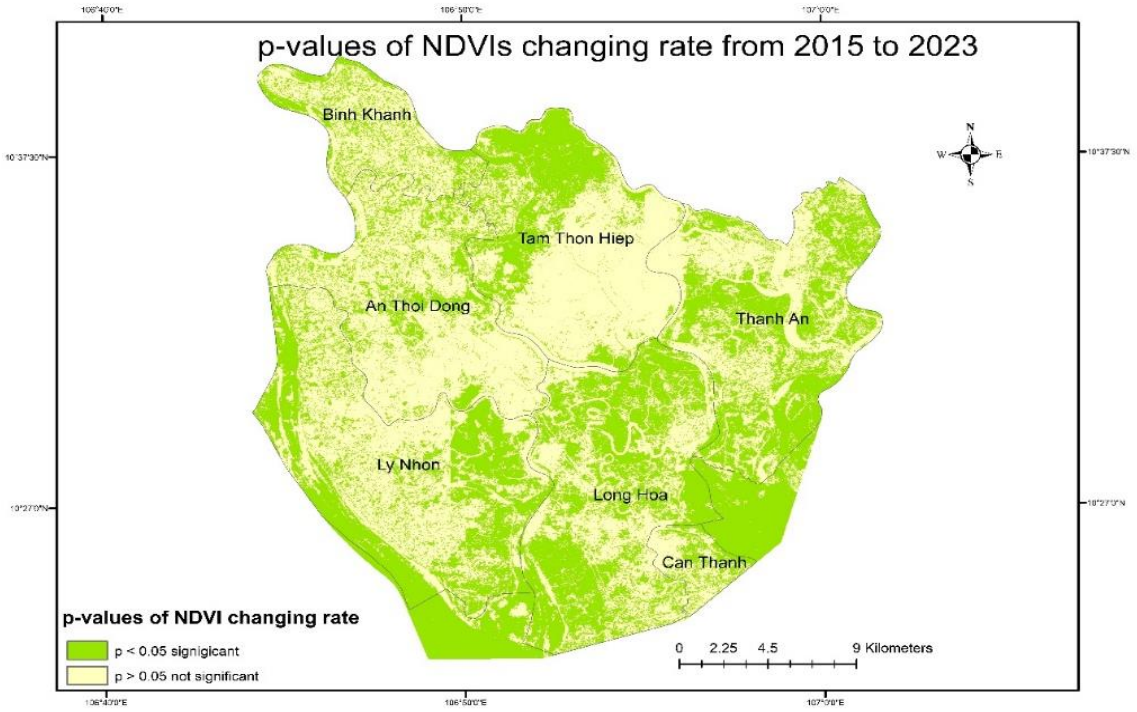

Figure 7b. p-values of NDVIs changing rate from 2015 to 2023.

As a consequence, the map of tendency of NDVI change from 2015 to 2023 was produced to visualize the areas statistically reduction or rise NDVI through time. According to figure 8, rapidly decreases take place at the transition areas between Binh Khanh - An Thoi Dong and An Thoi Dong - Ly Nhon. Other decreases are in Can Thanh. On the contrary, most of increase are observed in water areas. Some points of rapidly increases are in the core zone of mangrove forests.

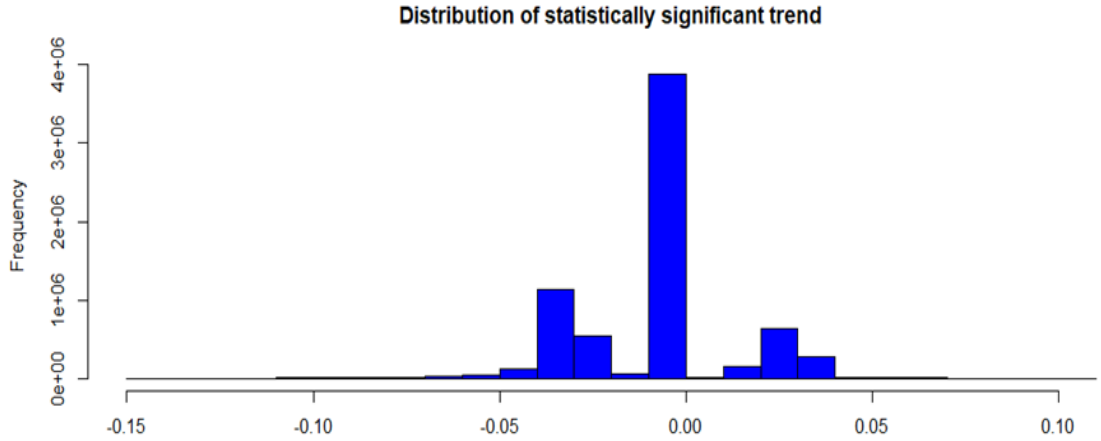

Figure 8a. Trending of NDVI change from 2015 to 2023.

Analyzing the spatial distribution results reveals specific points indicating a significant changes in NDVI, as determined by the linear regression model. The site exhibiting deposition tendencies from water flow demonstrates a statistically significant rise in NDVI. For instance, position 2 in Long Hoa and position 1 in Tam Thon Hiep showcase an increasing trend in NDVI. In other words, these sites have been continuously growth in mangrove forests over the past 9 years. Conversely, sites 3 and 4 experiencing NDVI declines denote consistent impacts over the same period, influencing the observed reduction in NDVI.

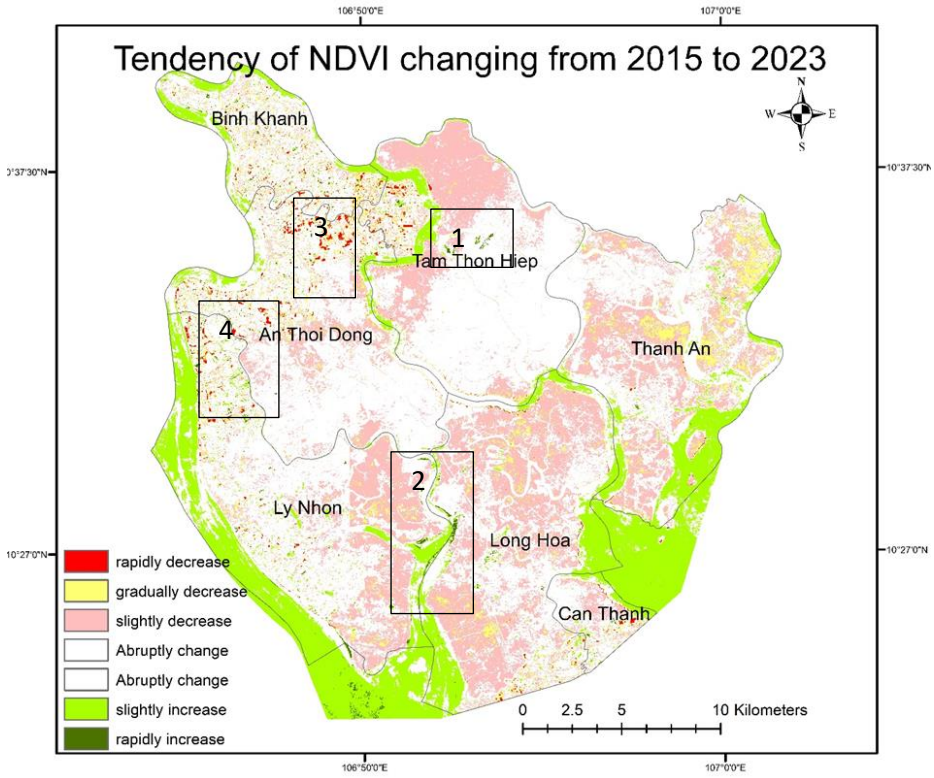

Figure 8b. Map of trending for NDVI change from 2015 to 2023.

3.4. Temporal analysis from 2015 to 2023

Table 2 indicates selected NDVI values which were extracted from random pixels, comparing to the associated p-values, slopes, and trends in NDVI changes. In brief, the trends observed are as follows: (1) NDVI exhibits either an increase or decrease without statistically reliable indications; (2) NDVI showcases either an increase or decrease with statistical reliability. However, in the linear regression analysis model, it demonstrates a consistent yearly increase or decrease in NDVIs. This suggests that pixels affected by sudden impacts resulting in abrupt NDVI changes will be omitted from the outcomes.

Table 2. Temporal analysis for NDVI from 2015 to 2023 at random sample point.

		NDVI from 2015 to 2023											
	Pixel	**2015**	**2016**	**2017**	**2018**	**2019**	**2020**	**2021**	**2022**	**2023**	**P-values**	**Slope values**	**Tendency**
1	1,000,000	0.55	0.24	0.39	0.32	0.22	0.2	0.35	0.23	0.1	0.03	-0.033	-0.03
2	1,500,000	0.14	0.12	0.25	0.44	0.36	0.43	0.43	0.49	0.29	0.04	0.034	0.03
3	1,755,000	-0.33	-0.23	-0.25	-0.19	-0.23	-0.21	-0.27	-0.16	-0.08	0.02	0.019	0.02
4	2,500,000	0.4	0.25	0.35	0.31	0.3	0.31	0.33	0.29	0.15	0.08	-0.015	0
5	2,755,000	0.49	0.58	0.66	0.63	0.69	0.62	0.68	0.48	0.38	0.43	-0.012	0
6	3,500,000	0.54	0.71	0.73	0.71	0.71	0.63	0.69	0.48	0.43	0.15	-0.022	0
7	3,555,000	0.26	0.58	0.68	0.58	0.64	0.55	0.63	0.43	0.38	0.95	-0.001	0
8	4,500,000	0.71	0.61	0.7	0.63	0.66	0.61	0.6	0.39	0.38	0.01	-0.037	-0.04
9	4,555,000	0.64	0.57	0.56	0.55	0.57	0.53	0.56	0.33	0.29	0.01	-0.035	-0.04
10	5,000,000	0.73	0.49	0.7	0.71	0.68	0.57	0.61	0.37	0.36	0.04	-0.037	-0.04

The graph in Figure 9 displays randomly selected NDVI values from specific pixels. Referring to the data table, these values are drawn from pixels positioned between the 1,500,000th and 4,500,000th. The graph represents the NDVI values across the years based on this selection. Utilizing linear regression analysis, three distinguished trends in the data emerge: gradually increase with a high R^2 correlation coefficient, low correlation with a low R^2, and moderate correlation with an R^2 in the middle of range.

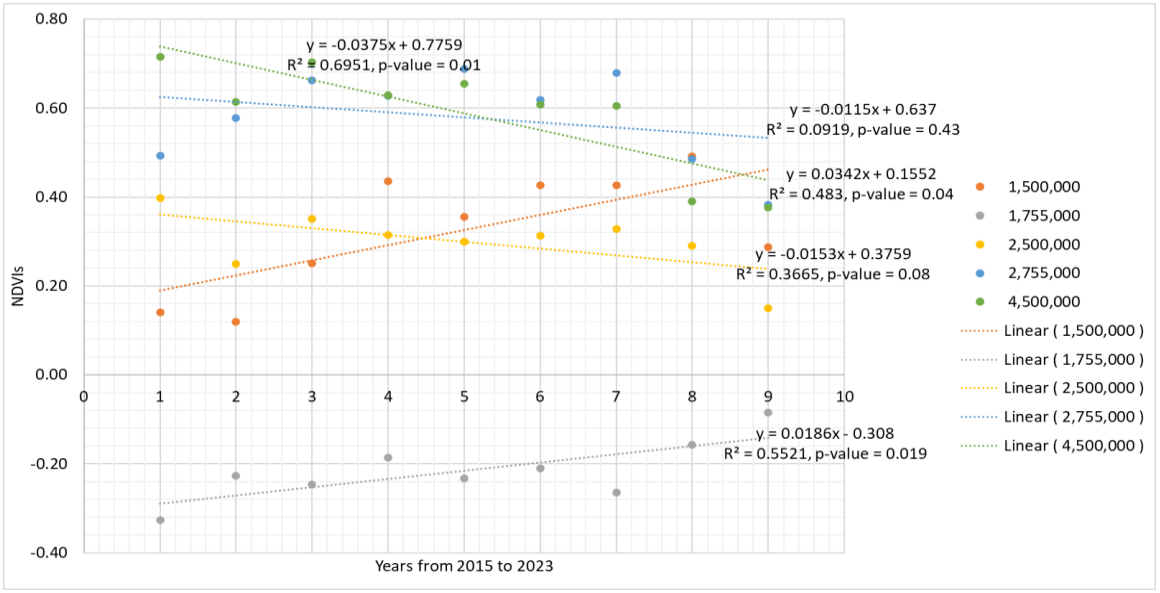

Figure 9. The linear regression for NDVI values at pixels.

Notably, the 4,500,000th pixel exhibits a significantly high R^2 value of 0.6951, while the 1,500,000th pixel shows a high increase over time with a medium R^2 of 0.483 and a p-value marginally reaching 0.04. At the 2,500,000th and 2,755,000th pixel, there's a consistent gradual reduction with a relatively R^2 of about 0.3665 and 0.0919, respectively. Similarly, p-values are insignificant in these two pixels. Thus, the more the R^2 value increases, the more the p-value tends to decrease below 0.05. However, the 1,755,000th pixel indicates that the R^2 slightly increase to 0.5521, while the p-value dramatically reduced to 0.019.

4. Conclusion

The results indicated that the decrease in average NDVIs from 2015 to 2023 was rationally deducible either from the downsizing of mangrove forest areas or the degradation of the mangrove forest. However, the annual NDVI statistic revealed there were areas with an acceleration of NDVI in comparison with the destruction of NDVI areas from 2015 to 2023. The significant declines occur rapidly at the transition zones between Binh Khanh and An Thoi Dong, as well as between An Thoi Dong and Ly Nhon. Additional declines are evident in Can Thanh. Conversely, the majority of increases are noted in aquatic regions. Certain locations exhibit rapid increases, particularly within the central core of mangrove forests.

This study presents a temporal statistical approach aimed at assessing NDVI changes within a defined timeframe. The main objective is not to quantify the direct expansion or reduction of mangrove forest areas. Instead, it seeks to indirectly evaluate mangrove forest quality through NDVI values in time series. Linear regression effectively models continuous processes like deposition or erosion. However, to evaluate other factors such as discrete human-made or sporadic impacts, alternative statistical models should be considered.

Notably, the unexpected increase in NDVI within water areas prompts further analysis, potentially associated with diverse processes like coastal erosion or deposition, environmental processes such as eutrophication and other influential factors that could impact these outcomes.

Author contribution statement: Conceived and designed the experiments; Analyzed and interpreted the data; contributed reagents, materials, analysis tools or data; manuscript editing: A.B.K.V.; Performed the experiments; contributed reagents, materials, analyzed and interpreted the data, wrote the draft manuscript: A.B.K.V.

Acknowledgements: The research utilized the available resources of Google Earth Engine (GEE), Sentinel-2 imagery, Geographic Information System (GIS), Google Earth, and the R programming packages, Ho Chi Minh City University of Natural Resources and Environment.

Competing interest statement: The authors declare no conflict of interest.

References

1. Shigeyuki, B. Studies in Can Gio mangrove biosphere reserve, Ho Chi Minh City, Viet nam. International Society for Mangrove Ecosystems (ISME), **2014**, 6, ISSN 0919-2646.
2. Vinh, T.V.; Marchand, C.; Linh, T.V.K.; Jacotot, A.; Nho, N.T.; Allenbach, M. Soil and aboveground carbon stocks in a planted tropical mangrove forest (Can Gio, Vietnam. Chapter 12 in Wetland Carbon and Environmental Management, Wiley. **2021**, pp. 229–245. doi: 10.1002/9781119639305.ch12.
3. Torell, M.; Salamanca, A.M. Wetlands Management in Vietnam's Mekong Delta: An Overview of the Pressures and Responses. Environmental Science, Geography, **2003**, pp. 1–19.
4. Vien, N.N.; Le, T.Q. Erosion and Accretion in Can Gio Mangroves. in Studius in Can Gio Mangrove Biosphere Reserve, HCMC, Viet Nam. *Int. Soc. Mangrove Ecosyst.* **2014**, *V6*, 31–36.
5. Hoan, H.D.; Kiet, B.N.T.; Binh, C.H.; Quy, P.V. Monitoring Riverbank Erosion in Can Gio mangroves. In Studius in Can Gio Mangrove Biosphere Reserve, HCMC, Viet Nam, **2014**, *V6*, 37–43.
6. Vien, N.N.; Le, S.V.; Miyagi, T.; Baba, S.; Chan, H.T. An Overview of Can Gio District and Mangrove Biosphere Reserve. **2014**. *ISSN 0919-2646 V6*.
7. Sugara, et al. Utilization of Sentinel-2 Imagery in Mapping the Distribution and Estimation of Mangroves' Carbon Stocks in Bengkulu City. *Geosfera Indonesia* **2022**, *7(3)*, 219. Doi:10.19184/geosi.v7i3.30294.
8. Hirata, Y.; Tabuchi, R.; Patanaponpaiboon, P.; Poungparn, S.; Yoneda, R.; Fujioka, Y. Estimation of aboveground biomass in mangrove forests using high-resolution satellite data. *J. For. Res.* **2014,** *19(1)*, 34–41. Doi:10.1007/s10310-013-0402-5.
9. Vu, T.T.P.; Pham, T.D.; Saintilan, N.; Skidmore, A.; Luu, H.V.; Vu, Q.H.; Le, N.N.; Nguyen, H.Q.; Matsushita, B. Mapping Multi-Decadal Mangrove Extent in the Northern Coast of Vietnam Using Landsat Time-Series Data on Google Earth Engine Platform. *Remote Sens.* **2022**, *14*, 4664. https://doi.org/10.3390/rs14184664.
10. Meneses-Tovar, C. NDVI as indicator of degradation. *Unasylva 238*, **2011**, *62(2)*, 39–46.
11. Le, H.T.; Tran, T.V.; Gyeltshen, S.; Nguyen, C.P.T.; Tran, D.X.; Luu, T.H.; Duong, M.B. Characterizing Spatiotemporal Patterns of Mangrove Forests in Can Gio Biosphere Reserve Using Sentinel-2 Imagery. *Appl. Sci.* **2020**, *10*, 4058. https://doi.org/10.3390/app10124058.
12. Schmid, J.N. Using Google Earth Engine for Landsat NDVI time series analysis to indicate the present status of forest stands. Thesis for: Bachelor of Science, 2017, pp. 33. doi: 10.13140/RG.2.2.34134.14402/6.
13. Townsend, J.T. Theoretical analysis of an alphabetic confusion matrix*. *Percept Psychophys* **1971**, *9*, 40–50.
14. Kuhnert, M.; Voinox, A.; Sppelt, R. Comparing raster map comparison algorithms for spatial modelling and analysis. *Photogramm Eng. Remote Sens*. **2005**, *71(8)*, 975–984.
15. Mchugh, M.L. Interrater reliability: the kappa statistic.
16. Ehsan, S.; Kazem, D. Analysis of land use-land covers changes using normalized

difference vegetation index (NDVI) differencing and classification methods. *Afr. J. Agric. Res.* **2013**, *8(37),* 4614–4622. Doi:10.5897/ajar11.1825.

17. Nguyen, T.P.C.; Le, T.H.; Nguyen, T.O.; Le, C.L.; Ha, T.C. Vegetation Indices for Spatio-Temporal Analysis of the Quality of Can Gio Mangrove for Biodiversity and Conservation. Proceeding of the IOP Conference Series: Earth and Environmental Science, Institute of Physics. **2023**, *1247(1)*, 012003. Doi: 10.1088/1755-1315/1247/1/012003.
18. Lap, Q.K.; Luong, V.N.; Hong, X.T.; Tu, T.T.; Thanh, K.T.P. Evaluation of mangrove rehabilitation after being destroyed by chemical warfare using remote sensing technology: A case study in can gio mangrove forest in mekong delta, southern Vietnam. *Appl. Ecol. Environ. Res*. **2021**, *19(5)*, 3897–3930. Doi: 10.15666/aeer/1905_38973930.
19. Nguyen, H.H.; Quang, P.D.; Nguyen, V.D.; Linh, D.V.K.; Manh, N.K. Management of forest resources and environment estimation of mangrrove carbon stocks using Sentinel 2a and field-based data in Tien Lang district, Hai Phong city. *Manage. Forest Resour. Environ.* **2020**, *10*, 48–58.
20. Nguyen, S.T.; Bui, T.X.; Chau, D.T. Monitoring mangrove forest changes from multi-temporal Landsat Data in Can Gio Biosphere Reserve, Viet Nam. *Wetlands* **2016**, *212*, 635–640. Doi: 10.1007/s13157-016-0767-2.

JOURNAL OF
HYDRO-METEOROLOGY

Research Article

Determine greenhouse gas emissions from landfills and suggest a household solid waste classification system in Dong Hoi, Quang Binh province

Doan Ha Phong[1]*, Nguyen Hue[2], Vu Van Doanh[3], Nguyen Quang Hieu[4]

[1] Vietnam Institute of Meteorology, Hydrology Science and Climate Change; Doanhaphong@gmail.com
[2] Department of Natural Resources and Environment of Quang Binh; nghue66@gmail.com
[3] Hanoi University of Natural Resources and Environment, vvdoanh@hunre.edu.vn
[4] Quang Binh Environment & Urban Development Joint Stock Company; qhieu1302@gmail.com

*Corresponding author: doanhaphong@gmail.com; Tel.: +84–913212325

Received: 17 October 2023; Accepted: 5 December 2023; Published: 25 March 2024

Abstract: The distribution network model is one of the sophisticated strategies being used in research to assess the state of household solid waste (HSW) management and calculate the quantity of greenhouse gas emissions from landfills in Nghia Ninh and Bao Ninh communes. Traditional and modern techniques are also being used in this study. The results have assessed the existing state of household solid waste (HSW) management for home sizes ranging from four to six people. The daily average for garbage per person is 0.31 kilogram. The corresponding CO_2 emissions from the two communes are 0.42 kg/person/day (Bao Ninh) and 0.47 kg/person/day (Nghia Ninh); study and survey data from these two districts show that the average cost for households to collect HSW is 27,000 VND/family/month. 2698.72 kg CO_2 equivalent per ton of garbage, the same amount of emissions from solid waste. Nghia Ninh and Bao Ninh communes, as well as the Dong Hoi city government in general, rely on it to limit the amount of waste that families emit into the environment while encouraging improved information exchange and sharing. Share responsibility for waste management and encourage waste separation at the source.

Keywords: HSW; GHG emission; MSW; Landfilling; Dong Hoi, Quang Binh.

1. Introduction

An estimated 60,000-70,000 tons of residential solid waste are produced daily in the nation as a whole, with 60% of that amount occurring in urban areas. The rest is burned to normal destruction, dumped into water sources, or buried in trash landfills [1]. Many case studies exist around the world; for example, in Putrajaya, Malaysia, community participation in solid waste segregation operations was achieved through a trash recycling program [2]. A significant link has been found between community engagement in recycling programs and attitudes toward solid waste classification (r = 0.343) and community knowledge about solid waste classification (r = 0.251), according to analytical results based on a survey of 382 persons. The study suggests ways to improve the community's capacity for recycling and classification in light of the analysis [2]. When researching the solid waste management system and the role of community engagement in Jigjiga town, Somali state, Ethiopia, it was discovered that social and environmental concerns still exist. The garbage collection system's solid waste management mechanism is ineffective... [3].

Similarly, the research “Community-based waste management: experiences of Asian countries” detailed this strategy in seven Asian countries. Difficulties in the model are caused by insufficient solid waste management policies, a lack of human resources, a lack of community awareness, and a lack of collaboration capability between the government and the community [4].

Dong Hoi City authorities at all levels have hastened the process of industrialization, modernization, and urbanization in recent years in an effort to increase the local economy and improve people's quality of life. The province encourages an approach that prioritizes environmental protection over economic benefits in communes such as Bao Ninh, Nghia Ninh, Thuan Duc, and Quang Phu, while also prioritizing investment in the service and tourism sectors and implementing solid waste management in daily life in accordance with Section 2, Article 75 to 80 of the Law on Environmental Protection 2020 [5]. Therefore, to properly conserve the environment, production processes must be considered and integrated with the surrounding ecosystem in addition to avoiding, managing, and treating waste between places with favorable development conditions. many advancements in the economy. Many groups, including Nghia Ninh, Duc Ninh, Loc Ninh, Thuan Duc, and Quang Phu, who reside in communes outside of Dong Hoi city, are adversely impacted by the urbanization process.

Landfilling is the most often used waste treatment method worldwide. Landfill cleaning technology has evolved greatly in recent years [6]. The majority of emerging Asian countries, including Vietnam, continue to process trash in open, uncovered landfills and engage in open dumping and burying without gas recovery. As a result, when sanitary landfill technology is employed, there may be no landfill gas collection system, which means that the majority of emissions are released untreated or uncontrolled into the atmosphere. Municipal solid waste (MSW) is anaerobically digested in open dumps and landfills to produce landfill gas (LFG), which is mostly carbon dioxide (CO_2) and around 60% methane (CH_4). LFG’s CO_2 component is of biological origin and is not a greenhouse gas, however LFG's CH_4 component contributes to global warming [7]. According to the IPCC, uncontrolled CH_4 emissions from landfills are the third-largest source of man-made CH_4 emissions. Numerous variables, including trash quantity and composition, moisture content, pH, and waste management practices, will affect the amount of methane generated in landfills. Methane concentrations in trash dumps rise as organic matter and moisture content rise [8].

The IPCC 2006 waste model may calculate emissions from a variety of solid waste disposal sites based on the default assumptions of a country or region’s specific waste composition, such as climate and landfill status. The IPCC Waste 2006 calculation model was used in this work to assess greenhouse gas emissions from typical waste treatment in landfills. Under the supervision of the IPCC, the first order (FOD) analytical model, which captures the rate of waste breakdown at the disposal site and delivers more accurate results than emissions estimates, has been suggested for usage [9].

Urbanization includes things like the loss of arable land, changes in the occupational structure, accessibility to urban life (which is mostly dependent on public services and consumer culture), gentrification and urban construction, and the emergence of several local environmental issues. Specifically, there is a lot of household solid waste, and because of the introduction of new materials, raw materials, and products, its qualities and composition have changed from before, making management challenging. The inability of local solid waste management to meet regulations results in significant environmental degradation on a small- to large-scale basis, negatively affecting the community's quality of life and health. Implementing the Research Team's “Determine the greenhouse gas emissions from landfills in the communes of Nghia Ninh and Bao Ninh, Dong Hoi city, Quang Binh province, and suggest a system for classifying household solid waste at the source” is crucial in light of the aforementioned concerns. essential and significant from a practical and scientific standpoint.

2. Materials and Methods

2.1. Description of the study area.

East of the city is the beach commune of Bao Ninh. Due to its advantageous location near the Nhat Le River and a lengthy shoreline, Dong Hoi (Quang Binh) is home to a large number of service restaurants that cater to tourists. One of the factors raising the possibility of environmental contamination is these commercial operations. The total area of Nghia Ninh commune is approximately 1,570 hectares, of which 145 hectares are used for agriculture, primarily for the production of rice.

A step toward increasing public awareness is the selection of two economically disparate communes in Dong Hoi City for the purpose of surveying and calculating greenhouse gas emissions for urban solid waste collection and treatment activities.

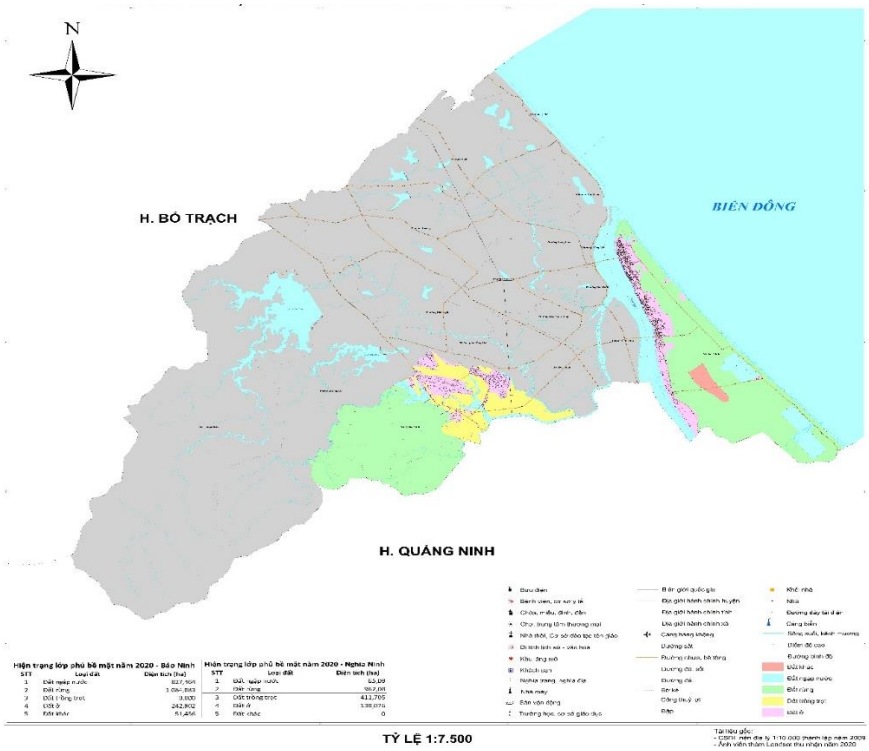

Figure 1. Map of the communes of Nghia Ninh and Bao Ninh.

2.2. Field survey method, determination of generation coefficient and waste composition

The study randomly selected 25 households living in two villages, Trung Nghia 5 and Trung Nghia 6, Nghia Ninh commune, and 25 households in My Canh and Ha Thon villages, Bao Ninh commune. Plastic bags to store waste for research households, and after 24 hours, return to use a scale to weigh the amount generated. Record the amount of waste and the demographics of each household.

Determine the emission coefficient:

$$\text{Emission coefficient} = \frac{Volume\ of\ household\ solid\ waste}{\text{Number of household members}} (\text{kg/person/day}) \quad (1)$$

Determine the composition of household solid waste:

Based on the instructions in Article 75, Law on Environmental Protection when distributing plastic bags for waste to people the study guided and distributed 3 bags marked: Solid waste capable of being reused and recycled; food waste; other HSW for households randomly selected from 4 villages in 2 communes, Nghia Ninh and Bao Ninh. Along with weighing to determine the emission coefficient, three types of weighing will be carried out to determine the composition by volume.

The CTR percentage component is calculated as follows:

$$\text{Ingredients \% by type} = \frac{Volume\ according\ to\ each\ type}{Total\ volume\ of\ solid\ waste\ of\ the\ sample} \times 100\% \quad (2)$$

Each commune chooses 25 families to deliver rubbish bags and weigh waste. These 25 homes were chosen at random depending on their living conditions in order to assess the association between income and the amount of solid trash created.

2.3. Sociological investigation methods

The study has developed 03 survey forms, of which: 01 survey form for local management officials, 01 form for households and 01 form for workers. Collection by self-management team. How to determine the sample: Based on Yamane's formula for calculating sample size [10].

$$\boldsymbol{n} = \frac{N}{1+N*e^2} \quad (3)$$

where n is the survey sample size; N is the total number of households in the study area; e: Acceptable error level (e ranges from 0.005 to 0.1; choose e = 0.1 to match the number of survey questionnaires and provide accurate results about the research object).

Due to limited time, human resources, and material resources, this study only conducted a survey with 100 random households in the two research communes. Along with that was a survey with 02 household solid waste collection workers and 02 local management officials. Details are as Table 1 below:

Table 1. Survey subjects in Nghia Ninh and Bao Ninh communes.

No.	Subject matter investigated	Quantity	Purpose
first	Officer in charge of environmental affairs in the area	02	Evaluate household waste management in the area. Collect information about waste collection equipment throughout the commune. Assess the impact of household waste on the locality. Assess people's awareness and level of compliance with the HSW classification.
2	Collection workers or self-management teams	02	Collect information about compliance awareness, waste collection situations, and difficulties. Collect information about equipment, tools, vehicles, and preventive measures.
3	Family	100 votes, including 46 votes in Bao Ninh commune and 54 votes in Nghia Ninh commune	Evaluate people's awareness when classifying household waste at source. People's assessment of household solid waste collection People's assessment of environmental fees and propaganda work Awareness about environmental protection.

Calculate the sample size using formula (3) with a marginal error of 0.1, or 10%, and the above sample size is sufficient.

2.4. SWOT method

This paper will identify the strengths, shortcomings, opportunities, and challenges in household solid waste management and source classification in two communes: Bao Ninh and Nghia Ninh. According to formula (3), survey samples in these places meet the criterion. Propose adequate solutions for identifying household solid trash at the source in the study region from there.

2.5. Data processing methods

The sociological investigation will utilize software like Word and Excel to synthesize, analyze, and present collected information and data scientifically.

2.6. SPSS data processing method

The study utilized SPSS software to assess the awareness, attitudes, and behavior of 100 households in Nghia Ninh and Bao Ninh communes regarding HSW management and classification.

2.7. Estimation of GHG emissions from landfilling

The following mathematical formula has been used in IPCC model to quantify GHG emissions from the landfilling:

$$DDOC_m = DDOC_{m(O)} \text{ x } e^{-kt} \quad (4)$$

where $DDOC_{m(0)}$ is the initial mass of decomposable degradable organic carbon (DDOC), when t=0 and e^{-kt}=1, k is the reaction constant and t is the time in years. $DDOC_m$ is the mass of DDOC at any time.

3. Results and discussion

3.1. Current status of HSW generation in Nghia Ninh and Bao Ninh communes

a) Sources of household solid waste generation

Sources of HSW generation in Nghia Ninh commune, through the commune's environmental status report, combined with actual investigation and survey, the main sources are identified as follows:

Table 2. Sources of household solid waste generation in Nghia Ninh commune.

Nghia Ninh commune			
No.	**Waste sources**	**Stationary sources**	**Solid waste composition**
first	Residential area	Households	Excess food; Goods packaging; Broken electronics and appliances; Leaves and tree branches are scattered.
2	Business and trading activities	People's markets and spontaneous markets	Plastic bags, foam, packaging; Excess food; Paper, plastic, glass, metal; Damaged fruits and vegetables;
3	Agencies, offices, schools	Primary and secondary schools in Nghia Ninh commune; Commune People's Committee; Commune medical station	Paper, plastic, glass, metal; Excess food; Broken items.
4	Traffic activities	Gathering areas and rest areas for container trucks	Goods packaging; Damaged goods; Broken items
5	Agricultural activities	Crop fields and cattle barns	Livestock waste; Damaged agricultural products; Packaging; Humus

The study reveals that waste generation in Bao Ninh commune is sourced from various sources, including residential areas and administrative agencies, in addition to similar waste sources in Nghia Ninh commune, including aquaculture and tourism business activities, as determined through data collection and analysis.

Table 3. Sources of household solid waste generation in Bao Ninh commune.

Bao Ninh commune			
No.	**Waste sources**	**Stationary sources**	**Solid waste composition**
first	Residential area	Households	Excess food; Goods packaging; Broken electronics and appliances; Leaves and tree branches are scattered.

Bao Ninh commune			
No.	**Waste sources**	**Stationary sources**	**Solid waste composition**
2	Business activities	People's market and shops	Plastic bags, foam, packaging; Excess food; Paper, plastic, glass, metal; Damaged fruits and vegetables;
3	Agencies, offices, schools	Primary and secondary schools in Bao Ninh; Commune People's Committee; Commune medical station	Paper, plastic, glass, metal; Excess food; Broken items.
4	Tourism activities	Resorts, hotels, restaurants, homestays...	Goods packaging; Excess food
5	Aquatic exploitation activities	Aquaculture areas and fishing grounds	Livestock waste; Damaged agricultural products; Packaging; Broken fishing gear; Mesh piece
6	Construction sites	Urban areas, hotels, resorts... are under construction	Leftovers; Paper, plastic, glass, metal; Broken tools

b) Volume of household solid waste generated

Through the process of survey, actual research and weighing of household solid waste in 50 households in the study commune. We get the results of the emission coefficient and amount of HSW of each study area as follows:

Table 4. Indicating the HSW discharge coefficient in the communes of Bao Ninh and Nghia Ninh.

TT	**Name of area investigated**	**Demographics were investigated**	**Mass of solid waste weighed during the day according to 3 types (kg)**			**HSW emission coefficient (kg/person/day)**
			Food solid waste	**Solid waste is recyclable**	**Solid waste is different**	
Nghia Ninh commune						
1	Trung Nghia 5 (15 households)	60	14.07	5.6	0.41	0.33
2	Trung Nghia 6 (10 households)	45	9.53	2.5	1.29	0.29
Total			23.6	8.1	1.7	
Average HSW emission coefficient (kg/person/day)						0.32
Bao Ninh commune						
1	My Canh (14 households)	59	16.26	6.95	0.92	0.42
2	Ha Thon (11 households)	45	12.71	5.3	0.5	0.4
Total			28.97	12.25	1.42	
Average HSW emission coefficient (kg/person/day)						0.41

Nghia Ninh Commune: Nghia Ninh commune with an area of 15.71 km^2, population of 5,317 people [11]0.

The investigation's findings show that there were 105 peoples living in 25 houses in the Nghia Ninh commune, generating a total of 32,796 (kg) of household solid trash every day. The average daily production of HSW in the ward is 0.31 kg per person, per survey results. Estimated total volume of solid trash generated by households in the ward:

$$0.31 \text{ (kg/person/day)} \times 5{,}317 \text{ (person)} = 1{,}648 \text{ (ton/day)}$$

The results are displayed in Table 4, where we can observe that the total emission coefficient is 0.13 kg/person/day, with the lowest emission amount in the research households being 0.13 kg/person/day and the greatest being 0.65 kg/person/day. Compared to the average household waste generation per capita in Quang Binh province in 2019 of 0.52 kg/person/day and the generation index of rural areas in the North Central and Central Coast regions of 0.51 kg/person/day [1], the average generation volume is 0.31 kg/person/day. People spend less time at home and more time in the fields and working regions, which accounts for the population's mostly agrarian lifestyle and somewhat lower living standards than in the surrounding area.

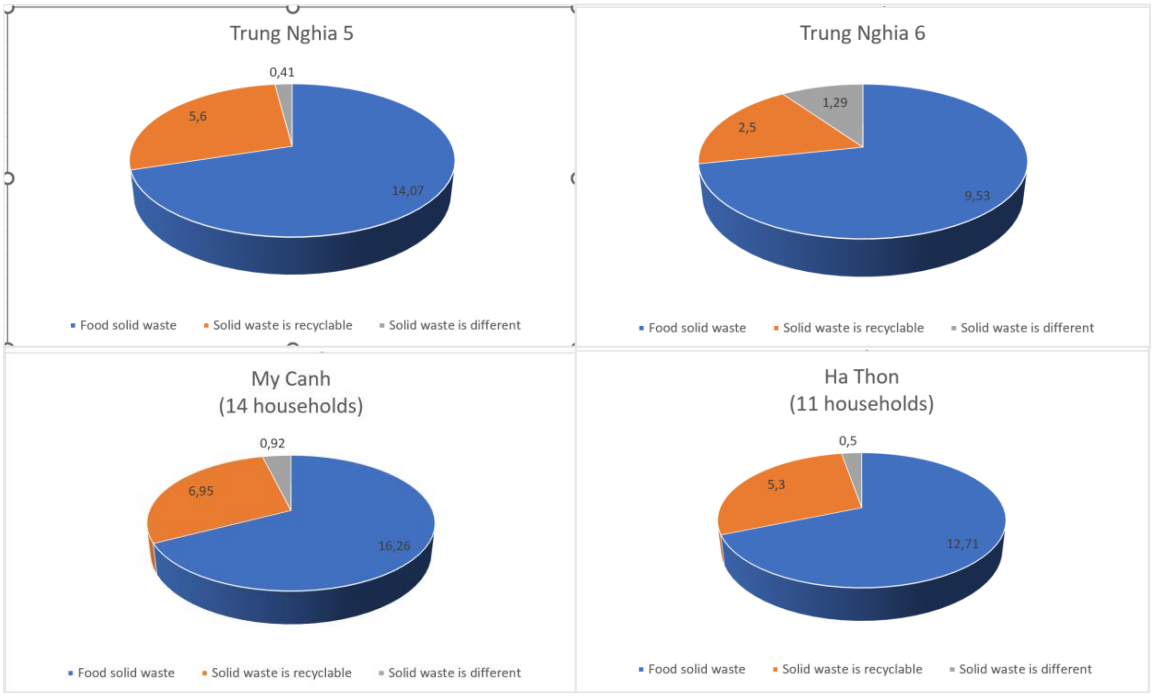

Figure 2. Mass of solid waste weighed during the day according to 3 types.

Bao Ninh commune: With an area of 17.67 km^2, the population is 11,136 people 00.

According to the results of the investigation, the total volume of household solid waste in 25 households in Nghia Ninh commune: 42.64 (kg/day), with 104 people in 25 households. According to survey results, the average amount of HSW generated per person in the ward is 0.41kg/person/day. Estimated total volume of household solid waste in the ward:

0.41 (kg/person/day) x 11,136 (person) = 4,565 (ton/day)

Table 4 displays the acquired data. It is evident that the research households had daily emission amounts ranging from 0.23 kg/person to 0.7 kg/person, with the lowest emission amount being 0.23 kg/person. The disparity is not so great, but in a commune with potential for tourists, household commerce and trading are rather active, which raises HSW. When compared to the average volume of household waste generated per capita in Quang Binh province in 2019 - 0.52 kg per person per day and the generation index of rural areas in the North Central and Central Coast regions 0.51 kg per person per day (as reported in the 2019 Environmental Status Report) [1-the average total generation coefficient is 0.41 kg/person/day. These differences are not very great. The sole steps in the waste treatment process in communes are collection, transportation to the waste treatment classification plant, production of biogas, and the use of organic mineral fertilizers 0. From the table above, we can calculate the average percentage composition of different types of HSW in the two study communes as follows:

Table 5. Household solid waste composition in the communes of Nghia Ninh and Bao Ninh.

TT	Investigation area	Composition % HSW		
		Food solid waste	**Solid waste is recyclable**	**Solid waste is different**
1	Nghia Ninh commune	70%	25%	5%
2	Bao Ninh commune	68%	29%	3%

Figure 3 there is a significant amount of organic matter in the HSW component; Metal, cardboard, wood, plastic, and glass are examples of recyclable and reusable materials; the following materials are inorganic, non-recyclable, and reusable; A negligible percentage of home solid waste is made up of hazardous materials such batteries and packaging that

contains chemicals for plant protection. The utilization of growth factors default discharge is the primary cause of the computation findings about 59.6% uncertainty 0.

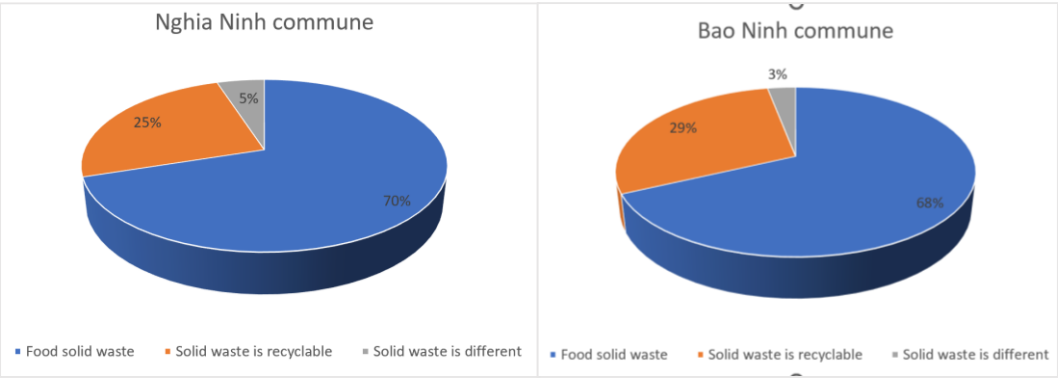

Figure 3. Household solid waste composition.

3.2. Analyze the connections between home solid waste and the age, occupation, and income of the households residing in the neighborhood

The volume and makeup of household garbage vary according on family size, occupation, and income, according to surveys conducted among homes in the communes of Nghia Ninh and Bao Ninh.

Income: Is a significant element influencing the amount and kind of solid waste that every home produces. According to the report, households earning at least $10 million will have greater shopping demands than households earning less than $10 million, which will result in a higher volume of HSW.

Occupation: Occupation is another crucial factor that has a big impact on the emissions that homes create. Since they labor most of the day, there won't be much demand for goods. People who work overtime, in government agencies or offices, or in homes where people work, trade, grow crops, clean, etc., typically have lower emissions than households.

Number of family members: Families with four or more individuals typically produce two to three kilograms of solid trash, and their solid waste composition is more varied than that of families with fewer members, per the survey.

Age: Based on the survey, it was discovered that respondents between the ages of 20 and 40 were more knowledgeable about HSW categorization than those over 45. Compared to older individuals, young people are more likely to have faster and better access to information, which encourages them to conserve the environment.

Along with Bao Ninh commune's advantages in growing tourism services, Nghia Ninh commune has elements that are comparable to those impacting the volume and composition of household solid trash. The tourist season is one of the reasons Bao Ninh communes is situated outside of the city center. Businesses, dealers, restaurants, lodging facilities, and other institutions all agree that during the low season, solid waste generation is quite low, averaging 2 to 3 kg, but it is extremely low during the tourist season. As a matter of fact, trash production rises. This indicates how closely the aforementioned parameters relate to the amount and make-up of solid trash generated by households as well as the province-wide average emissions.

3.3. Current status of household solid waste management

Sorting and recycling activities: Nghia Ninh commune had the largest percentage of households performing partial categorization, according to a survey conducted among 100 houses in the two communes. Not a single household completed complete classification. According to 50% of respondents, most people in the population work in agriculture and animal husbandry because people frequently make pet food, compost fertilizer, or gather

scraps to sell. Other types of HSW are also kept together and are rarely classified, and there is no suitable treatment method [15, 16].

While just 24% of households in Bao Ninh classify, food waste is still primarily collected and classified in small amounts. The biggest percentage of non-recycling is found in the Bao Ninh area, where 76% of the population is non-agricultural and each household has a small plot of land. In Nghia Ninh, 50% of the population is unclassified, and most of these houses are non-agricultural.

Households whose HSW has not been classified prior to collection believe that the following are the causes: Individuals have not been informed and encouraged to classify HSW; Collection vehicles do not fulfill the requirements for classification; There are no locations for waste groups to gather after classification; Collection and transportation activities:

Nghia Ninh commune: The commune's primary producers of solid waste are homes, individuals, a small number of business buildings, administrative spaces, and educational institutions. The principal constituents of this kind of garbage include food scraps, plastic, nylon, and organic waste from agricultural items. The homeowner's solid waste will be stored there until the collection team uses containers, hand carts, sweepers, small trucks, and other vehicles to order its loading onto tricycles at collection stations. Move garbage from the location of collection to the collecting site. It is necessary to dispose of solid trash in a way that makes it as easy as possible for collectors to access it in hospitals, schools, or other central locations. Household solid garbage is collected twice a week, between the hours of 5 and 8. The filling coefficient of the vehicle is 1.3-1.5. In certain heavily inhabited regions, the vehicle's filling coefficient can reach 2. These areas include Trung Nghia 4 village and market area. Vehicles are still in use today. Just let the container loose so that it can fall onto the road easily when hauling household solid trash. The majority of self-made collection vehicles are still simple carts and motorcycles.

Bao Ninh commune: The commune's primary industries include daily operations, tourism services, and aquatic exploitation. Thus, the majority of waste is composed of plastic, nylon, and leftover food waste. Garbage trucks, hand carts, motorbikes with bins on the back, and each household's allotted trash will all be used to collect the waste. At collection stations, solid garbage will wait to be placed onto tricycles. The frequency of collection was twice a week; in tourist locations, it occurs once or twice daily. The collection hours vary depending on the season and are from 3:00 to 6:00 p.m. To keep beaches and roadways clean, there are extra street cleaning crews.

The vehicle uses hand carts with extra walls surrounding spilled trash, and its filling factor ranges from 1.5 to 1.8. Right now, the following types of trash are being delivered to the waste treatment plant:

Inorganic waste A biogas line that combines the production of electricity and fertilizer is made from organic waste; products like shredded plastic, shredded nylon, rags, wood, etc., are used as raw materials for waste power lines; metals (iron, aluminum, copper...), plastics, glass, rubber, paper, etc., will be collected and sold for recycling.

The Dong Hoi - Bo Trach general waste landfill is where the debris will be buried (before being used as input material for the unburnt brick production process).

Waste fee collection activities: As of right now, the cost of home solid trash collection in the city is determined by Decision No. 36/2018/QD-UBND, which states 0: Families in communes and wards: 27,000 VND a month per household.

The collection cost in Nghia Ninh (69%) and Bao Ninh (76%), the two communes studied, is 27,000 VND per month per home. Most respondents in these communes believe the fee is excessive given their income. But according to 24% and 31% of Nghia Ninh and Bao Ninh communes, respectively, the price is reasonable given the quality of the services they receive.

Most respondents indicated that they would not choose to hire Nghia Ninh 65% and Bao Ninh 76% when asked whether they would be prepared to pay additional collection service costs because they believed the cost was reasonable. The remaining families are unsure, whereas those that selected Bao Ninh (22%), Nghia Ninh (26%), and other reasons wanted better services, better equipment, and more frequent collections.

3.4. GHG emission from the mix MSW landfilling

One liter of fossil fuel is required to treat one kilogram of solid waste. According to Tables 6 and 7, the amount of solid waste in the two communes is the same. If fossil fuels are used simultaneously, greenhouse gas emissions range from 44,4 to 49 tons per month. As a result, in urban waste treatment activities, developing approaches for identifying household solid waste at the source is critical.

Baseline survey results, which are comparable to the values in the communes mentioned above, will aid in increasing the accuracy of computing greenhouse gas emissions for solid waste in urban areas (better than 60%) of Dong Hoi City.

Table 6. GHG emissions at the landfill of Nghia Ninh commune.

Diesel consumption for operating matchineries at landfill	49000	L/month
Total waste handled at the landfill	49	tons/month
A diesel requirement	1000	L/ton of waste
Total energy in consumed diesel	36420	MJ/ton of waste
Default CO_2 emission factor for combustion	74100	kg CO_2/TJ
GHG emissions due to fossil fuel consumption	**2698.72**	**kg of CO_2 eq/ton of waste**

Table 7. GHG emissions at the landfill of Bao Ninh commune.

Diesel consumption for operating matchineries at landfill	44400	L/month
Total waste handled at the landfill	44.40	tons/month
A diesel requirement	1000	L/ton of waste
Total energy in consumed diesel	36420	MJ/ton of waste
Default CO_2 emission factor for combustion	74100	kg CO_2/TJ
GHG emissions due to fossil fuel consumption	**2698.72**	**kg of CO_2 eq/ton of waste**

3.5. Propose solutions to improve management efficiency

The management of household and individual solid waste in Quang Binh province is governed by a number of regulations on solid waste management, which include duties and powers pertaining to the classification, storage, collection, transportation, and treatment of domestic solid waste in the region, as well as the responsibilities and powers of agencies, organizations, communities, households, and individuals 0.

The following guidelines are used to categorize domestic solid waste produced by homes in the two communes: Reusable and recyclable solid waste (paper, plastic, metal, glass, etc.); Food waste (vegetable scraps, fruits, veggies, tubers, animal carcasses, plants, etc.); Other solid garbage from the home (bulky waste, non-recyclable waste, hazardous waste category).

Putting forward ideas for separating household solid waste at the source. According to the survey, while some people in the communes of Nghia Ninh and Bao Ninh have started using the separation at source and composting with biological products model, the great majority of people still do not classify garbage at source. Two strategies can be put forth to increase the effectiveness of local waste management, particularly the classification of household solid waste at the source in Nghia commune, when combined with the previously indicated scientific and practical foundation. These are Ninh and Bao Ninh:

Educating the public about the HSW classification system, source classification, and the way waste categories are categorized with an emphasis on scrap, cans, plastic boxes, and salable metal goods. In Bao Ninh (87% of households) and Nghia Ninh (91% of households), meetings are held, or environmental news is disseminated.

garbage groups need to be trained, and people in the communes of Nghia Ninh and Bao Ninh still don't comprehend the rules governing garbage classification. Need financial assistance (equipment and monthly labor wage) to support collection work in the communes of Nghia Ninh and Bao Ninh. Because the waste rates in the research regions are lower than those in the province as a whole, frequent health checks and staffing are carried out in tourism and heavily populated areas. Large trash containers and additional collection vehicles are required in places with congested roads and homes distant from collection points.

Create collection groups in communes or villages to assist environmental workers with rubbish collection; also, establish guidelines for the Collection Team and designate personnel to oversee and assist the team's operations. According to the survey, 67% of respondents think that labels are useful for collection and classification, and that garbage bags or expandable storage containers are required for sorting household solid waste.

4. Conclusion

The study illustrates the difficulties in gathering and categorizing the quantity of solid trash produced in households. In the communes of Nghia Ninh and Bao Ninh, the monthly cost of solid trash collection is 27,000 VND. Seventy-six percent of Nghia Ninh households and sixty-nine percent of Bao Ninh households value this fee. Based on research, the household solid waste generation coefficients for Nghia Ninh commune and Bao Ninh commune are 0.3 kg/person/day and 0.4 kg/person/day, respectively. Bao Ninh has a coefficient of 0.4 kg/person/day for domestic solid waste generation, compared to 0.3 kg/person/day for Nghia Ninh commune.

In line with the demands of socioeconomic growth, solid waste emissions in Quang Binh province are low at 0.52 kg/person/day and 0.51 kg/person/day in rural regions, according to the 2019 National Environmental Report. corresponding to one ton of garbage at 2698.72 kg CO_2 equivalent.

In both communes, the actual rate of garbage classification is low - 61 percent of homes have not received a classification. This type of waste management is used by 39% of homes; it primarily targets salable waste materials such cans, bottles, canned foods, leftover food, and fruit and vegetable peels. No household has yet received a thorough classification.

Author's contributions: Developing research ideas: D.H.P., V.V.D., N.H.; Data processing: D.H.P., V.V.D., N.H.; Write a draft of the article: D.H.P., V.V.D.; Edited article: N.Q.H.

Declaration: The authors declare that this article is the research work of the authors, has not been published anywhere, and is not copied from previous research; There is no conflict of interest within the author group.

References

1. Ministry of Natural Resources and Environment. National Environmental Report: topic on household solid waste management. 2019.
2. Malika, N.K.A.; Abdullah, S.H.; Manaf, L.A. Community participation on solid waste segregation through recycling program in Putrajaya. International on Environmental Forensics, 2015.
3. Birhanu, Y.; Berisa, G. Assessment of solid waste management practices and the role of public participation in Jigjiga Town, Somali Regional State, Ethiopia. *Int. J. Environ. Protect. Policy* **2015**, *3(5)*, 153–168.
4. Enayetullah, I.; Sinha, AHMM. (Eds). Community-based solid waste management: The Asian experience. Proceeding of the Regional Seminar on Community Based

Solid Waste Management. Dhaka, Bangladesh, Dhaka: Waste Concern Publication. 2000, pp. 19–20.
5. National Assembly of the Socialist Republic of Vietnam. Law on Environmental Protection 2020 No. 72/2020/QH14.
6. Manfredi, S.; Tonini, D.; Christensen, T.H.; Scharff, H. Landfilling of waste: accounting of greenhouse gases and global warming contributions. *Waste Manage. Res*. **2009**, *27*, 825–836.
7. Conestoga-Rovers & Associates (CRA). Landfill gas management facilities design guidelines, Richmond, British Colombia. Online available. 2010. Online available: http://www.env.gov.bc.ca/epd/munwaste/waste-solid/landfills/pdf/Design-guidelines-final.pdf (accessed 20 August 2012).
8. IPCC. Guidelines for National Greenhouse Gas Inventories, Prepared by the National Greenhouse Gas Inventories Programme, Eggleston HS Buendia L Miwa K Ngara T Tanabe, K (Eds.). Published: IGES, Japan. 2006.
9. Metz, B.; Davidson, O.R.; Bosch, P.R.; Dave, R.; L.A.; Meyer (eds). Contribution of Working Group III to the Fourth Assessment Report of the Intergovernmental Panel on Climate Change. Cambridge University Press, Cambridge, United Kingdom and New York, USA. IPCC, 2007.
10. Yamane, T. Statistics: An introductory analysis (2nd eds). New York: Harper and Row. 196711. Nghia Ninh Commune People's Committee. Report on the socio-economic situation in 2022.
12. Bao Ninh Commune People's Committee. Report on the socio-economic situation in 2022.
13. Department of Natural Resources and Environment of Quang Binh province. Report No. 37/BC-UBND dated February 15, 2023, Report on environmental protection work in 2022 of Quang Binh province. 2023.
14. Hoa, V.X.; Thuc, T. Calculate greenhouse gas emissions from solid waste landfill activities for the base year 2014 and assess the uncertainty of the results. *J. Clim. Change Sci*. **2017**, *4*, 70–77.
15. Electronic information portal of Ha Nam province. Launching the "Waste classification at source" model in Dinh Xa and Trinh Xa communes. 2022. Online available: https://phuly.hanam.gov.vn/Pages/ra-mat-mo-images-of-rac-thai-at-nguontai-xa-dinh-sa-va-trinh-xa.aspx.
16. Anh, L. Waste classification at source in Da Nang: Identifying shortcomings and limitations. 2022. Online available: https://baotainguyenmoitruong.vn/phan-loai-rac-tai-nguon-o-da-nang-nhan-diennhung-ton-tai-han-che-348471.html.
17. Quang Binh Provincial People's Committee. Decision No. 36 on adjusting maximum price regulations for household waste collection and transportation services using state budget capital in Appendix No. 03 issued together Decision No. 48/2017/QD-UBND dated November 30, 2017 of the People's Committee of Quang Binh province. 2018.
18. People's Committee of Quang Binh province. Decision No. 14/2023/QD-UBND Promulgating detailed regulations on household solid waste management of households and individuals in Quang Binh province, decision Based on the Law on Environmental Protection 2020, Circular No. 02/2022/TT-BTNMT, Decree No. 08/2022/ND-CP. 2023.

JOURNAL OF
HYDRO-METEOROLOGY

Research Article

Risk of groundwater pollution and proposals for sustainable development in Binh Thuan province, Vietnam

Huynh Phu[1]*, Tran Thi Minh Ha[2]

[1] HUTECH University; HUTECH Institute of Applied Sciences; h.phu@hutech.edu.vn
[2] Tay Nguyen University, Buon Ma Thuot - Dak Lak Province; ttmha@ttn.edu.vn

*Correspondence: h.phu@hutech.edu.vn; Tel.: +84–966687548

Received: 9 December 2023; Accepted: 22 January 2024; Published: 25 March 2024

Abstract: Groundwater serves as one of the important sources of water supply for Binh Thuan province, Vietnam during dry seasons. This water source is concentrated in Quaternary sediments with two aquifers qh and qp. Geophysical methods have been applied, performing geological drilling, observing and monitoring boreholes. Determine the characteristics of the qh and qp aquifers, located along the coast of Binh Thuan province. Our research has shown that these reservoirs are contaminated. Water sources are at high risk of being contaminated with mineral oil, radioactive, organic, bacterial and saline contamination. The article warned about water resource risks in Binh Thuan province and proposed remedial measures to ensure water resources for Binh Thuan province.

Key words: Aquifers; Binh Thuan Province; Ground Water; Salinization.

1. Introduction

Binh Thuan is a coastal province in the South-Central region, with a sea length of 192 km extending from Ca Na to Binh Chau (Figure 1). Binh Thuan has to “face to face” the phenomenon of eawater infiltrating into the land up to nearly 20 km in some places. Solving the problem of water shortage has been difficult. Currently, Binh Thuan province still has to cope with salinization. The study results identified the salinization boundaries of the aquifers in Binh Thuan province. Since then, the authors have made offers to minimize the negative impacts on water resources, serving sustainable development.

Since 1992, the United Nations has chosen March 22 every year as World Water Day. The theme of World Water Day 2022 is “Groundwater” to draw attention to the hidden and always valued water resource but has not been fully recognized for its value in sustainable development policy planning. Geophysical methods used in exploration include: i) Seismic methods are a group of methods that use seismic waves or sound waves to study the environment. The results of the exploration are the location of reflection/refraction boundaries, the speed of wave propagation in rock (or water) masses, and possibly the physical and mechanical structural characteristics of the rock and soil [1]; ii) Gravity method measures the Earth's gravity, thereby determining the density distribution (or density) of rock masses [2]; iii) Magnetic method to measure the Earth’s magnetic field [3]; iv) Electrical methods are a system of methods that use voltage or constant current (DC) to study the environment through electrodes inserted into the ground, to determine the distribution of electrical conductivity characteristics of blocks or rock layer [4]; v) Electromagnetic methods are a system of methods that use electromagnetic fields to study the environment, and usually do not use electrodes. The survey results are the conductivity distribution in soil and rock, but are often expressed in resistivity [5]; vi) Radioactive exploration includes methods for

characterizing and distributing natural or forced radiation in rocks and soil [6]; vii) Geothermal exploration: Measure temperature distribution in soil and rock to determine the heat source and rock state properties [7]; viii) Seismoelectrical: Research and application of electromagnetic fields generated in soil and rock under the impact of compressive elastic waves (longitudinal P waves) to predict nearby earthquakes, search and explore underground water or potentially valuable minerals. related to quartz. However, it is still rarely used [8].

Binh Thuan province's underground water resources are divided into 2 porous aquifers, 4 aquifers and fissure aquifer zones, geological formations that are extremely poor in water and contain no water. The results of assessing the exploitable reserves of underground water in Binh Thuan province show that the distribution area of freshwater layers is about 4,080.7 km^2, the exploitable reserve is 652,290 m^3/day and night [9]. Currently, the underground water reserves of Binh Thuan province are distributed in different aquifers, coastal sand dune areas with an exploitation depth of 30-40 m, in some places it is 80-100 m. Groundwater in the coastal area of the entire province is the most volatile. Mining titanium-zircon minerals requires a large amount of water, and water sources here are very scarce, and at the same time discharges a large amount of wastewater that contains radioactive substances that may be higher than allowed levels. Titanium-zircon mining technology is being applied here with the mining pit always being flooded [10]. In Binh Thuan, underground water is very important. Only 40% of domestic water demand in the province comes from surface water, the rest most people and water plants exploit underground water sources, especially hotels serving coastal tourists in the province [11].

Figure 1. Location of the study area.

The purpose of this study is to evaluate the current status of groundwater quality of the qh and qn aquifers of Binh Thuan province, Vietnam; Consider the water quality of these aquifers. Based on the results obtained, the study determined the risk of groundwater pollution and proposed solutions for sustainable development of the province.

2. Data collection and methods

2.1. Data collection

In this study, materials were utilized: (1) Groundwater research topics and projects are addressed in these documents; (2) Geological and hydrogeological research results from Binh Thuan province; (3) Documentation of field investigations in Binh Thuan province for 2016,

2018, 2020, and 2021; (4) Binh Thuan province's seaside vision for zoning distribution and groundwater resource protection by 2030; (5) Boreholes that exploit underground water in Binh Thuan province have parameters; (6) Monitoring, sampling, and analysis of water samples are the results of the author's work.

2.2. Methods

2.2.1. Data collection and analysis

The formation of porous aquifers occurs in unconsolidated sediments from the Quaternary era. The hydraulic properties of laminar water are present in them, and they are mostly found in unpressured aquifers. The Quaternary unconsolidated sediments are an underground hydraulic system that runs continuously throughout the region in essence. Water-permeable and water-repellent materials are alternately present in this heterogeneous entity. The water table in these sediments is typically less than 2 meters deep. Contamination of porous water is a common occurrence. Also, coastal water is slightly salty, while underground water is saline due to seawater intrusion. The dynamics of open water fall under both seasonal changes and coastal dynamics. Ground water levels fluctuate significantly with the seasons and extremes of water levels are reached more slowly than rainwater and surface water.

The study has sampled water in aquifers qh and qp, located along the coast of Binh Thuan province. Water samples were analyzed by 24 parametrs (pH, $CaCO_3$, TDS, NH^{4+}, Cl^-, SO_4^{2-}, ΣFe, NO_2, NO_3, COD ($KMnO_4$), Florua (F^-), Xianua (CN^-), Phenol, Asen (As), Cadimi (Cd), Pb, Cr^{6+}, Cu, Zn, Mn, Hg, Se, E. Coli, Coliform. The analysis results for water samples are compared with National Technical Regulation on Drinking Water Quality of Viet Nam.

2.2.2. Geophysical methods

Geophysical methods are amazingly effective for the in-depth study of structures. Geophysical methods allow determining the geological structures, aquifer boundary, water storage zone, saltwater/ freshwater boundary based on the difference in resistivity of the studied objects [12]. In saline water the resistivity values change suddenly (low resistance, Figure 2 shows from blue to yellow). From this, we have determined the salinization boundary. In addition, we also determined the thickness of the Quaternary sediments. That is the basis for us to determine the thickness of the aquifers. The geophysical lines are designed by us in the direction perpendicular to the coastline (Figure 3).

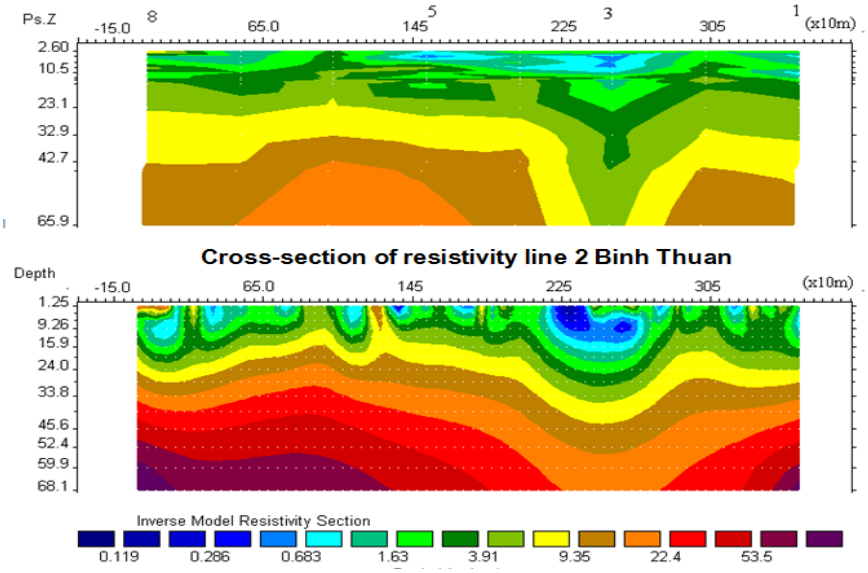

Figure 2. Resistivity section of line 2 Binh Thuan.

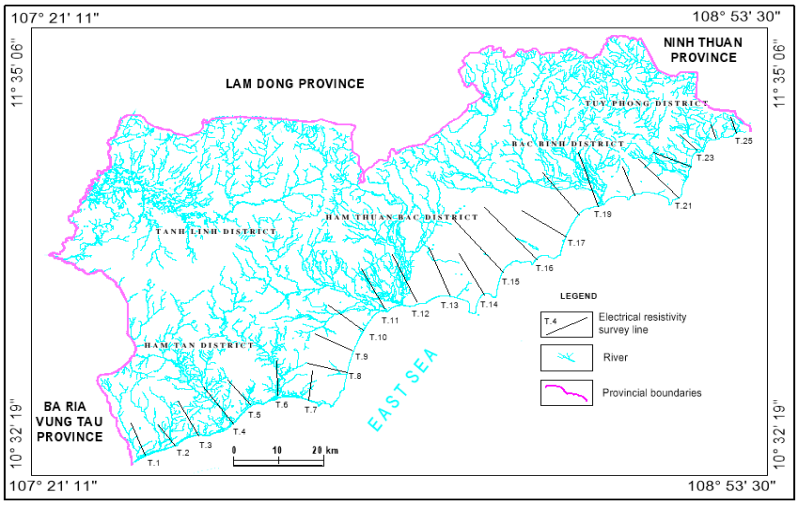

Figure 3. The diagram of the resistivity survey.

We used Schlumberger equipment with device distance ABmax = 350m, MNmax = 25m (study depth from 50÷90 m). The resistivity survey method determines the change of geological structure with depth.

The resistivity values were identified by:

$$\rho = K\frac{\Delta U}{I} \quad (1)$$

where I is an amperage; ΔU is the voltage; K is determined.

$$K = \pi\frac{AM \times AN}{MN} \quad (2)$$

Symmetrical depth method according to the diagram of figure 4.

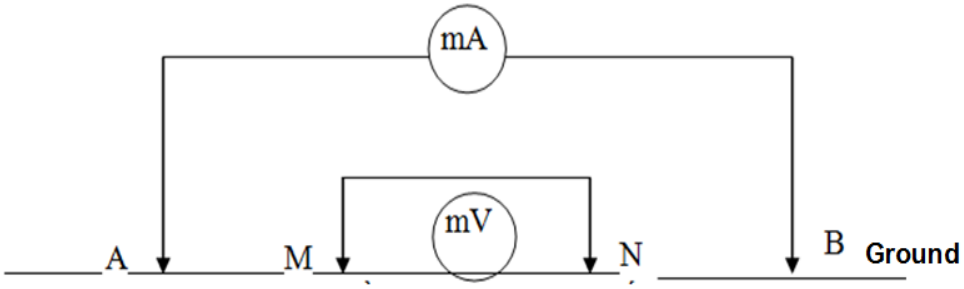

Figure 4. Diagram of method Schlumberger.

Network of measuring points: The distance between the lines is from 5km to 8km and the average distance between the measuring points is 500m. Measurement points were identified by GPS Montana 680.

2.2.3. Field observation

Field observation is a very important method, it has helped the authors to directly observe geological phenomena, geomorphological processes. Field observations have helped us to research, determine the resistivity survey, location of borehole.

2.2.4. Geological drilling method

With hundreds of wells collected from geological projects, hydrogeology helped the authors determine the thickness of aquifers. The documentation of the wells helped the authors to divide the sedimentary layers.

Coarse sediments are the distribution of groundwater, fine-grained sediments are not suitable for storing water. We did additional drilling to verify geophysical measurement results, and also took sample types (see section 2.2.5). From there, identifying the thickness of the sedimentary layers associated with the aquifers will be determined more accurately.

2.2.5. Methods of monitoring and sampling boreholes

We took water samples from drilled wells in Binh Thuan province. The results of the analysis have been compared with the National Technical Regulation on Groundwater Quality of Ministry of Natural Resources and Environment in Vietnam: 09/2023/ MONRE (Table 1).

Table 1. Table of water quality standards for groundwater (Vietnamese Standards: 09/2023/MONRE).

TT	Parameters	Units	Vietnamese standards: 09/2015/ Monre
1	pH		5.8 - 8.5
2	$CaCO_3$	mg/l	500
3	TDS	mg/l	1500
4	Amonium (NH^{4+})	mg/l	1
5	Cloride (Cl^-)	mg/l	250
6	Sulpate (SO_4^{2-})	mg/l	400
7	Total Fe	mg/l	5
8	Nitrite (NO_2)	mg/l	1
9	Nitrate (NO_3)	mg/l	15
10	COD ($KMnO_4$)	mg/l	4
11	Fluoride (F^-)	mg/l	1
12	Cyanide (CN^-)	mg/l	0.01
13	Phenol	mg/l	0.001
14	As	mg/l	0.05
15	Cd	mg/l	0.005
16	Pb	mg/l	0.01
17	Cr^{6+}	mg/l	0.05
18	Cu	mg/l	1.0
19	Zn	mg/l	3.0
20	Mn	mg/l	0.5
21	Hg	mg/l	0.001
22	Se	mg/l	0.01
23	E. Coli	MNP/	0
24	Coliform	100ml	3

2.2.6. Sample analysis method

Water samples were analyzed for 24 parameters. Samples analyzed at Nation Lab Nation Lab. VLAT 1-1.0517; ISO/IEC 17025.2017 and Institute of Environmental & Circular Economy Sothern_ IECES (Table 1).

3. Results and discussion

3.1. Characteristics of aquifers

Research results showed that Binh Thuan province has 7 aquifers, including porous aquifer and fractured aquifer [13–15]. In this article, we only refer to the porous aquifer, because the fault aquifer belongs to the low-productivity aquifer type, which is not the subject of this study.

In porous aquifers, water exists and circulates ceaselessly in the gaps between particles of non-cohesive matter. As for bulk materials, they are often described in terms of the grain size of individual particles such as sand, pebbles, gravel, etc., widely distributed porous aquifers, forming coastal plains and valleys of rivers and streams.

a) Porous aquifers in unclassified Quaternary sediments (q)

Porous aquifers in unclassified Quaternary sediments (q) are formed by the deluvial sediments (dQ), deluvial - proluvial (dpQ), eluvial - deluvial (edQ) and aluvial - deluvial (adQ). The aquifer thickness varies from 0.5m to 7.0m, in some places up to 17.0m. (LK1016 - Ham Tan). The common thickness is 3m - 5m. The total distributed area of the porous aquifers in unclassified Quaternary sediments is about 128 km^2. The compositions of the sediments include debris, sand, gravel, silt, clay, pebble, rock, etc, discrete texture. Deep of water level of the wells is from 2.83m - 5.98m deep, with average of 4.18m. Porous aquifer in unclassified Quaternary sediments belong to the low yield aquifer category. The test results of the water pump are shown in Table 2.

Table 2. Results of experimental water pump of pits and wells of the porous aquifer in unclassified Quaternary sediments (q).

Value	Static Water Level (m)	Discharge (l/s)	TDS (g/l)	permeability coefficient (m/ng)
Maximum	5.98	0.85	0.18	2.80
Minimum	2.83	0.03	0.04	0.14
Medium	4.18	0.28	0.15	1.10

The source of supply for this aquifer is mainly rainwater, surface water and from aquifers located above. The drainage area is the hydrological network in the area. Research results have shown that the water level often rises in the rainy season and wells dry up in the dry season. The water level changes between 2 seasons from 2m to 4m. Porous aquifers in unclassified Quaternary sediments have had discontinuous distribution, forming narrow bands, thin thickness, low productivity aquifers.

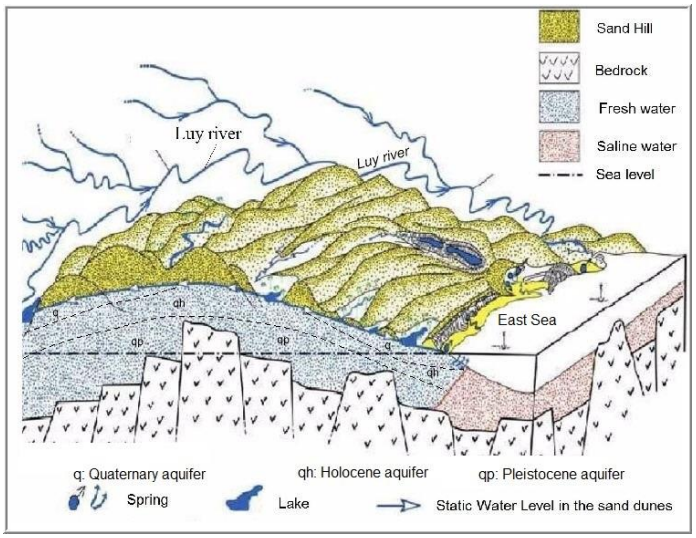

Figure 5. Map of Binh Thuan province Hydrogeology.

b) Porous aquifer in Holocene sediments (qh)

Porous aquifer in Holocene sediments is made up of marine sediments (mQ_2^2, mQ_2^{2-3}, mQ_2^3), marine sediments - marshy (mbQ_2^2, mbQ_2^{2-3}, mbQ_2^3), wind origin sediments (vQ_2^2, vQ_2^{2-3}, vQ_2^3), alluvial sediments - marine (amQ_2^{2-3}), alluvial sediments (aQ_2^{2-3}, aQ_2^3). They are distributed in the Vinh Hao deltas, Tuy Phong delta, Bac Binh delta, Ham Thuan Bac delta, along with the valley of Phan river, valley of Dinh river, valley of

Long Song river the valley of Phan river, Bau Sen area, Ham Tan area, Thuan Quy area, Tan Thanh area, etc. Total distributed area is 983 km^2. The compositions of the sediments include debris, sand, gravel, silt, clay, pebble, rock, etc, discrete texture. Holocene aquifer thickness ranges from 1m - 2m to 20m - 40m, with an average of about 10m. The water capacity of Holocene sediments is very erratic and depends on the composition of sediment, distributed location, and thickness of the rock.

Experimental results of pumping water in pits and wells in Holocene aquifers showed that: The water had no pressure, the water depth was from 0.5m to 5.0m. The water flow at these outcrops ranged from 0.01 liters to 0.3 liters per second. The main source of supply for the Holocene aquifer was rainwater; Water level in rainy and dry seasons was from 0.3m to 0.4m. The experimental water pumping results showed that the flow of the well ranged from 0.06 liters - 0.91 liters per second, an average of 0.45 liters per second; seepage coefficient ranged from 2.0 meters - 3.0 meters per day, well flow ranged from 0.2 liters - 0.4 liters per second.

Table 3. Experimental pumping results of pits and wells in low-yield areas of Holocene aquifers.

Value	Static Water Level (m)	Discharge (l/s)	Draw- down (m)	TDS (g/l)	permeability coefficient (m/ng)
pits					
Maximum	4.5	0.91	4.33	5.91	4.53
Minimum	0.3	0.06	1.03	0.07	0.72
Medium	1.86	0.45	1.85	1.23	2.55
wells					
Maximum	11.55	0.99	25.8	1.987	4.76
Minimum	0.05	0.054	0.29	0.05	0.02
Medium	2.64	0.33	6.61	0.84	1.34

Table 4. Experimental pumping results of pits and wells in high-yield areas of Holocene aquifers.

Value	Static Water Level (m)	Discharge (l/s)	Draw- down (m)	TDS (g/l)	permeability coefficient (m/ng)
Pits					
Maximum	4.1	4.44	3.56	1.11	46.93
Minimum	0.0	1.00	1.16	0.11	3.13
Medium	1.90	1.75	2.08	0.57	12.92
wells					
Maximum	6.17	2.00	9.33	0.165	11.63
Minimum	0.88	1.10	0.74	0.045	0.77
Medium	2.92	1.33	4.51	0.11	2.80

In general, water in the Holocene was super freshwater to saline water, TDS ranged from 0.045 grams - 1.987 grams per liter, the frequent values ranged from 0.5 grams - 0.7 grams per liter. The low-yield sediments, distributed in the coastal area, have high TDS due to salinization from seawater. Checking 38 constructions, up to 7 waterworks were salinization (M = 1.6 grams - 5.91 grams per liter). The groundwater changed seasonally, closely related to surface water and rainwater. The groundwater level monitoring results of well BBM11 showed the highest water level in October (water level depth: 1.0 m) and the water level was lowest in May (water level depth: 1.58 m), the water level difference of the season rainy and dry season was 0.58 m [16].

Most of Holocene aquifers distributed in Phan Thiet area have been affected by salinity. Freshwater was only available at a depth of < 5.0 m, from 5.0 m or more, the water has been

contaminated with salt (resistivity survey results by Geophysical methods, gave small resistivity values, corresponded to high salinity values of water).

In summary, the Holocene aquifer had a discontinuous distribution. Level of water storage was from low- yield to medium - yield. Porous aquifer in Holocene sediments could be water supply small scale, in the estuary areas of the Cai river, Phan river. Porous aquifers in Holocene sediments were salinization.

c) Pleistocen aquifer (qp)

Porous aquifers in Pleistocene sediments (qp) are made up of alluvial sediments (aQ23, aQ22-3), alluvial marine sediments (amQ12-3, amQ13.2), marine sediments (mQ12-3, mQ13.2, mQ12.1)); marine - marsh sediments (mbQ12-3, mbQ13.2), wind source sediments (vQ13), deluvial - proluvial (dpQ) and eluvial - deluvial (edQ). They are distributed mainly in low-lying plains from Tuy Phong to Ham Tan, along Highway 1A, Ham Hiep, Ham Phu, Ham Liem, along Ca Tot river, Ca Ty river, etc. Total surface area is about 1,414 km^2.

The compositions of the sediment include: the upper part is quartz sand, sand, clayey sand, siltstone, the lower part is pebbles, gravel, dark gray, yellowish gray, discrete texture. The thickness of the Pleistocene aquifer varies by region: in Ham Tan - Phan Thiet area, it is from 10m - 15m; in Bac Binh: from 8m - 12m; in Tuy Phong: from 5m - 14m.

The low-yield area is distributed in Vinh Hao, Lien Huong, Hong Thai, Phan Thiet, Tan Thang, Ham Tan, etc. The ingredient of sediments includes quartz sand, mixed sand, sand, and clay, which covers an area of about 1,634 square kilometers. The Pleistocene aquifer has a level of water from 1.5 m to 3.0 m. Experimental pumping results of wells in the Pleistocene aquifer showed that: discharge the wells varied from 0.07 liters to 0.91 liters per second, with an average of 0.31 liters per second; Permeability coefficient was from 1.0m to 2.0m per day.

Table 5. Experimental pumping results of pits and wells in water-poor regions of the Pleistocene aquifer (qp).

Value	Static Water Level (m)	Discharge (l/s)	Draw-down (m)	TDS (g/l)	permeability coefficient (m/ng)
pits					
Maximum	5.50	0.91	4.20	0.77	4.00
Minimum	0.90	0.07	1.11	0.067	0.84
Medium	2.64	0.31	1.73	0.29	1.68
wells					
Maximum	104.0	0.9	33.3	2.05	3.18
Minimum	0.2	0.04	0.09	0.02	0.01
Medium	4.89	0.32	8.00	0.52	0.63

- The test results of the water-pump showed: Average-yield water storage area has water level depth from 0.4m - 66.96m, the value from 3.0m to 6.0m.

Table 6. Experimental pumping results of pits and wells in high yield area of the Pleistocene aquifer (qp).

Value	Static Water Level (m)	Discharge (l/s)	Draw- down (m)	TDS (g/l)	permeability coefficient (m/ng)
Pits					
Maximum	4.10	2.56	2.31	1.69	9.60
Minimum	1.10	1.00	1.04	0.05	0.84
Medium	2.53	1.81	1.69	0.46	3.91
wells					
High	66.96	3.50	18.30	2.16	7.18
Low	0.40	1.00	1.10	0.044	0.167
Moderate	13.88	1.89	8.29	0.32	2.36

The Pleistocene aquifer was mainly super freshwater to freshwater, in some places, it is salt-water (M = 1.69 grams - 2.16 grams per liter). TDS was from 0.044 grams - 2.16 grams per liter, frequent values were from 0.2 grams - 0.5 grams per liter. Water in the Pleistocene aquifer changeed with the seasons, closely related to surface water and rainwater. The results of monitoring at wells HTM4 showed that the water level was highest in September (water depth: 0.23m) and lowest water level in April (water depth: 2.1m). Supply for Pleistocene aquifer was mainly surface water and rainwater. Most of the distributed area of the Pleistocene aquifers of Phan Thiet area was in the salinization. This was an important aquifer to provide domestic water, and social-economic development [16].

3.2. Water quality in Binh Thuan

The analysis results of 1949 water samples of the Holocene aquifer showed that there were 162 Samples beyond the limit. In which the COD indicator has the highest % samples beyond the limit (73.8%), there are 12 indicators % samples beyond the limit (Table 7).

Table 7. Underground analysis results of Holocene aquifer.

Nº	Parameter	Samples	Units	content			Vietnamese Standards: 09/2015/ MONRE	Samples beyond the limit	Samples beyond the limit
				Min	Max	medium			
1	pH	217		5.91	8.39	7.41	5.5 - 8.5	0	0
2	$CaCO_3$	191	mg/l	6.00	1944	110	500	3	1.6
3	TDS	217	mg/l	31.5	49436.0	1110.3	1500	20	9.2
4	Amonium (NH^{4+})	191	mg/l	0.007	0.21	0.06	0.1	40	20.9
5	Cl^-	217	mg/l	2.8	27882.4	542.4	250	36	16.6
6	SO_4^{2-}	191	mg/l	0.12	465.84	18.70	400	1	0.5
7	Total Fe	195	mg/l	0	11.13	0.84	5	3	1.5
8	NO_2	191	mg/l	0.01	1.14	0.06	1.0	1	0.5
9	NO_3	191	mg/l	0.08	68.20	4.61	15	16	8.4
10	COD	46	mg/l	0.00	192.40	31.01	4	36	78.3
11	F^-	8	mg/l	0.049	5.244	1.380	1.0	2	25
12	CN^-	8	mg/l	0.002	0.006	0.003	0.01	0	0
13	Phenol	8	mg/l	<0.001	<0.001	<0.001	0.001	0	0
14	As	8	mg/l	<0.001	0.023	0.001	0.05	0	0
15	Cd	8	mg/l	<0.001	0.002	<0.001	0.005	0	0
16	Pb	8	mg/l	<0.001	0.003	0.001	0.01	0	0
17	Cr^{6+}	8	mg/l	<0.001	<0.001	<0.001	0.05	0	0
18	Cu	8	mg/l	<0.001	0.002	0.001	1.0	0	0
19	Zn	8	mg/l	0.004	0.022	0.013	3.0	0	0
20	Mn	8	mg/l	0.028	0.617	0.173	0.5	1	12.5
21	Hg	8	mg/l	<0.001	<0.001	<0.001	0.001	0	0
22	Se	8	mg/l	<0.001	0.003	<0.001	0.01	0	0
23	E. Coli	3	MNP /100 ml	0	0	0	KPH	0	0
24	Coliform	3		4	1100	735	3	3	100
	Total	**1949**						**162**	

Analysis results of 1459 water samples of Pleistocene aquifer showed that 104 samples exceeded the limit. In which the COD parameter had the highest % of samples exceeding the limit (58.3%), there were 11 parameters that exceed the limit (Table 8). Therefore, the pollution level of the Holocene aquifer was higher than that of the Pleistocene aquifer. Compared with Vietnam standards 09/2015 of the Ministry of Natural Resources and Environment, coastal water quality tends to be salty polluted; The content of SO_4^{2-} and total Iron is higher than the standard.

Table 8. Results of underground analysis of Pleistocene aquifers.

No	Parameter	Samples	Units	Content			Vietnamese Standards: September 2015/Monre	Samples beyond the limit	Samples beyond the limit
				Min	Max	medium			
1	pH	151		5.33	9.77	7.31	5.5 - 8.5	1	0.7
2	$CaCO_3$	146	mg/l	5.00	1616	155	500	5	3.4
3	TDS	151	mg/l	35	6872	507	1500	12	7.9
4	Amonium (NH^{4+})	146	mg/l	0.004	0.21	0.05	0.1	18	12.3
5	Cl^-	151	mg/l	1.8	3483.6	155.2	250	21	13.9
6	SO_4^{2-}	146	mg/l	0.14	325.52	13.27	400	0	0
7	ΣFe	150	mg/l	0	12.68	0.62	5	3	2
8	NO_2	146	mg/l	0.01	1.13	0.06	1.0	1	0.7
9	NO_3	146	mg/l	0.08	290.40	13.07	15	23	15.8
10	COD	24	mg/l	0.06	51.30	10.85	4	14	58.3
11	F^-	8	mg/l	0.049	0.451	0.154	1.0	0	0
12	CN^-	8	mg/l	0.001	0.003	0.001	0.01	0	0
13	Phenol	8	mg/l	<0.001	<0.001	<0.001	0.001	0	0
14	As	8	mg/l	<0.001	0.003	<0.001	0.05	0	0
15	Cd	8	mg/l	<0.001	0.001	<0.001	0.005	0	0
16	Pb	8	mg/l	<0.001	0.001	<0.001	0.01	0	0
17	Cr^{6+}	8	mg/l	<0.001	0.001	<0.001	0.05	0	0
18	Cu	8	mg/l	<0.001	0.001	0.001	1.0	0	0
19	Zn	8	mg/l	0.005	0.055	0.024	3.0	0	0
20	Mn	8	mg/l	0.009	0.885	0.168	0.5	0	0
21	Hg	8	mg/l	<0.001	0.001	<0.001	0.001	0	0
22	Se	8	mg/l	<0.001	<0.001	<0.001	0.01	0	0
23	E. Coli	3	MNP	4	1100	521	KPH	3	100
24	Coliform	3	/100ml	93	1100	764	3	3	100
	Total	**1459**						**104**	

3.3. Saline Boundary

The analysis results of 24 parameters in Table 10 and Table 11, it shows that salinization of Holocene and Pleistocene aquifers has occurred. The Holocene aquifer has 20 saline samples, accounting for 9.2% of the total samples analyzed (Table 7). The Pleistocene aquifer has 12 samples that have exceeded the limit, accounting for 7.9% of the total samples analyzed. Thus, the saline level of the Holocene aquifer is higher than that of the Pleistocene aquifer.

One cause of salinization of aquifers in Binh Thuan province is that titanium mining enterprises have used sea water to select ore, seawater has infiltrated aquifers qh, qp. In addition, it is also contaminated with mineral oil and radiation (α, β), organic and bacteria [16]. From the resistivity survey results and sample analysis results (Table 7, Table 8), we have determined the saline intrusion boundary of Binh Thuan province. The saline boundary has $M \geq 1$g/l. In addition, at the saline sites, there were saline concentrations higher than 1g/l, which were outside this saline boundary (Figure 6).

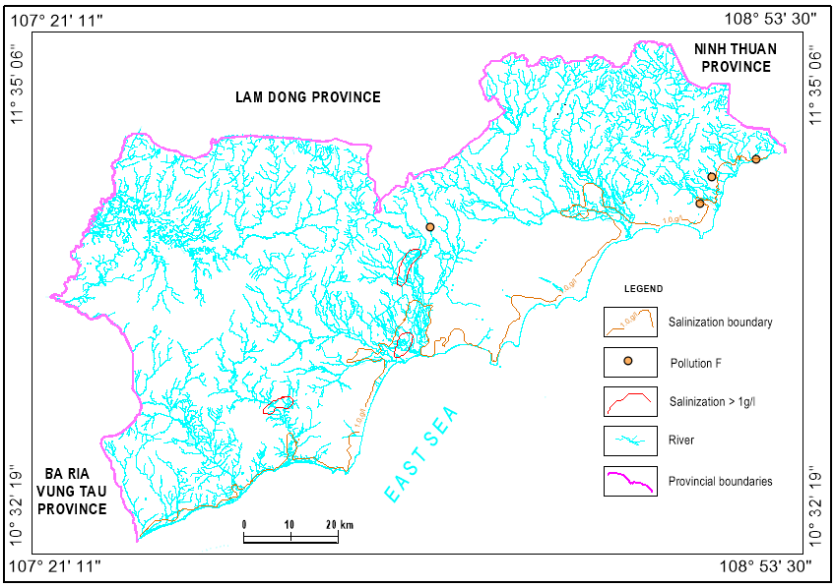

Figure 6. Map of groundwater pollution in Binh Thuan province.

3.4. Sustainable development of water resources solutions for Binh Thuan province

Domestic water shortage in Binh Thuan province often occurs in the dry season, in some areas people have to buy freshwater. Currently, Binh Thuan province also has no solution. Based on the Study of the characteristics of aquifers in Binh Thuan province, the authors have identified areas with water storage capacity (qp aquifer). These aquifers are distributed in Tuy Phong, Phan Thiet, Ham Tan.

Refer to the experience of some countries around the world [17–20]. The study has proposed solutions for sustainable development of water resources for Binh Thuan province as follows:

3.4.1. Planting forests to increase cover, prevent soil erosion, increase water storage capacity

- Planting forests to keep the land and prevent erosion

Experiments have proven that the force of rainwater falling on the forested area is much weaker than in the non-forested area due to the barrier of the forest canopy. Research results have also shown that the level of erosion in non-forested areas is 30 to 35 times higher than in forested areas.

- Forest canopy contributes to reducing floods and droughts

In places where there is no forest, when it rains heavily, the soil is eroded by rainwater, filling upriver beds and stream beds. When water does not drain in time, it overflows into low-lying areas causing flooding. Where there is no forest, the soil cannot hold water causing drought. In the dry season, the streams in Binh Thuan no longer have water, people dig holes in the stream bed but there is no water.

- Forests contribute to the protection of groundwater resources.

Rainwater falling into the forest will be partially retained and gradually wetted down to the soil and rock layers, forming underground flows, then flowing down to the low places to form rivers and streams. It is an important source of water for domestic and agricultural uses. Thus, forests not only reduce drought, but also protect groundwater.

3.4.2. Saving water in agricultural production such as drip irrigation, sprinkler irrigation

This is a highly effective method of Saving water. This method has been successfully applied in many countries around the world, such as Israel. Binh Thuan province is applying this method to agricultural production (Figures 7a-7b).

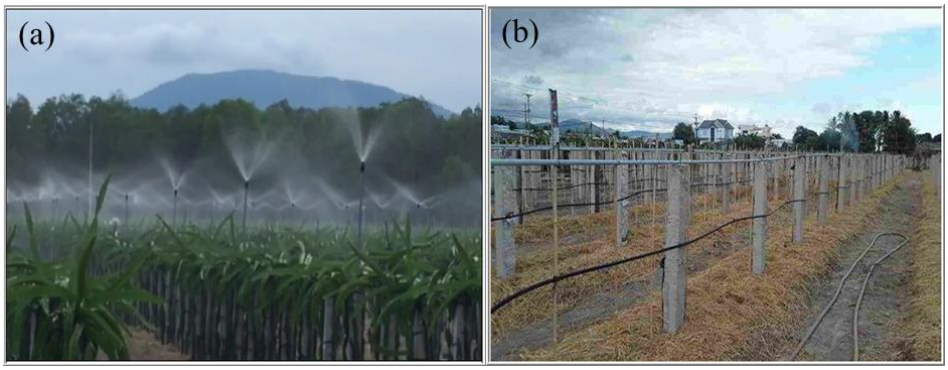

Figure 7. Save water in agricultural production: a) Sprinkler irrigation; b) Drip irrigation.

3.4.3. Not licensed to mine Titan in the coastal area

Binh Thuan is a province located in the drought areas of Vietnam. In the dry season, people often suffer from water shortages. Titan ore is distributed mainly along the 192 km coastline, located in the sand layers, with a total area of about 782 km^2. Distribution depth titanium ore from 30-50 m [21]. Mining titan consumes a lot of water. According to calculations, taking titanium ore in 1m^3 of sand requires 2 m^3 of water. If mining titan huge impact on people's lives and economic sectors (agriculture, tourism, Commerce, wind electricity, forestry). Therefore, not licensed to mine Titan is necessary work.

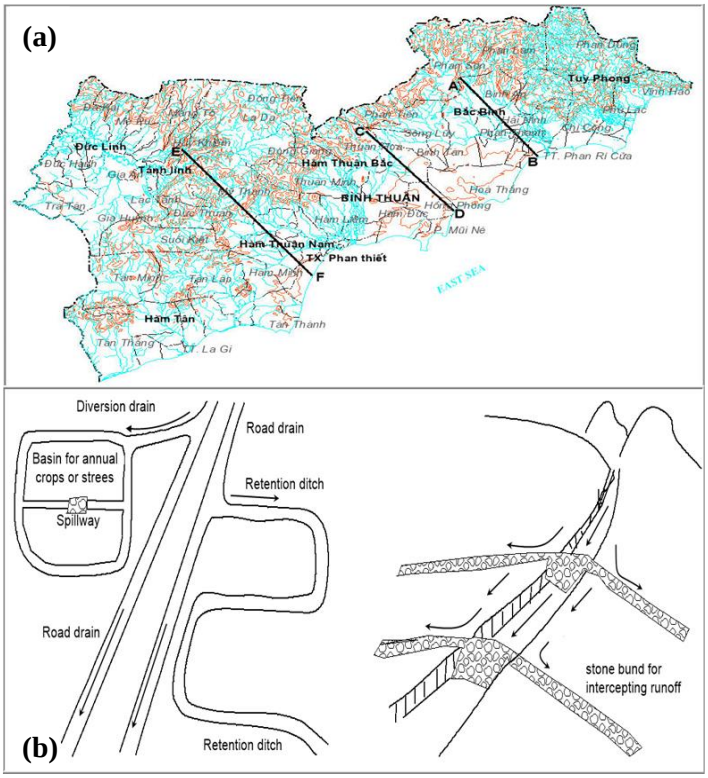

Figure 8. Lead rainwater along with the lines AB, CD, EF and store into the rainwater reservoir, do not allow water flows into the East Sea.

3.4.4. Build water storage, do not allow water flows into the sea

This is a model that has been successfully applied in the world [17–18, 21]. When the rainy season comes, many areas of Binh Thuan province are flooded (Ham Thuan Bac district, Tanh Linh district). We have studied geology, geomorphology, hydrogeology, structure of aquifers to come up with a plan to build water storage (on the face and under the ground).

Build concrete dam rainwater collection, prevents rainwater flow into the sea, preventing the salinization of seawater into the continent. We have designed for rainwater to flow along lines AB, CD, EF (Figure 8a). The water storage (Figure 8b) is arranged in appropriate positions on both sides of the axes AB, CD, and EF. That is the systems of rainwater retaining wall, reservoir rainwater, do not allow water flows into the East Sea.

3.4.5. Water replenishment for aquifers

The water replenishment for aquifers has been developed in several countries around the world [19–20]. The reference to the literature and the combination of our research results are

the basis for us to choose the appropriate positions. Water replenishment was rainwater. Areas were selected based on the following conditions:

- Determine the permeability coefficient of the soil cover on the topographic surface in the selected areas for water storage.
- Check the wetting ability of the unsaturated zone and check for the existence of tarnished areas in the unsaturated zone that may adversely affect the water quality.
- Check the water transmission capacity of aquifers.
- Field investigation of geology, hydrogeology, geochemistry to select the distribution areas of surface sediments with high permeability coefficient in Binh Thuan. The results of Field investigation geology, hydrogeology determined that the sand strip at the seaside distributed from Phan Ri to Ham Tan - Binh Thuan, has satisfied the above conditions. These are suitable areas for the arrangement of construction systems that add rainwater to the qp aquifer. Rainwater is added to underground aquifers in the following manner:
- Create a rainwater reservoir at a location with a permeability coefficient of 2-7 m/day, rainwater will seep through the sand layers to the qh underground aquifer.
- Collect rainwater in the drainage ditch and put it in a suitable location to add rainwater for the underground aquifer (Figure 9).

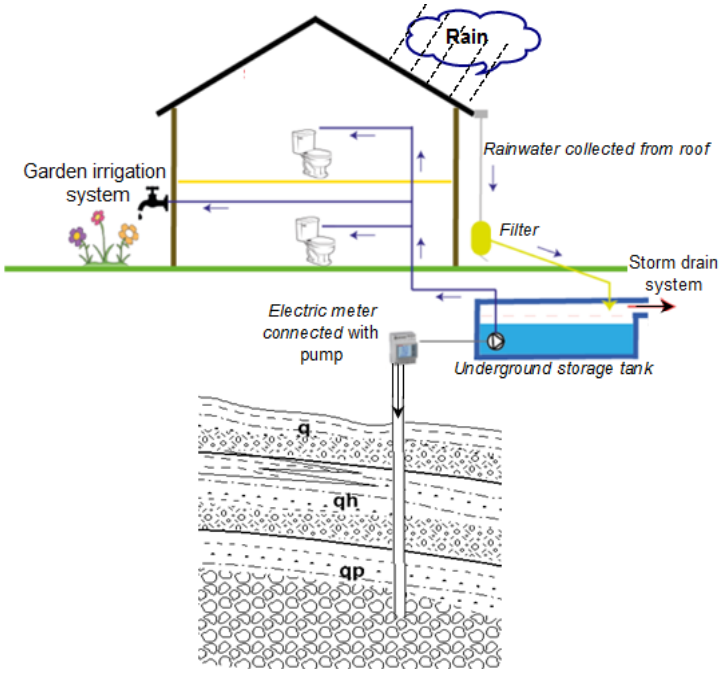

Figure 9. Rainwater collection for domestic water use and addition to aquifer qp.

- Build underground storage tanks under buildings for rainwater collection and add rainwater to the aquifer with wells (Figure 10).

According to [18], rainwater is collected into underground storage tanks, which then provides for the needs of use water in buildings. We recommend that it is necessary to design boreholes and an additional water pump to the qp aquifer (Figure 8 and Figure 9).

3.4.6. The subsurface dam method.

This method has been applied in some countries around the world such as India, Japan. In Vietnam, the model of an underground dam on sand, preventing water loss has been successfully built in My Thanh (Binh Thuan). The underground dam was made of bentonite soil cement with a length of 370m, a depth of 5m to 9.5m, forming a cobblestone tank with a capacity of nearly 200,000 m^3, ensuring the operation of My Thanh water plant for 3 months in the dry season [19, 21].

From this model, it can be extended to similar areas in the territory of Vietnam. In addition, it is possible to build a sand barrier dam at the foot of the coastal dunes of Binh Thuan province. This sand barrage traps rainwater contained in the sand layer and prevents seawater infiltration (Figure 10).

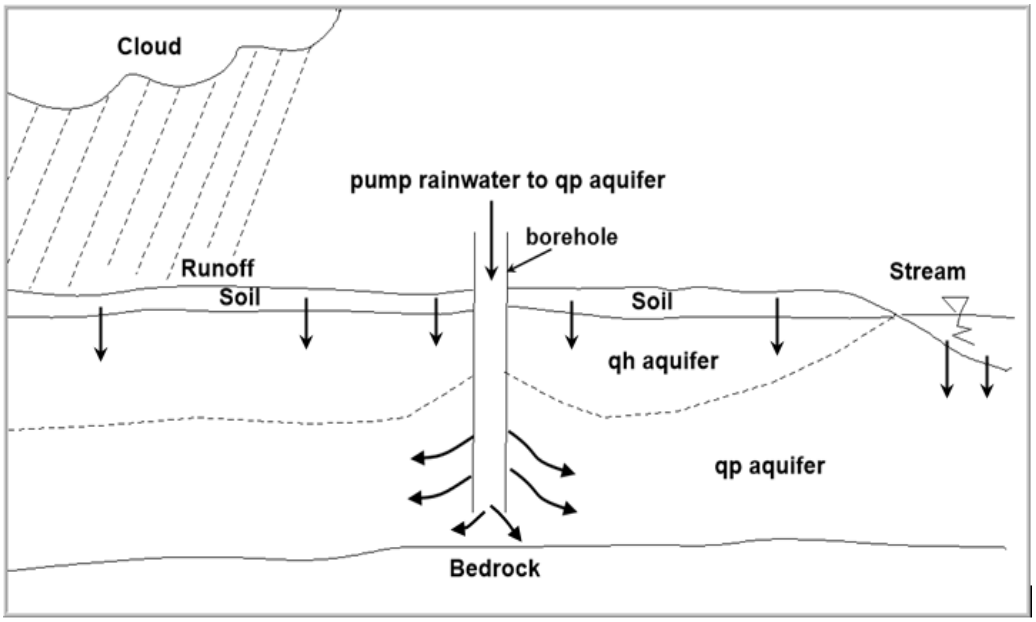

Figure 10. Rainwater addition to aquifer qp.

3.4.7. Sand dam

Binh Thuan province has many rivers. In the dry season, they have no water. The sand dam can be built for water storage. This model has been present in many countries around the world such as India, South Africa, Kenya (Figure 11).

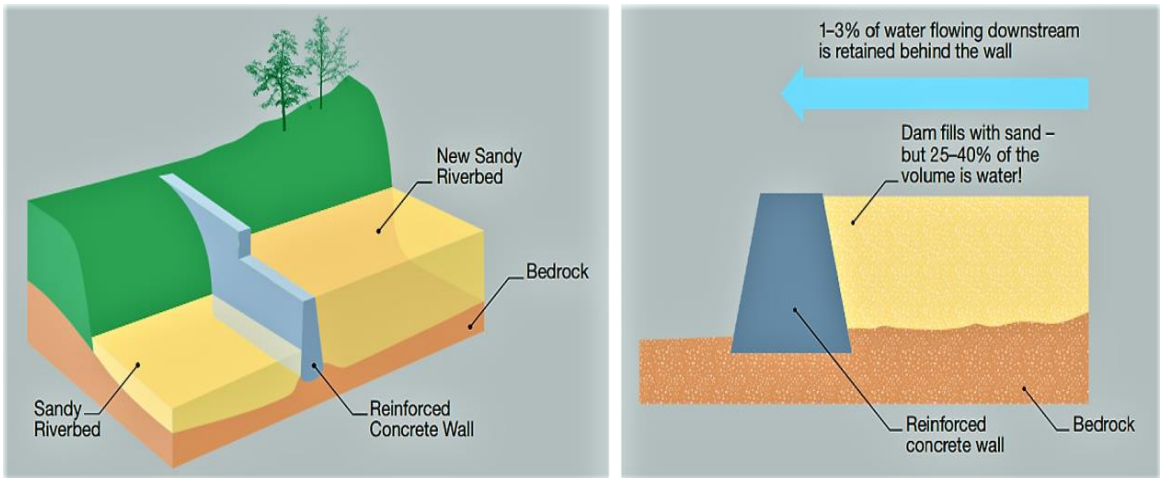

Figure 11. Left: Schematic cross-section of a sand dam. Right: Sand accumulates until the dam is completely full of sand up to the spillway. Water is stored within the sand, protected and filtered, making up to 40% of the total volume [19].

3.4.8. Manufacturing seawater purifier

Vietnam has successfully made seawater purifier into freshwater, power reached 91 million liters of fresh water per day, named “Made in Vietnam”. Vietnam has exported seawater purifiers to Saudi Arabic. We also made this device, power from 400 m^3 to 600m^3 per day [20] (Figure 12). Seawater purifier has been installed in Binh Thuan, Ben Tre, and Can Tho provinces. The defect of this device is the high price.

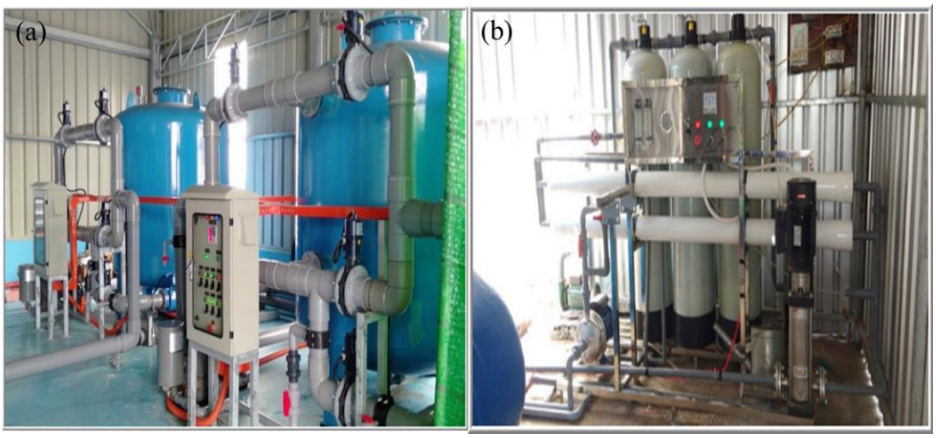

Figure 12. Seawater purifier [20].

4. Conclusions

Binh Thuan is the place with the least distribution of rainfall compared to other regions in the territory of Vietnam. The groundwater of Binh Thuan province is taken from Quaternary sediments and these aquifers have been polluted. Currently, the process of salinization into aquifers qh and qp is taking place strongly and tends to increase. Groundwater is mainly taken from qh and qp aquifers, some places have been polluted. The reserves of these two aquifers are not large because the aquifer has a thin thickness (from 3-5m to 30-50m). Water resources of Binh Thuan province are at high risk of being contaminated with mineral oil, radioactive (α, β), organic, bacterial, and salinity. Binh Thuan province often suffers from water shortage in the dry season and is at high risk of pollution. The authors' recommendations on mitigating water shortages were applied in Binh Thuan province. The collection of rainwater has been used, and at the same time, pumping rainwater into the qp aquifer, underground dam method, sand dam construction, construction of a rainwater drainage system in the Northwest - Southeast direction, increasing the mobility of water. Solutions for sustainable development of water resources not only help Binh Thuan province but also can be applied well to other provinces in the territory of Vietnam. The article studies the highly significant risk of groundwater pollution and provides an assessment of the possibility of groundwater pollution to have appropriate solutions to ensure sustainable development.

Authors contribution: Constructing research idea: H.P., T.T.M.H.; Select research methods: H.P; Data processing: H.P., T.T.M.H.; Sample analysis: H.P., T.T.M.H.; Take samples: H.P., T.T.M.H.; Writing original draft preparation: H.P., T.T.M.H.; Writing review and editing: H.P., T.T.M.H.

Acknowledgments: This study was carried out under the sponsorship of the Binh Thuan main Rivers Water Quality Research Project, under the Institute of Environmental & Circular Economy Sothern_ IECES.

Conflicts of interest: The authors declare that this article was the work of the authors, has not been published elsewhere, has not been copied from previous research; there was no conflict of interest within the author group.

References

1. Ardau, F.; Balia, R.; Barbiere, G.; Barocu, G.; Gavaudo, E.; Ghilieri, G.; Vernier, A. Geophysical and hydrogeological studies in a coastal plain affected by salt water intrusion: SAGEEP 2000. *Conf. Proc*. **2000**, 223–231.
2. Khanh, V.T. at al. Report on the results of underground water planning in the dunes at the seaside Binh Thuan in the period 2005 - 2010. 2006.

3. Khuyen, N.M. Study on formation characteristics of groundwater at river catchment at the seaside Ninh Thuan and Binh Thuan. Ph.D. thesis, National Library Archives, 2015.
4. People's Committee of Binh Thuan province. Zoning distribution and protect groundwater resources at the seaside in Binh Thuan province, vision to 2030, 2021.
5. DGMVN (Department of Geology and Minerals of Vietnam) 2012-2013. Results of groundwater monitoring in Binh Thuan province.
6. Thanh, L.N. et al. Coastal pollution at the site titanium exploitation in Thien Ai area, Bac Binh district, Binh Thuan province, 2011.
7. Department of Jobs, Precincts and Regions © 2021. Online avaliable: https://agriculture.vic.gov.au/farm-management/.
8. Francis Shaxson and Richard Barber. Food and Agriculture Organization of the United Nations Rome (FAO). Optimizing soil moisture for plant production. FAO Soils Bulletin, 2003, 79, pp. 107. https://doi.org/10.1007/978-3-319-75115-3_18.
9. Online avaliable: https://vikaspedia.in/energy/environment/rainwater-harvesting-1/rain-water-harvesting-techniques-to-augment-ground-water.
10. Online avaliable: https://washmatters.wateraid.org /Report - Rainwater harvesting for recharging shallow groundwater.
11. Hamilton, L.S. Forests and water. Food & Agriculture Organization of the United Nations (FAO), 2005, pp. 94.
12. N-Cerwass. Research on groundwater exploitation in the South Central Coastal Provinces Socialist Republic of Vietnam, 2009.
13. Pacey, A.; Cullis, A. Rainwater harvesting - the collection of rainfall and runoff in rural areas. IT Publications, London, 1986, 8(1), 119–120.
14. DGMVN (Department of Geology and Minerals of Vietnam). Mineral Resources of Binh Thuan Province, 2006.
15. Online avaliable: https://www.fao.org/
16. Misra, A.K. Rainwater Harvesting and Artificial Recharge of Groundwater, 2019.
17. Online avaliable: https://sswm.info/es/sswm-solutions-bop-markets/.
18. Dung, N.Q. Research and build model of rainwater collection, hosted, anti-loss groundwater for living and production in Ninh Thuan, Binh Thuan regions, 2018.
19. ED (n.y). Pioneers of Sand Dams. Brentford: Excellent development (ED), 1984-2011. Online avaliable: https://sswm.info/sites/default/files/reference_attachments/ED%20Editor%20ny%20Pioneers%20of%20Sand%20Dam.pdf.
20. Phu, H.; Dong, D.V. The salinization water treatment works for breeders with a power of 400- 600 m^3/day. CP Vietnam Joint Stock Company in Ninh Thuan and Bac Lieu, 2020.
21. Phu, H. Project "Making a list of water sources and establishing water resource protection corridors in Binh Thuan province to manage, exploit, use and protect water resources". (Phu My Institute for Environmental Technology and Water Resources Development), 2022.

JOURNAL OF
HYDRO-METEOROLOGY

Research Article

The trend of erosion and accretion of the western coast of the Mekong Delta, the section from Ca Mau Cape to Kien Giang

Duyen Chau My Nguyen[1], Vy Huynh Thuy Duong[1], Long Ta Bui[1]*

[1] Faculty of Environment and Natural Resources, University of Technology, Vietnam National University, Ho Chi Minh City; nguyenduyen91@hcmut.edu.vn; vy.duonghthuyvy@hcmut.edu.vn; longbt62@hcmut.edu.vn

*Correspondence: longbt62@hcmut.edu.vn; Tel.: +84–918017376

Received: 8 January 2024; Accepted: 06 February 2024; Published: 25 March 2024

Abstract: Natural processes and human-caused activities, including coastal erosion, constantly threaten coastal areas. This phenomenon is dangerous because the permanent loss of land leads to the transformation of the coast. In recent years, coastal erosion has become increasingly complicated in the Mekong Delta, especially in the western coastal area of Cape Ca Mau. This study aims to provide updated results of the changing trend of accretion/erosion of the coastline from Cape Ca Mau to Kien Giang in 2021-2023. Specifically, the rate and area of erosion/accretion considered. Remote sensing and GIS tools are used. As a result, in Ngoc Hien district, Ca Mau, the erosion rate is 55.66 m/year, and the erosion area is 47.21 hectares, ranking highest compared to other districts in the same study area. The results also show that the Kien Giang coastal area has a more moderate erosion process than the accretion process. In contrast, on the coast of the Ca Mau Cape area, the erosion and accretion process are complexly interwoven, especially in the Dat Alluvial Plains area Cape - Ngoc Hien (Ca Mau).

Keywords: Coastal erosion; Landsat8 OLI/TIRS; GIS; Mekong Delta; Ca Mau - Kien Giang.

1. Introduction

Coastal erosion is one of the important issues in coastal management. To adapt to it and prevent it where possible and necessary, it is important to recognize the spatial and temporal scale of the phenomenon as well as its causes [1]. The coastal environment constantly changes due to human activities and various physical processes. This increases environmental degradation, including erosion or accretion along many coastal areas. Coastlines are predicted to face unprecedented pressure this century as climate change causes changes in sea levels, storm patterns, waves, and tides. This forecast of increasing pressure is driving a reassessment of current coastal management practices [2–6]. Due to the special importance of the Mekong Delta to world food security, accretion, erosion, and land loss in this area are the subject of many studies [7, 8].

The decrease in sediment is considered an essential factor causing coastal erosion in the Mekong Delta today [9]. However, human activities cannot be ruled out; for example, sand mining at the river bottom can lead to currents, changing sediment deposition [10]. Mud and sand are trapped behind dams, leading to a decrease in coastal sediment supply, which is considered the overarching cause of decreased sediment supply to the coast, leading to coastal erosion [11–13]. To evaluate hydrodynamics and sediment transport, 2- and 3-dimensional models have been used [14–17]. These studies have focused on clarifying sediment's seasonal distribution and mud dependence on meteorological,

hydrological, oceanographic, tide, wave, and storm surges. To evaluate the scope and extent of sedimentation and erosion processes as well as determine the concentration of suspended matter (SPM) over time, remote sensing methods have been used [18]–[21]. The modelling and remote sensing approaches have highlighted how the fine sediment dynamics and morphology of major tropical deltas, such as the Mekong River, will respond to changing flow influences and coastal zones.

In this study, the Cape Ca Mau - Kien Giang (CM-KG) area of the Mekong Delta - located in the southwest of Vietnam with a coastline of more than 340 km, was selected. Here, many riverbank and coastal erosion occur every year and are on the rise [9]. The results of remote sensing image analysis in 2016-2020 show that the erosion trend has increased rapidly in the study area [22–25]. The CM-KG area has a shore retreat speed and ocean advance speed of -9.8 m/year and +24.3 m/year, with an average speed of 0.7 m/year. Erosions occurred strongly in 2018-2020, reflected in the area of land loss, increasing 2.7 times (from 250 hectares to 617 hectares) compared to 2016-2018. In 2016-2018, the area of accretion was up to 1122 hectares; however, by 2018-2020, the accretion area had decreased nearly ten times [26].

There have been many studies around the world using remote sensing image data to classify soil water from multi-temporal satellite images and then overlay them to identify and evaluate shoreline changes [27–29]. Specifically, the study [30] used Landsat 3, 5 and 8 images to create maps, calculate the rate of shoreline change in the Kanyakumari area - the southern boundary of India, located in Tamil Nadu and predict the period 2030-2040. The study [31] initial data was obtained from 1:25,000 topographic maps and multi-temporal satellite images (2006-2015) downloaded from the Google Earth archive focusing on the Kuwaru coastal area south of Yogyakarta special region facing the Indian Ocean. The study [4] the period (1990-2016) was analysed using Landsat 5, 7, and 8 images. The study focused on long-term coastal erosion analysis of the entire Karnataka coast. In Vietnam, research related to shoreline changes is of special interest. The study [32] Landsat seven images from 2001 to 2017 were used to evaluate Ca Mau coastal coastline changes using the Alesheikh ratio method (2006). The study [33] used the ENVI 4.7 tool to process remote sensing images and evaluate changes in the East and West coasts of Ca Mau. The study [34] researched using Landsat 8 images to assess changes in the Cua Dai coastline in 2016-2021 with a shoreline extraction technique based on two indices: AWEI index (*Automatic Water Extract Index*) and NDWI (*Normalization Differentiation Water Index*) and shoreline change calculation technique DSAS (*Digital Shoreline Analysis System*) [35].

In the above context, based on updated satellite data and remote sensing methods, this study clarified the sedimentation and erosion trends in the Western region - taking the coastal area of Ca Mau province - Kien Giang as a research case study. This study aims to clarify the range of accretion/erosion levels in the selected area, 2021-2023, using the integrated DSAS method, remote sensing, and GIS. The novelty of this research topic is reflected in the choice of research area and updated data. Previously, the west coast from Cape Ca Mau to Kien Giang was rarely chosen for a separate study. Meanwhile, the shoreline fluctuations in Dat Mui, Vien An (Ngoc Hien district), and Dat Moi (Nam Can district) communes are complicated by continuous sedimentation and erosion. The results show that applying remote sensing and GIS to assess shoreline changes is feasible and effective.

2. Materials and Methods

2.1. Study area

The research area is from Ngoc Hien district - Ca Mau, stretching to Ha Tien - Kien Giang. This area belongs to the Mekong Delta, mainly delta, with large estuaries and interlaced canals divided into ten sections corresponding to five Kien Giang and five districts of Ca Mau (Figure 1). Districts in Kien Giang province include Ha Tien-Kien

Luong, Hon Dat, Rach Gia, An Bien, and An Minh. Districts in Ca Mau province include U Minh, Phu Tan, Tran Van Thoi, Nam Can and Ngoc Hien.

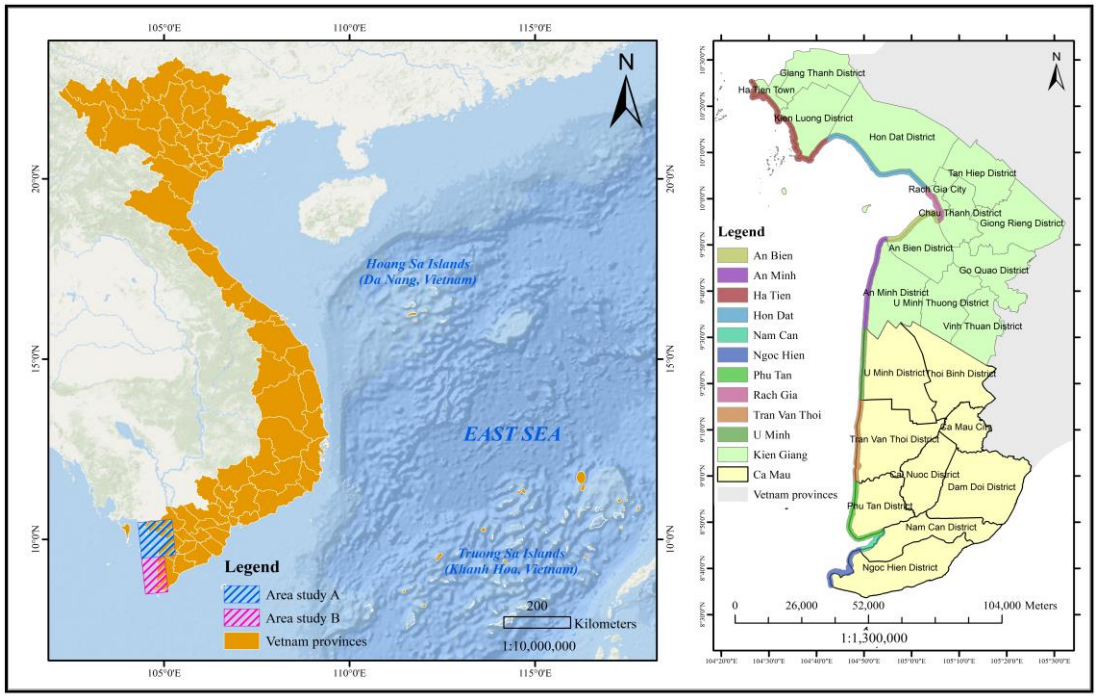

Figure 1. Study location map Ca Mau Cape - Kien Giang.

2.2. Data

The remote sensing images used in this study are Landsat8 OLI/TIRS Collection 2 Level 1 images from the Landsat 8 satellite launched on April 10, 2013. The United States Geological Survey - U.S. Geological Survey (USGS) provided the image free of charge from the website https://earthexplorer.usgs.gov/. Landsat8 OLI/TIRS Collection 2 Level 1 satellite images were taken in 11 image channels with different wavelengths and resolutions. However, the study only uses five image channels with a resolution of 30m × 30m, processed according to the WGS-84 UTM reference system, applied to area 49. Image interpretation results help evaluate erosion developments over time according to erosion area and distance parameters (Table 1). The satellite's imaging cycle is 16 days; a reasonable time to choose images is during the dry season months, with little rain and little cloud cover (Table 2).

Table 1. OLI and TIRs sensor characteristics of Landsat 8 satellite images [36].

Bands	**Wavelength** (micrometers)	**Resolution** (meters)
Band 1 - Coastal aerosol	0.43-0.45	30
Band 2 - Blue	0.45-0.51	30
Band 4 - Red	0.64-0.67	30
Band 5 - Near Infrared (NIR)	0.85-0.88	30
Band 7 - Shortwave Infrared (SWIR) 2	2.11-2.29	30

Table 2. Image data used in the study.

Year	**Day/month**	**Data set name**
2021	04/03	LC08_L1TP_126053_20210304_20210312_02_T1
	21/04	LC08_L1TP_126054_20210421_20210430_02_T1
2022	02/01	LC08_L1TP_126053_20220102_20220106_02_T1
	18/01	LC08_L1TP_126054_20220118_20220123_02_T1
2023	06/02	LC08_L1TP_126053_20230206_20230209_02_T1
	10/03	LC08_L1TP_126054_20230310_20230320_02_T1

2.3. Methods and implementation steps

In recent decades, remote sensing technology has developed rapidly as a tool to collect geospatial and atmospheric data with applications ranging from geoscience to economics. Currently, several methods are used to analyze coastline change, of which the Digital Shoreline Analysis System (DSAS) is considered an effective and widely used tool [31]. DSAS can integrate with ArcGIS software to analyze geographic information and calculate shoreline change rates in space and time. DSAS supports ArcGIS software to calculate the shoreline change rate over time by creating transect lines orthogonal to the set distance, thereby calculating the resulting shoreline change rate and matching the statistics in the attribute table. The distance between the transects is set, and the transects are constructed perpendicular to the Baseline baseline. The combination of DSAS and satellite images has been applied to several studies by [32–34]. Classifying surface cover types and analyzing changes is one of the most common applications of remote sensing. One of the most basic classification tasks is distinguishing water bodies from dry land surfaces. Landsat images are one of the most widely used data sources in remote sensing of water resources. The Automated Water Extraction Index (AWEI) was introduced to improve classification accuracy in areas with dark surfaces that other classification methods often fail to classify accurately [37]. The NDWI index (Normalized Difference Water Index - normalized difference water index) is often used to detect and distinguish areas with surface water from other objects [38]. In this study, the main steps include:

Step 1: After downloading and decompressing remote sensing images, they are inserted into ENVI 5.2 software to standardize the images. Convert the numerical values on the image to the value of physical radiation at the sensor. Then, the values of physical radiation at the sensor are converted to the value of reflection in the upper atmosphere of the object (object). AWEI calculation is essential to highlight land and water objects. Then, export the file in .tiff format and import it into ArcGIS to digitize the shoreline of the study area at the same scale. The result is to extract the shoreline for each year of study [25, 26].

Step 2: Use the DSAS tool to analyze accretion/erosion rates under the changes of the extracted shorelines. Calculate the distance and area of accretion/erosion over each year. Calculating and analyzing the shoreline is carried out as follows: Determine the baseline and calculated shorelines; Create transect lines perpendicular to the shore; Calculate the rate of shoreline change. Based on the collected data, the start-end rate (EPR) method was chosen to analyze the results. Formulas used: [25, 26]

EPR = Rate of change/ Total time to monitor changes (m/year)

where the rate of change is the distance between two coastlines, the total time of monitoring changes is the time between the oldest and newest coastlines [21].

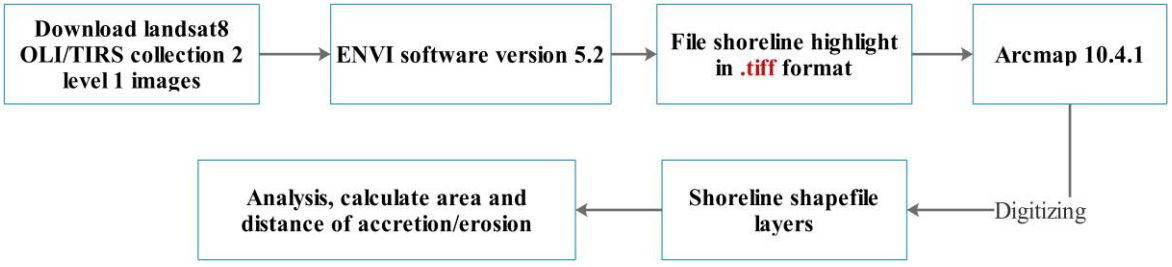

Figure 2. Study structure diagram.

3. Results and discussion

The area selected is a new land deposited by alluvium, formed by two ocean currents in the East Sea and the Gulf of Thailand, receiving alluvium from the Mekong River. The area is plain, has many rivers and canals, is a low, flat terrain, and is often flooded. The average height is 0.5m to 1.5m above sea level. The terrain direction gradually tilts from North to

South, from Northeast to Southwest. U Minh and Tran Van Thoi low-lying areas are inland "hanging depressions" limited by natural dikes of the Ong Doc, Cai Tau, and Trem river systems and high land edges along the West Coast. This hanging depression stagnates water all year round and becomes a swamp. The study of shoreline delineation and segmentation is shown in Figure 3; the results are analyzed and discussed in subsections.

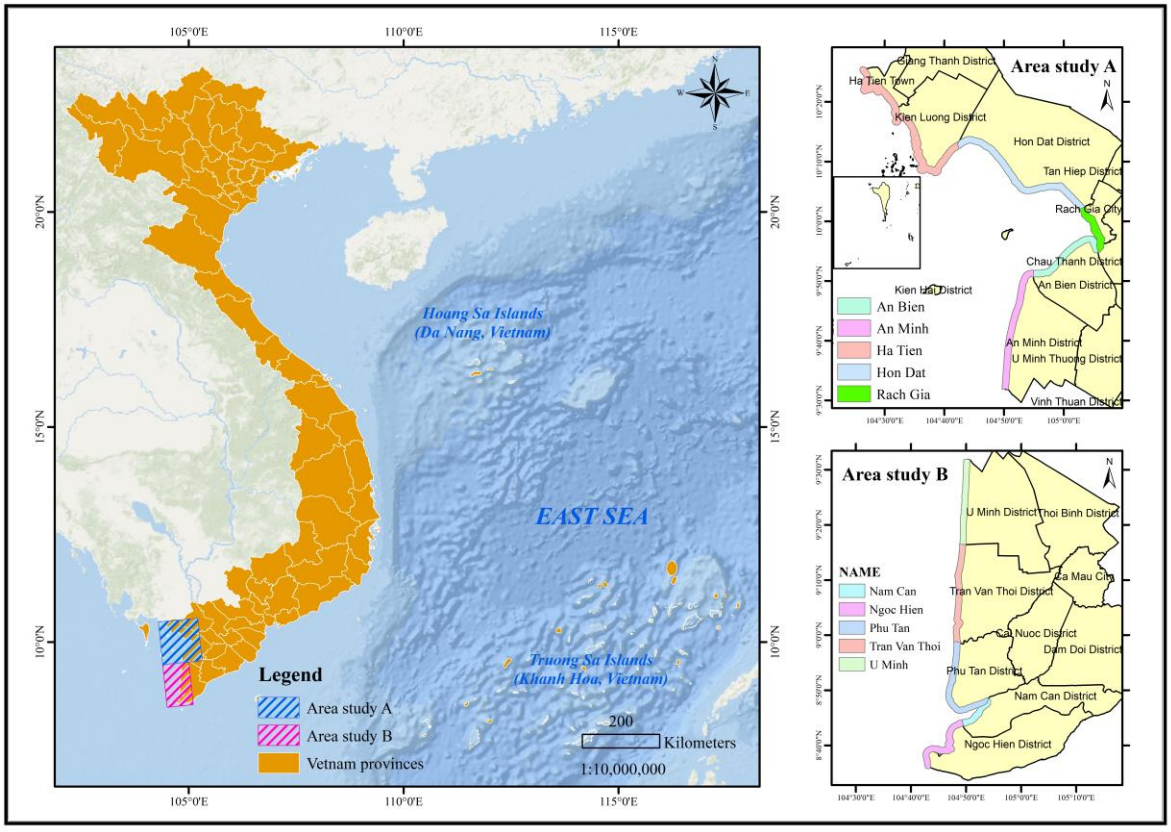

Figure 3. Delineation of the shoreline of typical accretion/erosion areas in Ca Mau - Kien Giang provinces in the period 2021-2023.

3.1. The accretion/erosion at Ha Tien - Kien Luong - Hon Dat districts

In Ha Tien - Kien Luong, in the period 2021-2022, the accretion/erosion rate is 18.08 m/year and 42.08 m/year, respectively, and the accretion/erosion area is 12.79 ha and 36.01 ha, respectively. In 2022-2023, the accretion/erosion rate is 11.34 m/year and 32.30 m/year, and the accretion/erosion area is 18.71 ha and 30.16 ha, respectively. In 2021-2023, the accretion/erosion rate is 11.16 m/year and 41.14 m/year, and the accretion/erosion area is 22.79 ha and 32.71 ha, respectively. Based on Figure 4A, the area of Binh An - Kien Luong commune is an erosion area.

At Hon Dat, in 2021-2022, the accretion/erosion rate is 19.49 m/year and 28.06 m/year, respectively, and the accretion/erosion area is 30.68 ha and 5.58 ha, respectively. In 2022-2023, the accretion/erosion rate is 18.56 m/year and 15.55 m/year, and the accretion/erosion area is 2.20 ha and 3.51 ha, respectively. In 2021-2023, the accretion/erosion rate is 17.60 m/year and 27.80 m/year, and the accretion/erosion area is 30.46 ha and 6.64 ha, respectively. Figure 4B clearly shows the erosion area in the Binh Giang and Binh Son commune. The results also show that between 2021-2022 and 2022-2023, the erosion rate will decrease, most clearly occurring in the area of Binh Giang commune and Binh Son commune; erosions only appear in Binh An commune. Some accretion locations are 2021-2022, accretion in Son Kien commune, and 2022-2023 in Binh Son commune (Figure 4C). The variation in accretion/erosion area is shown in Figure 4D.

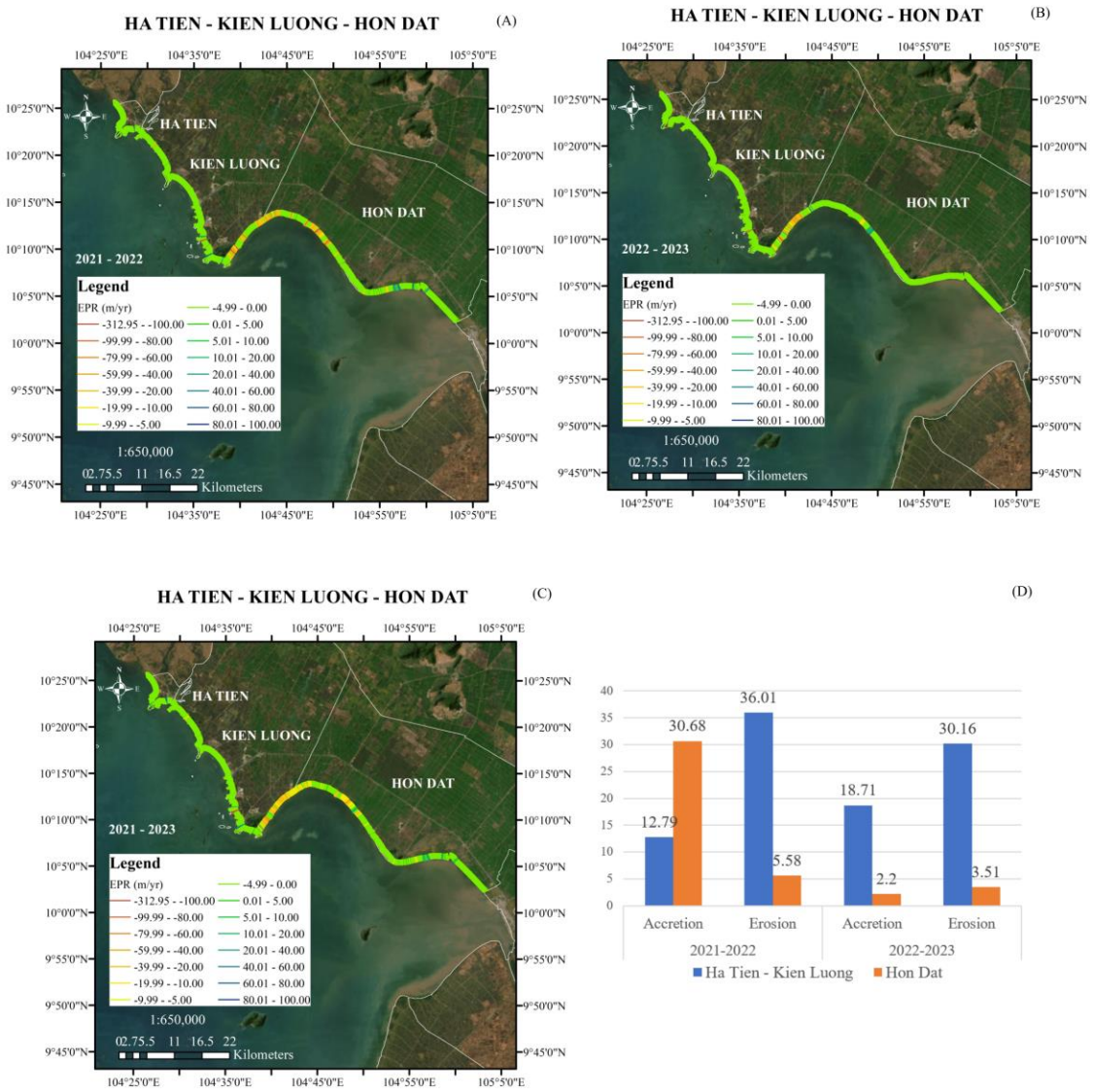

Figure 4. Map and chart showing erosion/accretion rate in TX. Ha Tien, Kien Luong, Hon Dat districts.

3.2. The accretion/erosion at Rach Gia - An Bien districts

In Rach Gia, in 2021-2022, the accretion/erosion rate is 11.16 m/year and 23.58 m/year, and the accretion/erosion area is 12.87 ha and 15.93 ha, respectively. In 2022-2023, the accretion/erosion rate is 16.43 m/year and 21.26 m/year, and the accretion/erosion area is 15.02 ha and 7.09 ha, respectively. In 2021-2023, the accretion/erosion rate is 15.40 m/year and 29.04 m/year, and the accretion/erosion area is 21.68 ha and 17.93 ha, respectively.

In An Bien, in 2021-2022, the accretion/erosion rate is 0.49 m/year and 42.94 m/year; the accretion/erosion area is 5.05 ha and 27.92 ha, respectively, Figure 5A. In 2022-2023, the accretion/erosion rate is 10.24 m/year and 24.96 m/year, and the accretion/erosion area is 9.39 ha and 17.24 ha, respectively. In 2021-2023, the accretion/erosion rate is 6.74 m/year and 26.27 m/year, and the accretion/erosion area is 9.21 ha and 29.59 ha, respectively. Based on Figure 5B, the Tay Yen commune area is an erosion area. The results show that the erosion rate will decrease between 2021-2022 and 2022-2023, most clearly in the Tay Yen - An Bien commune area. Some locations have accretion changes, such as erosions in 2021-2022 in An Hoa ward and accretion in 2022-2023. In Rach Soi ward, erosion has continuously increased over the years (Figure 5C). The variation in accretion/erosion area is shown in Figure 5D.

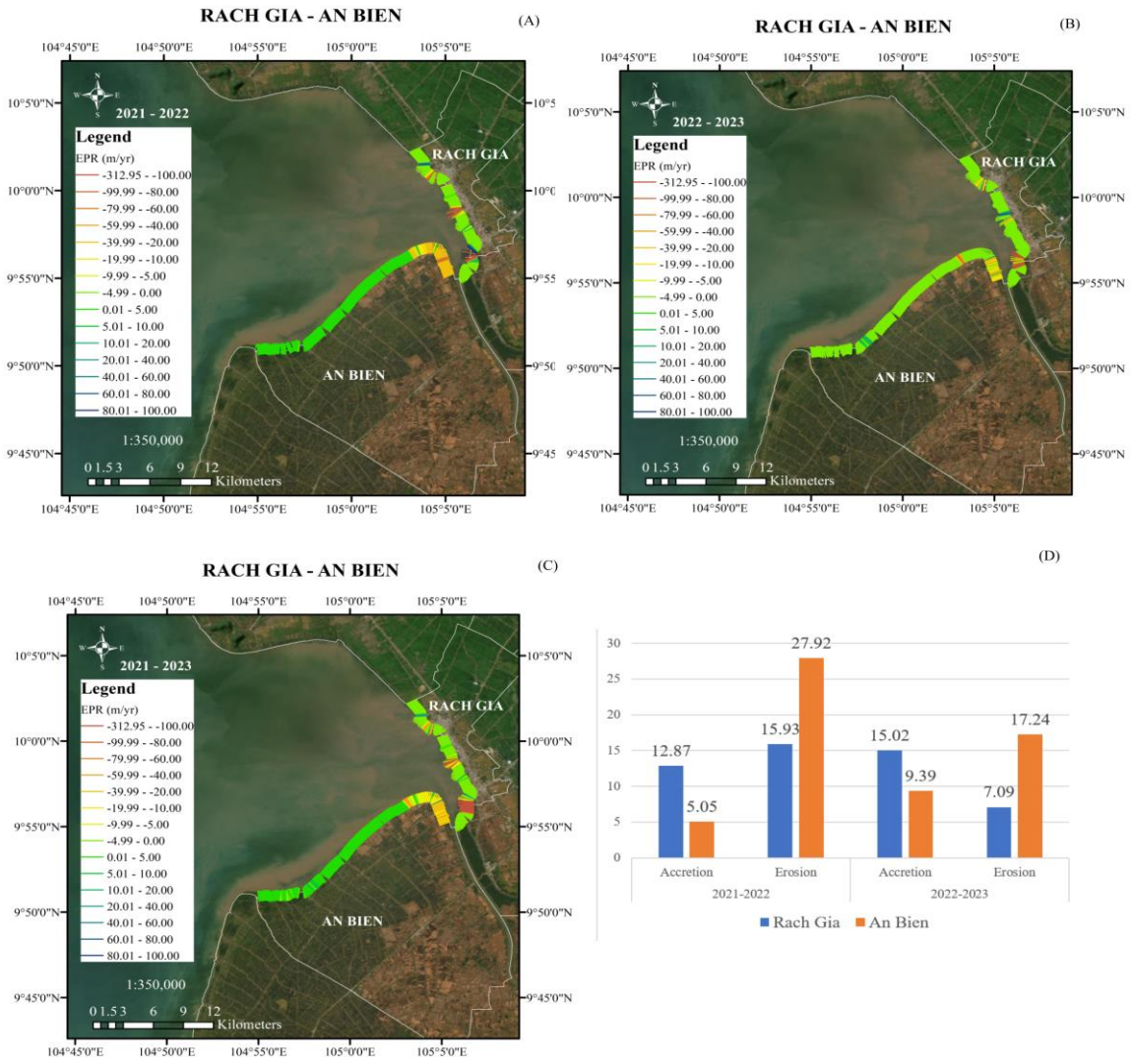

Figure 5. Map and chart showing erosion/accretion rate in Rach Gia, An Bien districts.

3.3. The accretion/erosion at An Minh - U Minh districts

In An Minh, in 2021-2022, the accretion/erosion rate is 15.87 m/year and 11.93 m/year, and the accretion/erosion area is 16.21 ha and 7.18 ha, respectively (Figure 6A). In 2022-2023, the accretion/erosion rate is 4.13 m/year and 18.94 m/year, and the accretion/erosion area is 0.79 ha and 2.32 ha, respectively (Figure 6B). In 2021-2023, the accretion/erosion rate is 8.48 m/year and 10.43 m/year, and the accretion/erosion area is 11.87 ha and 5.05 ha, respectively. Figure 6 shows the Van Khanh commune and Van Khanh Dong commune as accretional areas.

In U Minh, in 2021-2022, the accretion/erosion rate is 13.35 m/year and 6.77 m/year, and the accretion/erosion area is 10.25 ha and 6.61 ha, respectively (Figure 6A). In 2022-2023, the accretion/erosion rate is 12.57 m/year and 4.80 m/year, and the accretion/erosion area is 10.30ha and 4.87ha, respectively (Figure 6B). In 2021-2023, the accretion/erosion rate is 11.52 m/year and 8.85 m/year, and the accretion/erosion area is 10.06 ha and 5.12 ha, respectively (Figure 6C). Based on Figure 6, the area of Khanh Hoi commune and Khanh Tien commune is an accretion area.

Analysis results show that erosion and accretion are interwoven in An Minh-U Minh, but accretion is predominant. Between 2021-2022 and 2022-2023, the accretion rate in this area decreased, but An Minh district only has an increased erosion rate. The variation in accretion/erosion area is shown in Figure 6D.

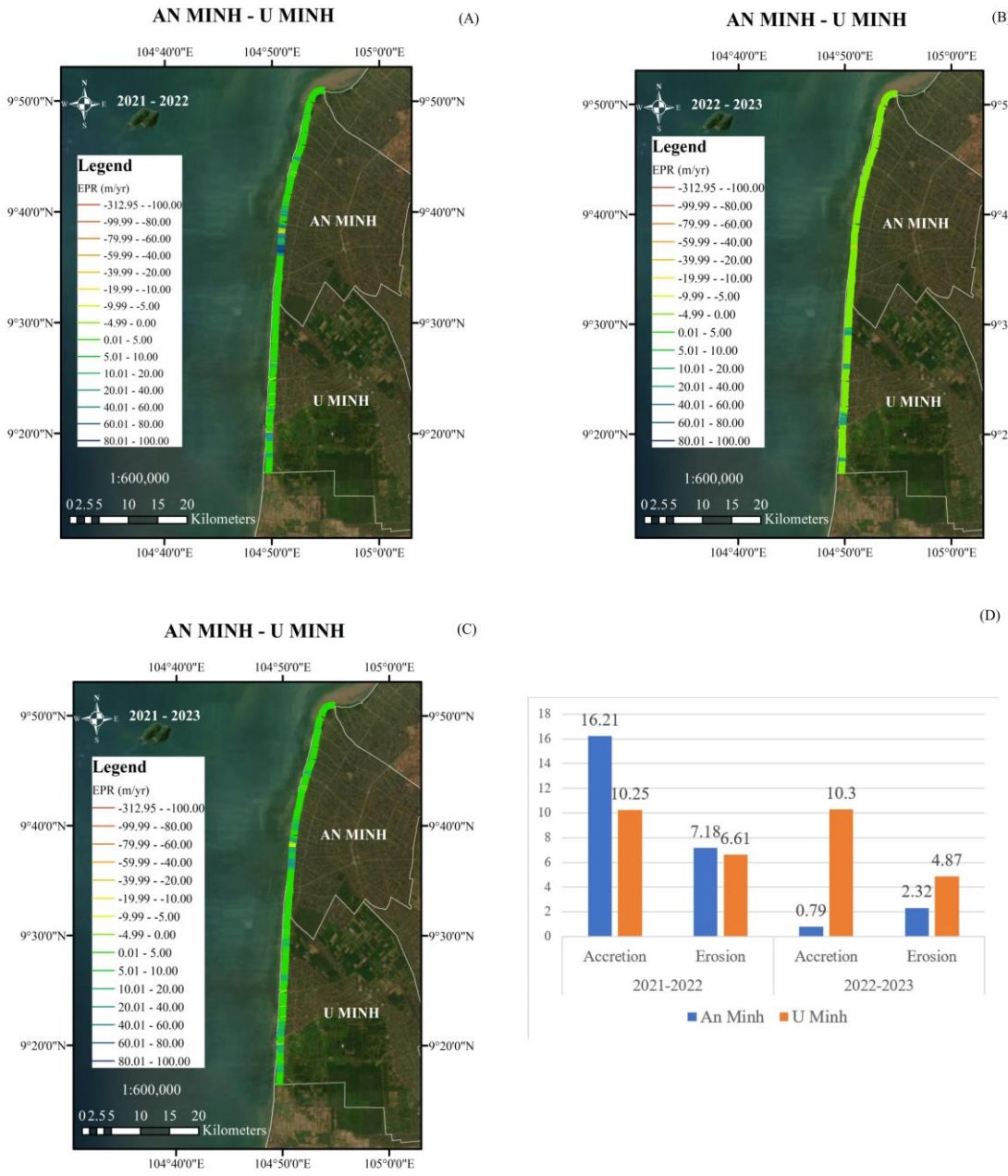

Figure 6. Map and chart showing erosion/accretion rate in An Minh and U Minh districts.

3.4. The accretion/erosion at Tran Van Thoi district

At Tran Van Thoi, in 2021-2022, the accretion/erosion rate is 19.41 m/year and 7.02 m/year, and the accretion/erosion area is 20.05 ha and 3.36 ha, respectively (Figure 7A). In 2022-2023, the accretion/erosion rate is 16.29 m/year and 5.55 m/year, and the accretion/erosion area is 26.17 ha and 4.95 ha, respectively (Figure 7B). In 2021-2023, the accretion/erosion rate will be 17.65 m/year and 6.49 m/year, and the accretion/erosion area will be 19.99 ha and 5.24 ha, respectively. Figures 7A-C show that the area of Khanh Hai commune, Song Doc town, and Phong Dien commune is the accretional area. The variation in accretion/erosion area is shown in Figure 7D.

Analysis results show that erosion and accretion are interwoven in the Tran Van Thoi area, but accretion is the main. Although the accretion rate will decrease between 2021-2022 and 2022-2023, the accretion area will still increase, and the erosion area will increase slightly. The variation in accretion/ erosion area is shown in Figure 7D.

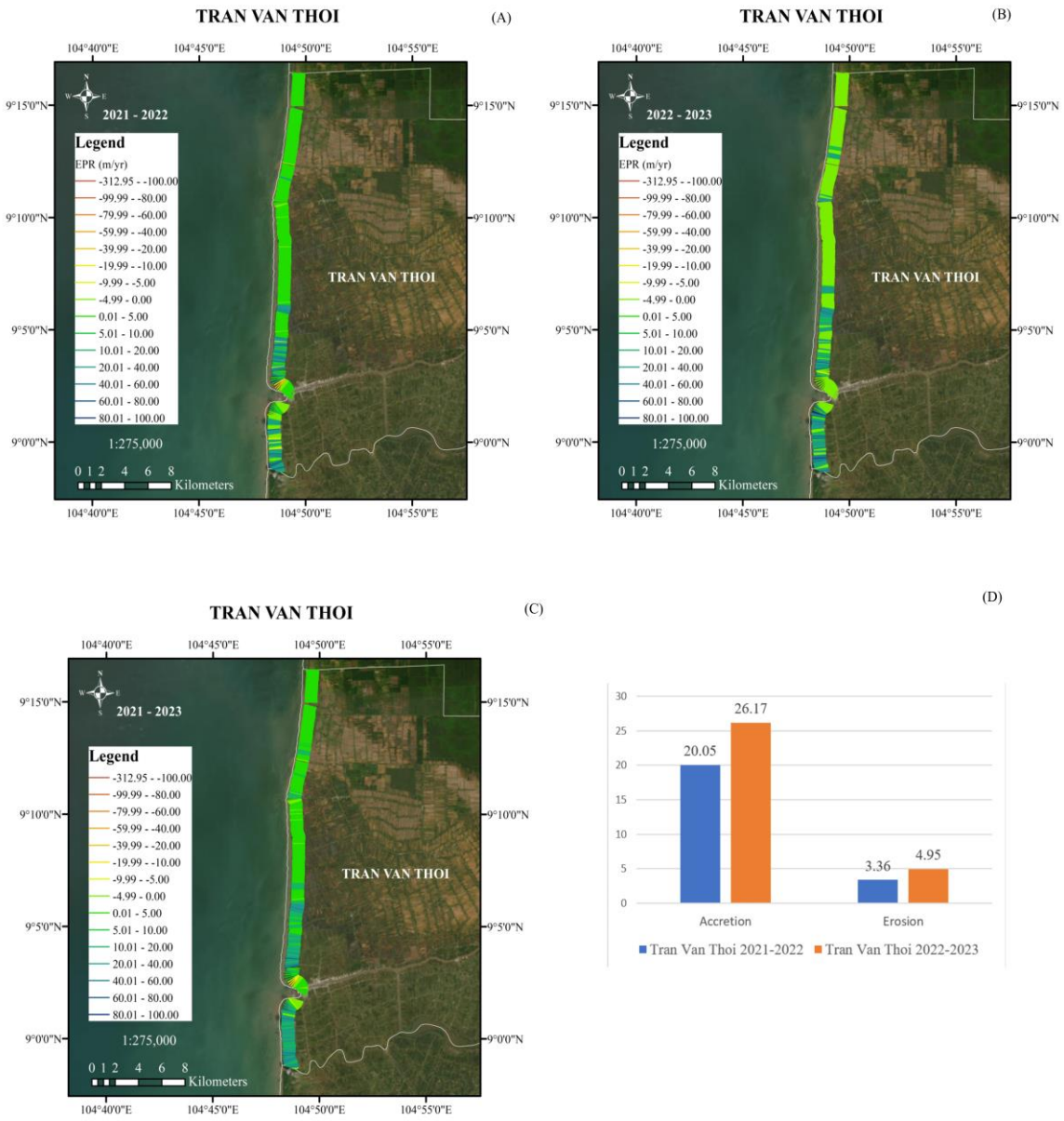

Figure 7. Map and chart showing erosion/accretion rate in Tran Van Thoi district.

3.5. The accretion/erosion at Phu Tan - Nam Can - Ngoc Hien districts

In Phu Tan, in 2021-2022, the accretion/erosion rate is 15.39 m/year and 10.04 m/year, and the accretion/erosion area is 30.71 ha and 8.03 ha, respectively. In 2022-2023, the accretion/erosion rate is 13.74 m/year and 4.39m/year, and the accretion/erosion area is 40.80 ha and 5.18 ha, respectively. In 2021-2023, the accretion/erosion rate is 15.95m/year and 9.30m/year, and the accretion/erosion area is 30.68 ha and 7.87 ha, respectively. Figure 6 shows the area of Phu Tan commune to Cai Doi Vam commune shows an accretion trend but is still slightly eroded.

In Nam Can, in 2021-2022, the accretion/erosion rate is 10.95 m/year and 37.73 m/year, and the accretion/erosion area is 3.67 ha and 10.52 ha, respectively Figure 8 A. In 2022-2023, the accretion/erosion rate is 8.92 m/year and 25.99 m/year, respectively, and the accretion/erosion area is 4.23 ha and 26.39 ha, Figure 8B. In 2021-2023, the accretion/erosion rate is 9.34 m/year and 33.88 m/year; the accretion/erosion area is 4.61 ha and 32.71 ha, respectively. The results shown in Figure 8 show that the areas of Dat Moi and Lam Hai communes have an erosion trend.

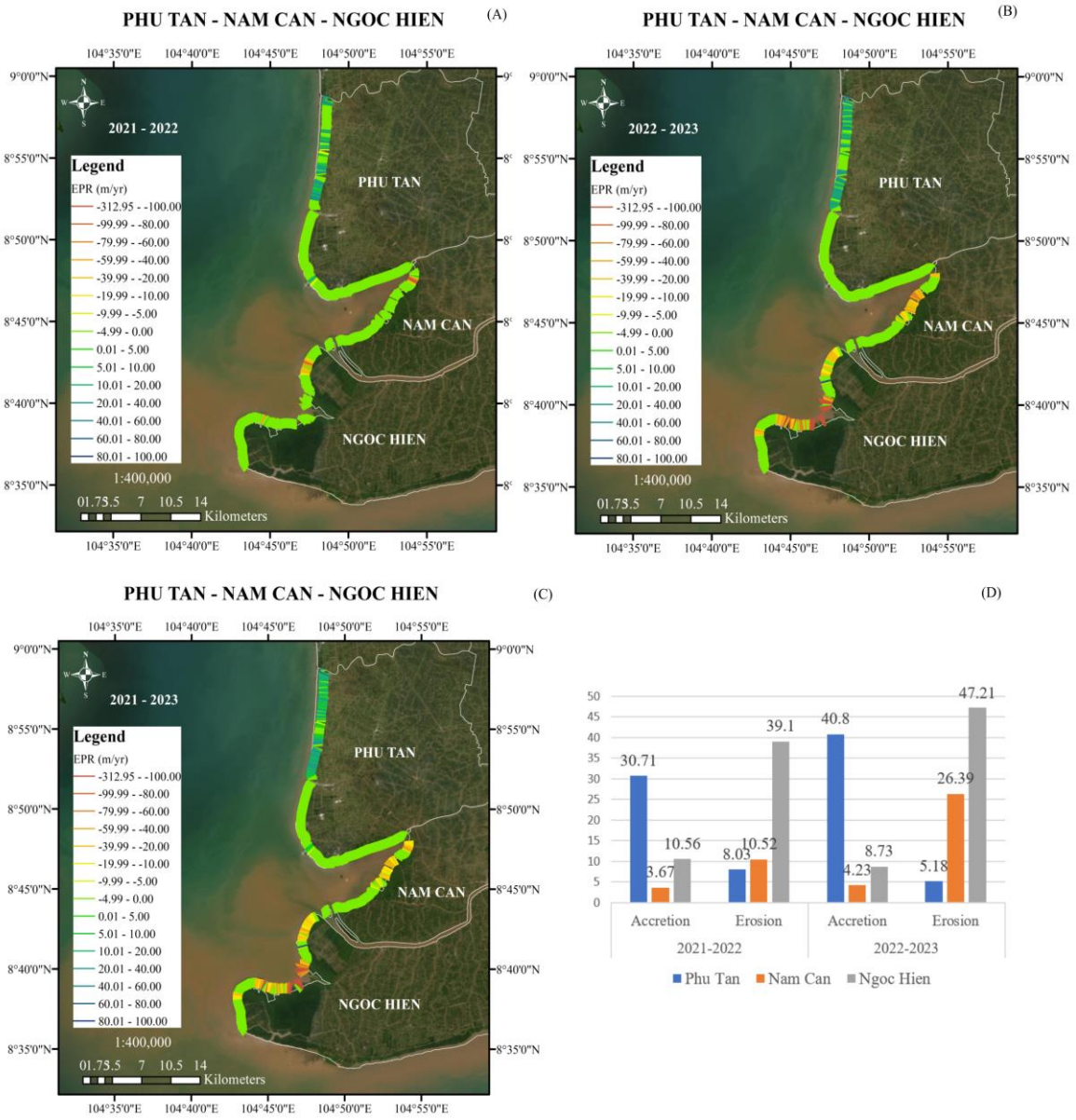

Figure 8. Map and chart showing erosion/accretion rates in Phu Tan, Nam Can and Ngoc Hien districts.

In Ngoc Hien, in 2021-2022, the accretion/erosion rate is 16.89 m/year and 36.53 m/year, respectively, and the accretion/erosion area is 10.56 ha and 39.10 ha, respectively. In 2022-2023, the accretion/erosion rate is 9.09 m/year and 55.66 m/year, and the accretion/erosion area is 8.73 ha and 47.21 ha, respectively. In 2021-2023, the accretion/erosion rate is 11.55 m/year and 47.79 m/year, and the accretion/erosion area is 9.39ha and 44.73 ha, respectively. The interpretation results in Figure 8 show that the areas of Vien An and Dat Mui communes are severely eroded.

General assessment shows that erosion and accretion are complexly interwoven yearly at Phu Tan - Nam Can - Ngoc Hien. In both periods, Phu Tan district was mainly accreted from Phu Tan commune to Cai Doi Vam commune. In 2021-2022, erosion will occur in Dat Moi - Nam Can commune and Vien An - Ngoc Hien commune area. By 2022-2023, erosion will expand further in Dat Moi commune, Lam Hai commune - Nam Can and is especially serious in Ngoc Hien district, from Vien An commune to Dat Mui commune. The variation in accretion/erosion area is shown in Figure 8D.

4. Conclusion

Evaluation results based on the shoreline extraction technique using the AWEI index and DSAS tool to calculate the current state of the shoreline over the years clearly show the trend of erosion/accretion on the coast of the Mekong Delta, the section from Ca Mau Cape to Kien Giang.

Although the trends of accretion/erosion in the study area are mixed, in the study period 2021-2023, the total area of accretion is 170.74 hectares, while the total area of erosion is 257.34 hectares. Thus, the increasing trend of erosion is a potential risk for the area. The results also show that the area of land loss in 2022-2023 is 115.43 hectares, an increase compared to the area of land loss in 2021-2022 of 109.37 hectares.

Next, it is necessary to clarify the mechanism of the formation of erosion and accretion zones by modelling seasonal hydrodynamic factors and mud and sediment factors received from the upstream to the river mouth. From the above results, we can determine the importance of applying remote sensing image analysis combined with GIS to monitor coastline changes. This method gives quick results and is less time-consuming but still ensures results, so this will be a helpful choice in shoreline protection, prevention, and management.

Author contribution statement: Developing research ideas, drawing up a draft writing plan, editing the manuscript, revising the manuscript version: L.T.B.; Process data: processing, first manuscript writing: D.C.M.N; GIS, Process data: V.H.T.D.

Acknowledgments: This research was funded by Vietnam National University Ho Chi Minh city (VNU-HCM), grant No: B2023-20-23. The authors would like to thank the Ho Chi Minh City University of Technology for the support of time and facilities from the Ho Chi Minh City University of Technology (HCMUT), VNU-HCM for this study.

Competing interest statement: The authors declare no conflict of interest.

References

1. Uścinowicz, G.; Uścinowicz, S.; Szarafin, T.; Maszloch, E.; Wirkus, K. Rapid coastal erosion, its dynamics and cause – An erosional hot spot on the southern Baltic Sea coast. *Oceanologia* **2023**. doi: 10.1016/j.oceano.2023.12.002.
2. Agate, J.; Ballinger, R.; Ward, R.D. Estuarine, coastal and shelf science satellite remote sensing can provide semi-automated monitoring to aid coastal decision-making. *Estuar. Coast. Shelf Sci.* **2024**, *298(8)*, 108639. doi: 10.1016/j.ecss.2024.108639.
3. Senevirathna, E.M.T.K.; Edirisooriya, K.V.D.; Uluwaduge, S.P.; Wijerathna, K.B.C.A. Analysis of causes and effects of coastal erosion and environmental degradation in southern coastal belt of Sri Lanka special reference to unawatuna coastal area. *Procedia Eng.* **2018**, *212*, 1010–1017. doi: 10.1016/j.proeng.2018.01.130.
4. Sowmya, K.; Sri, M.D.; Bhaskar, A.S.; Jayappa, K.S. Long-term coastal erosion assessment along the coast of Karnataka, west coast of India. *Int. J. Sediment Res.* **2019**, *34(4)*, 335–344. doi: 10.1016/j.ijsrc.2018.12.007.
5. Neelamani, S. Coastal erosion and accretion in Kuwait - Problems and management strategies. *Ocean Coast. Manag.* **2018**, *156*, 76–91. doi: 10.1016/j.ocecoaman.2017.05.014.
6. George, L.; Androws, X.; Krishnan, A.; Kumar, A.; Kannan, R.; Muthusankar, G.; Balasubramani, K. Assessment of shoreline changes and associated erosion and accretion pattern in coastal watersheds of Tamil Nadu, India. *Nat. Hazards Res.* **2023**. doi: 10.1016/j.nhres.2023.09.008.
7. Schmitt, K.; Albers, T. Area coastal protection and the use of bamboo breakwaters in the Mekong Delta. *Coastal Disasters Clim. Change VN Eng. Plann. Perspect.* **2014**, 107–132.
8. Nhan, N.H. Synthesis report of the formation and development mechanism of coastal accretion areas and scientific and technological solutions for sustainable socio-

economic development in Ca Mau coastal area-Code:ĐTĐL.2011.T/43. (In Vietnamse). Ho Chi Minh City, 2015.

9. Anthony, E.J.; Brunier, G.; Besset, M.; Goichot, M.; Dussouillez, P.; Lap, N.V. Linking rapid erosion of the Mekong River delta to human activities. *Sci. Rep.* **2015**, *5*, 4–9. doi: 10.1038/srep14745.
10. Brunier, G.; Anthony, E.J.; Goichot, M.; Provansal, M.; Dussouillez, P. Recent morphological changes in the Mekong and Bassac river channels, Mekong delta: The marked impact of river-bed mining and implications for delta destabilisation. *Geomorphology* **2014**, *224*, 177–191. doi: 10.1016/j.geomorph.2014.07.009.
11. Manh, N.V.; Dung, N.V.; Hung, N.N.; Kummu, M.; Merz, B.; Apel, H. Future sediment dynamics in the Mekong Delta floodplains: Impacts of hydropower development, climate change and sea level rise. *Glob. Planet. Change*. **2015**, *127*, 22–33. doi: 10.1016/j.gloplacha.2015.01.001.
12. Gugliotta, M.; Saito, Y.; Nguyen, V.L.; Ta, T.K.O.; Nakashima, R.; Tamura, T.; Uehara, K.; Katsuki, K.; Yamamoto, S. Process regime, salinity, morphological, and sedimentary trends along the fluvial to marine transition zone of the mixed-energy Mekong River delta, Vietnam. *Cont. Shelf Res*. **2017**, *147*, 7–26. doi: 10.1016/j.csr.2017.03.001.
13. McLachlan, R.L.; Ogston, A.S.; Allison, M.A. Implications of tidally-varying bed stress and intermittent estuarine stratification on fine-sediment dynamics through the Mekong's tidal river to estuarine reach. *Cont. Shelf Res.* **2017**, *147*, 27–37. doi: 10.1016/j.csr.2017.07.014.
14. Xing, F.; Meselhe, E.A.; Allison, M.A.; Weathers, H.D. Analysis and numerical modeling of the flow and sand dynamics in the lower Song Hau channel, Mekong Delta. *Cont. Shelf Res.* **2017**, *147*, 62–77. doi: 10.1016/j.csr.2017.08.003.
15. Vo, Q.T.; Reyns, J.; Wackerman, C.; Eidam, E.F.; Roelvink, D. Modelling suspended sediment dynamics on the subaqueous delta of the Mekong River. *Cont. Shelf Res.* **2017**, *147(7)*, 213–230. doi: 10.1016/j.csr.2017.07.013.
16. Ogston, A.S.; Allison, M.A.; Mullarney, J. C.; Nittrouer, C.A. Sediment and hydro-dynamics of the Mekong Delta: From tidal river to continental shelf. *Cont. Shelf Res.* **2017**, *147*, 1–6. doi: 10.1016/j.csr.2017.08.022.
17. Thai, N.H.; Thuy, N.B.; Dang, V.H.; Kim, S.; Hole, L.R. Impact of the interaction of surge, wave and tide on a storm surge on the north coast of Vietnam. *Procedia IUTAM* **2017**, *25*, 82–91. doi: 10.1016/j.piutam.2017.09.013.
18. Loisel, H.; Mangin, A.; Vantrepotte, V.; Dessailly, D.; Dinh, D.N.; Garnesson, P.; Ouillon, S.; Lefebvre, J.P.; Mériaux, X.; Phan, T.M. Variability of suspended particulate matter concentration in coastal waters under the Mekong's influence from ocean color (MERIS) remote sensing over the last decade. *Remote Sens. Environ.* **2014**, *150*, 218–230. doi: 10.1016/j.rse.2014.05.006.
19. Liu, C.; He, Y.; Des, E.W.; Wang, J. Changes in the sediment load of the Lancang-Mekong River over the period 1965-2003. *Sci. China Technol. Sci.* **2013**, *56(4)*, 843–852. doi: 10.1007/s11431-013-5162-0.
20. Heege, T.; Kiselev, V.; Wettle, M.; Hung, N.N. Operational multi-sensor monitoring of turbidity for the entire Mekong Delta. *Int. J. Remote Sens.* **2014**, *35(8)*, 2910–2926. doi: 10.1080/01431161.2014.890300.
21. Fleifle, A.E. Suspended Sediment Load Monitoring Along the Mekong River from Satellite Images. *J. Earth Sci. Clim. Change* **2013**, *04(06)*, 160. doi: 10.4172/2157-7617.1000160.
22. Hoang, T.B. Research and find solutions and technologies to prevent river bank erosion in Bac Lieu and Ca Mau provinces. Report Scientific Conference 12/27/2017: Southern institute of water resources research, HCM city, 2017.
23. Linh, B.; Bui, L. Modelling bank erosion dependence on natural and anthropogenic factors – Case study of Ganh Hao estuary, Bac Lieu - Ca Mau, Vietnam. *Environ. Technol. Innov.* **2020**, *19*, 100975. doi: 10.1016/j.eti.2020.100975.

24. Xuan, N.T.; Duyen, C.M.N.; Long, B.T. Simulating $PM_{2.5}$ dust pollution and analyzing related factors – The case of Ca Mau province, Vietnam. *J. Hydro-Meteorol.* **2023**, *756(12)*, 42–58.
25. Phuong, P.V.T.; Hanh, P.T.H.; Long, B.T. Application of remote sensing, GIS to assess the rate and range of coastal erosion in the Mekong River Delta, from Tien Giang to Soc Trang Province. *VN J. Hydrometeorol.* **2023**, *754*, 9–25. doi: 10.36335/vnjhm.2023.(754).9-25.
26. Pham, H.T.H.; Bui, L.T. Mechanism of erosion zone formation based on hydrodynamic factor analysis in the Mekong Delta coast, Vietnam. *Environ. Technol. Innov.* **2023**, *30*, 103094. doi: 10.1016/j.eti.2023.103094.
27. Hoang, T.T.; Dao, K.N.; Pham, L.T.; Van, N.H. Analysis of riverbank changes in Ho Chi Minh city in the period 1989 - 2015. *Sci. Technol. Dev. J. Sci. Earth Environ.* **2019**, *2(2)*, 80–88. doi: 10.32508/stdjsee.v2i2.496.
28. Elkafrawy, S.B.; Basheer, M.A.; Mohamed, H.M.; Naguib, D.M. Applications of remote sensing and GIS techniques to evaluate the effectiveness of coastal structures along Burullus headland-Eastern Nile Delta, Egypt. *Egypt. J. Remote Sens. Sp. Sci.* **2021**, 24(2), 247–254. doi: 10.1016/j.ejrs.2020.01.002.
29. Attar, I.M.S.A.; Basheer, M.A. Multi-temporal shoreline analysis and future regional perspective for Kuwait coast using remote sensing and GIS techniques. *Heliyon*. **2023**, *9(9)*, e20001. doi: 10.1016/j.heliyon.2023.e20001.
30. Chrisben, S.S.; Gurugnanam, B. Coastal transgression and regression from 1980 to 2020 and shoreline forecasting for 2030 and 2040, using DSAS along the southern coastal tip of Peninsular India. *Geod. Geodyn.* **2022**, *13(6)*, 585–594. doi: 10.1016/j.geog.2022.04.004.
31. Mutaqin, B.W. Shoreline changes analysis in Kuwaru coastal area, Yogyakarta, Indonesia: An application of the digital shoreline analysis system (DSAS). *Int. J. Sustain. Dev. Plan.* **2017**, *12(7)*, 1203–1214. doi: 10.2495/SDP-V12-N7-1203-1214.
32. Tinh,T.V.; Phong, D.H. Applying remote sensing and gis for study change in coastal areas of Ca Mau cap. *VN J. Hydrometeorol*. **2017**, *684*, 41–53.
33. Thanh, N.T. Analysis and evaluation of erosion and deposition processes in Ca Mau by remote sensing and GIS. *VN J. Hydrometeorol*. **2021**, *721*, 66–79. doi: 10.36335/vnjhm.2021(721).66-79.
34. Quynh, C.K.N.; Hanh, P.T.H.; Long, B.T. Assessment of the shoreline evolution and coastal erosion trends along Cua Dai beach, Hoi An City, Quang Nam. *VN J. Hydrometeorol.* **2022**, *736(1)*, 41–53. doi: 10.36335/VNJHM.2022(736(1)).41-53.
35. Thin, V.T.; Duan, P.V.; Thi, N.V.; Hung, N.V.; Van, N.H. Landsat8 disposal service photo identification phase fluctuations and coating plant. *J. Forestry. Sci. Technol*. **2015**, *N1*, 73–83.
36. U.D. of the Interior. What are the band designations for the Landsat satellites? USGS, 2014.
37. Feyisa, G.L.; Meilby, H.; Fensholt, R.; Proud, S.R. Automated Water Extraction Index: A New Technique for Surface Water Mapping Using Landsat Imagery. *Remote Sens. Environ.* **2014**, 23–35. doi: 10.1016/j.rse.2013.08.029.
38. Teng, J.; Xia, S.; Liu, Y.; Yu, X.; Duan, H.; Xiao, H.; Zhao, C. Assessing habitat suitability for wintering geese by using normalized difference water index (NDWI) in a large floodplain wetland, China. *Ecol. Indic.* **2021**, *122*, 107260. doi: 10.1016/j.ecolind.2020.107260.

JOURNAL OF
HYDRO-METEOROLOGY

Rerearch Article

A study on the application of computational models as support tools in urban flood management along the Cai Nai river in Can Tho city

Nguyen Van Hong[1], Nguyen Thao Hien[1]*

[1] Sub-Institute of Hydrology Meteorology and Climate Change;
nguyenvanhong79@gmail.com; nthien2710@gmail.com

*Correspondence: nthien2710@gmail.com; Tel.: +84–934720858

Received: 8 February 2024; Accepted: 14 March 2024; Published: 25 March 2024

Abstract: Urbanization processes often lead to flooding issues, hindering the development of cities in Vietnam. For cities undergoing planning, initial solutions are crucial. To avoid replicating old urban structures, lacking green spaces, and missing water retention systems, this paper applies Low Impact Development (LID) solutions within the Storm Water Management Model (SWMM) framework for flood management in the new urban area along the Cai Nai River, located in the new residential area of Hung Thanh Ward, Cai Rang District, Can Tho City. The integration of SWMM with LID serves as a useful tool towards sustainable urban development, aiming for a more modern and intelligent city. This tool helps managers and investors save costs and time in selecting suitable solutions tailored to the planning characteristics of the study area, ensuring effectiveness during implementation. The paper proposes constructing two scenarios: current status and planned; comparing flow rates before and after urbanization for a major rainfall event on April 2, 2023. Subsequently, LID solutions are introduced and evaluated for effectiveness through each calculated scenario.

Keywords: Urban flooding; Cai Nai; Can Tho; SWMM; LID.

1. Introduction

The study area is located within the residential area of Hung Thanh Ward, Cai Rang District, Can Tho City. The computational scope is bordered as follows: to the Northwest: adjacent to the Can Tho River; to the Southeast: adjacent to the road leading to the Can Tho Bridge (National Highway 1A); to the Northeast: adjacent to the planned bridge and Tran Hoang Na road, and to the Southwest: adjacent to the Cai Nai Canal. The total research area is 365,740 m^2 (Figure 1).

In general, Can Tho has a tropical monsoon climate with few storms, hot and humid weather year-round, and no cold season. The rainy season lasts from May to November, and the dry season runs from December to April of the following year. The average annual temperature is around 28°C, with an average of about 2 hours of sunshine per day throughout the year. The average annual rainfall is approximately 1,600 mm, with average humidity ranging from 82% to 87%. Due to the influence of the tropical monsoon climate, Can Tho benefits from favorable temperature conditions, heat radiation regimes, and high and stable sunlight levels throughout the two seasons [1].

The river, canal, and creek network here is quite dense. The two channels adjacent to the research area, Cai Nai and Can Tho, are both influenced by the main flow of the Hau River (Figure 1), so the hydrological regime of the area is strongly affected by tidal dynamics, upstream flow, and localized rainfall patterns., upstream flow and localized rainfall patterns. The hydrological regime is distinctly divided into two seasons: the flood season from July to

December and the dry season from January to June. Rainfall is the primary source of water supply for river flow. Additionally, factors such as tides and meteorological conditions impact the flow. Tides from the East Sea penetrate deeply inland and significantly influence the hydrological regime of the delta. During the flood season, tides also contribute to increased water levels in the river system, hindering flood drainage [1].

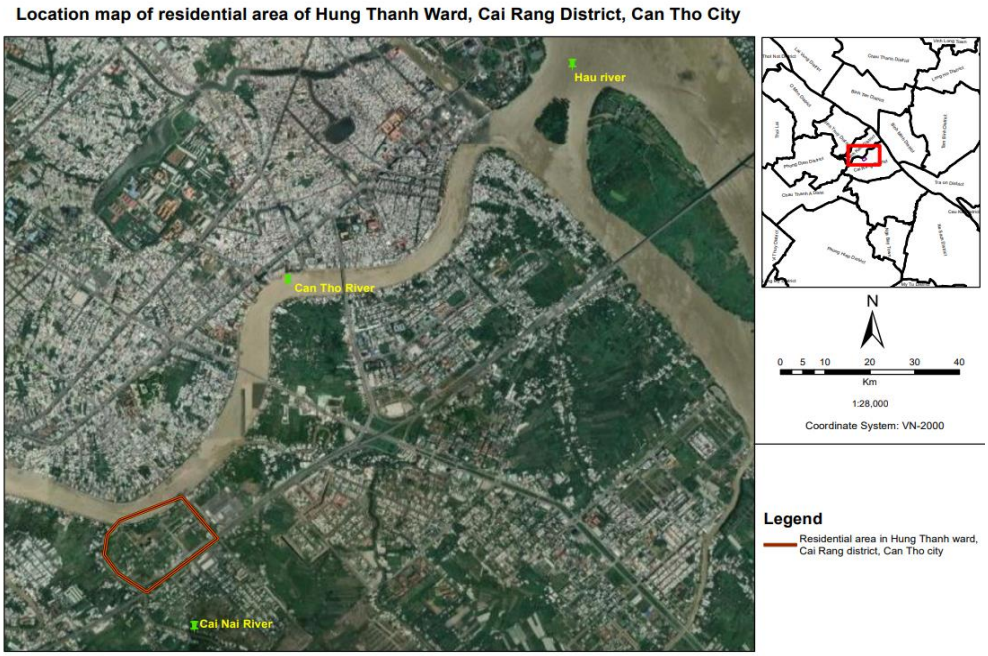

Figure 1. Location map of residential area of Hung Thanh Ward, Cai Rang District, Can Tho City.

During the land use survey, the research area is still undergoing investment planning, with a considerable amount of vacant land (Figure 2). This is why it is necessary to implement solutions to minimize flooding caused by excessive urbanization, avoiding the repetition of old urban structures, lack of green spaces, and inadequate water retention facilities. The integration of Low Impact Development (LID) with the Storm Water Management Model (SWMM) offers effective solutions suitable for the urban planning characteristics of residential areas, villas, apartments, schools, integrated areas, etc., saving costs, time in selection, and ensuring effectiveness during implementation.

Figure 2. Current land use status in the residential area.

The Storm Water Management Model (SWMM) and Low Impact Development (LID) sustainable development solutions are commonly applied in scientific research before being evaluated and implemented in practice. The studies [2,5] assess decentralized flood mitigation approaches to enhance permeability and rainwater storage capacity, addressing

urban flooding issues through various structures such as green roofs, permeable pavement materials, and tree boxes, designed for different rainfall and tidal conditions. The study [3] evaluates the applicability of sustainable urban drainage solutions (SUBS) in urbanizing areas of Binh Chanh district, Ho Chi Minh City, through two scenarios: Scenario 1 enhances temporary storage capacity for rainwater reuse, while Scenario 2 reduces peak flow rates. The study [4] incorporates GIS tools to assess urban flooding in the Metro residential area of Ninh Kieu district, Can Tho province, under various urbanization scenarios.

The studies [6, 7, 9] suggest that urban expansion leads to increased impermeable areas, resulting in increased surface flow, particularly in urban and large city areas. Additionally, urban flooding is influenced by various factors such as climate, land cover characteristics, and surrounding river networks. To mitigate flood damage and control flow, these areas have developed combined LID solutions in urban stormwater management using SWMM software. Specifically, the study [6] further simulates 2.5 and 10-year recurrence cycles for two rainfall events in the city, evaluating methods to effectively reduce peak flow volumes and runoff in stormwater drainage systems. The study [8] additionally applies the Monte Carlo method to simulate annual flow processes based on LID, analyzing correlations between flow indices, peak flows, and total suspended solids (TSS) runoff. This study not only assesses reducing overflow flow but also calculates water source pollution when flooding occurs. The study [10] advances flood mitigation research methods by optimizing spatial allocation of integrated LID with SWMM using MATLAB as the platform for a residential area in Western Canada. The study [19] ues of LID in various BMP scenarios aims to minimize urban stormwater runoff and reduce pollutant load through cost-effective and environmentally friendly approaches within a modernized platform on a Python-based web framework. The outcomes yield performance metrics concerning total flow volume, pollutant loadings, and construction costs for each LID solution in every BMP scenario, resulting in a 75% reduction in overall volume control, peak flow reductions ranging from 22% to 46%, and up to 32% pollutant removal.

Overall, most LID/SUBS solutions simulated in SWMM-based studies demonstrate effectiveness in enhancing infiltration capacity, extending runoff concentration time, and reducing urban surface runoff flow.

For urban areas undergoing planning processes, particularly the new urban area along the Cai Nai River, Hung Thanh Ward, Cai Rang District, Can Tho City, initial solutions are highly imperative. To avoid replicating old urban structures lacking green spaces and water retention facilities, among other deficiencies, the application of LID solutions within the SWMM urban drainage management model serves as a valuable tool in the initial stages of design, monitoring, and technical infrastructure construction to mitigate future urban flood risks.

2. Materials and Methods

2.1. Research methodology framework

To achieve the research objectives, which involve applying LID solutions to mathematical models for urban flood management, the following research methodology framework is proposed in Figure 3:

- Conduct field investigations, site surveys, and gather relevant documents.
- Utilize correlation equations to establish a database, serving as input parameters for the SWMM urban drainage model.
- Set up the SWMM model and perform calibration and validation of the model.
- Select appropriate LID solutions and incorporate the assumptions of these solutions into the mathematical model.

- Evaluate the effectiveness of flood reduction provided by the LID solutions through two scenarios: current conditions and post-urbanization.

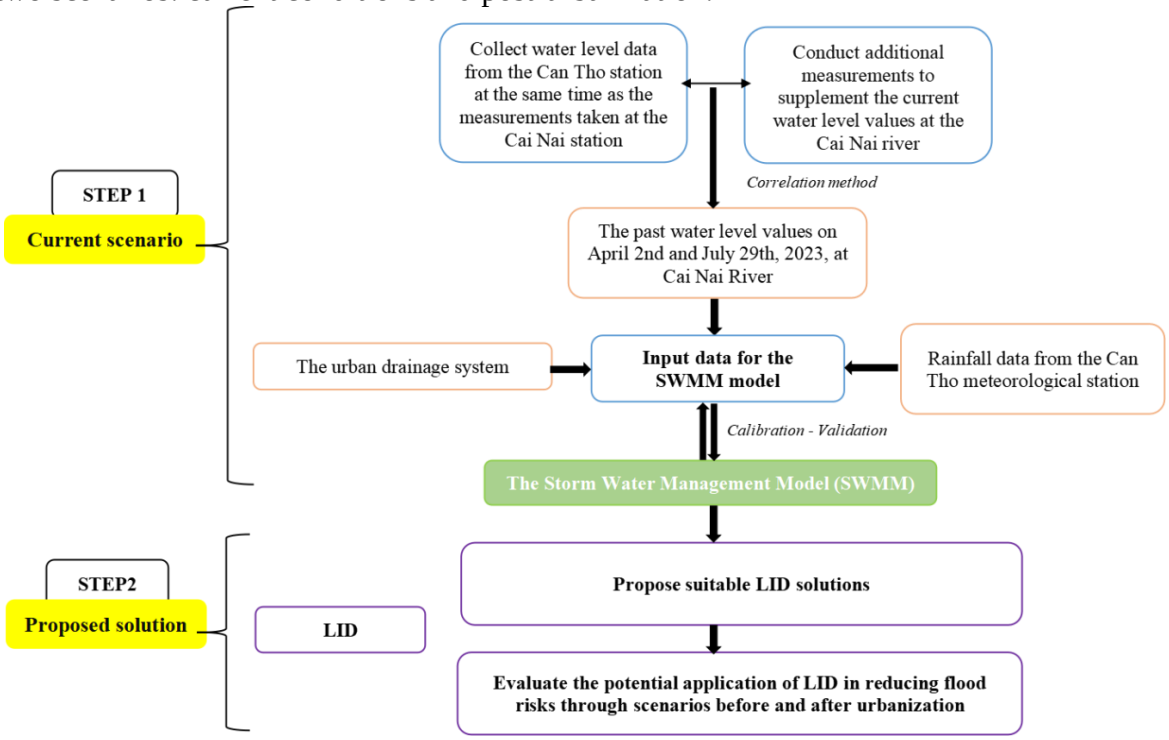

Figure 3. Research framework.

2.2. Using correlation equations to interpolate urban flooding calculation data

The research area is a newly planned residential area along the Cai Nai River, Cai Rang District, Can Tho City. To calculate the urban drainage model, it is necessary to input water level data at the urban runoff outlet. For this area, the representative water level at the runoff point is assumed to be the water level at Cai Nai, although this location does not have a hydrological station. Therefore, to ensure consistent data, the nearest hydrological station, Can Tho station (on the Hau River), was chosen to calculate and interpolate the water level at Cai Nai.

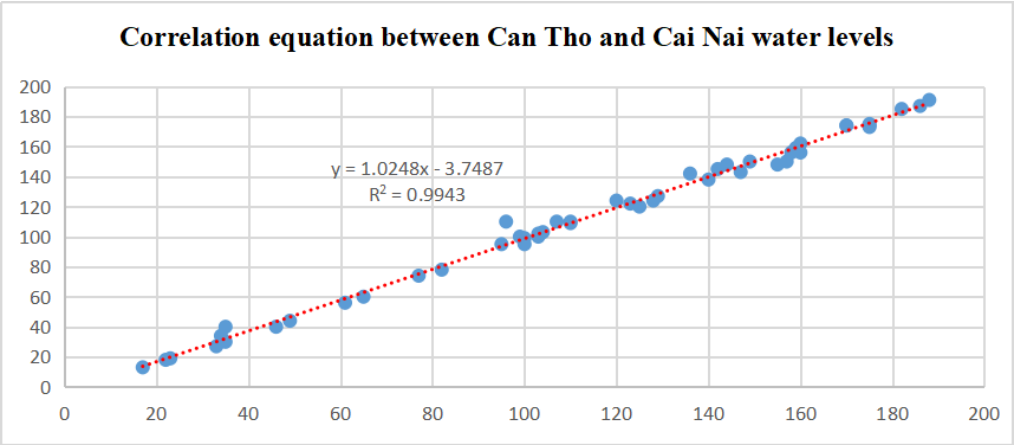

Figure 4. Correlation equation between Can Tho and Cai Nai water levels.

To find the most accurate and reliable water level values for the residential area at Rạch Cai Nai based on data from the Can Tho hydrological station, the study uses a single-variable correlation equation to interpolate water level values.

The data used in the calculation are obtained from actual measurements at the Can Tho station and a location at Cai Nai in the research area from November 1 to November 3, 2023.

A correlation equation is established based on the water level values over the three days. From this, we obtain correlated variables to support flooding calculations for past rainfall events (Figure 4).

2.3. SWMM and LID in urban water management applications

2.3.1. SWMM model (Storm Water Management Model)

The SWMM model [11, 20] (Storm Water Management Model) was developed by the United States Environmental Protection Agency (EPA) in 1971 [22] and was enhanced to Version 5.1 in 2015 [23]. EPA-SWMM is a computer program used to simulate hydrological, hydraulic, and water quality processes for both closed and open drainage networks within a watershed (urban or rural).

For the purposes of this study, the model supports dynamic simulation of rainfall-runoff processes for urban areas, calculating both the flow rates from each watershed to the outlet culvert and the inundation levels when manholes overflow.

SWMM uses a collection of nodes (manholes) and conduit segments connected through each manhole to describe the drainage network system. Additionally, this network is composed of various components: Subcatchments (watersheds), Raingages (rainfall stations), Junctions (nodes), Storage Units (detention basins), Pumps, Regulators (control valves or check valves), and Outfalls.

2.3.2. LID solutions

LID (Low-Impact Development) solutions are suitable and effective approaches in urban environmental management. Instead of constructing deep, straight drainage systems or underground sewers to quickly drain stormwater, sustainable drainage systems seek to delay stormwater runoff and consider rainwater as a valuable resource by incorporating green ecological principles with existing drainage technical principles to reduce the burden on drainage systems reasonably. The purpose of this solution is to mitigate urban flooding, replenish groundwater, minimize environmental pollution, and create green spaces in urban areas.

LID utilizes principles such as conserving and restoring natural landscape features, minimizing impervious surfaces to create a system of areas with drainage, infiltration, and treatment functions, to utilize rainfall as a resource rather than a waste. Widely applied, LID can maintain or restore the hydrological and ecological functions of watersheds. LID is regarded as a sustainable stormwater management system.

2. Setting up the storm water management model (SWMM) for urban drainage

2.1. Setting up the culvert elevations and terrain of the research area

Based on actual cross-sectional data of the Cai Nai at coordinates 10°00.089’; 105°45.810’, the current ground elevation is determined to be 2.41 meters.

From the above data, the study interpolates the elevation values of the ground, depth of manholes, and culvert bottom elevations for the

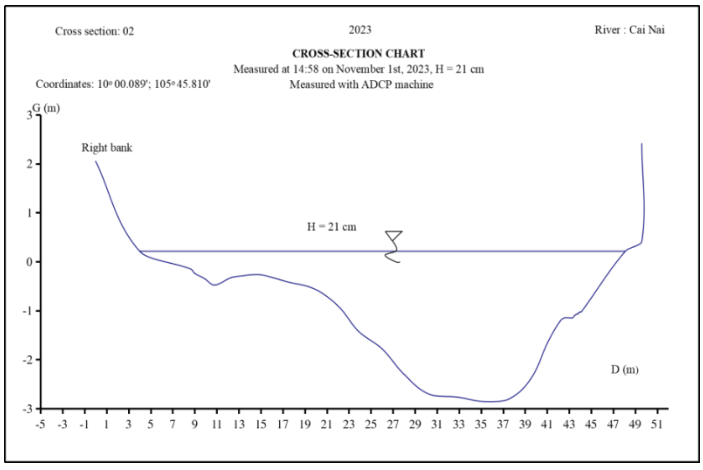

Figure 5. Cross-sectional elevation profile of the Cai Nai River.

SWMM urban drainage model, serving to calculate surface runoff and hydraulic flow in the drainage system.

2.2. Setting up the culvert, manhole, and discharge gate network

The urban stormwater drainage system consists of a combination of manholes and culverts with varying diameters designed to discharge directly into the Cai Nai at three discharge gates: CX3, CX4, and CX5. This system collects water through closed gates, arranged beneath the sidewalks, and then directs it to the river channel. Pre-cast reinforced concrete pipes with diameters of D400, D600, D800, and D1000 are used (Figure 6).

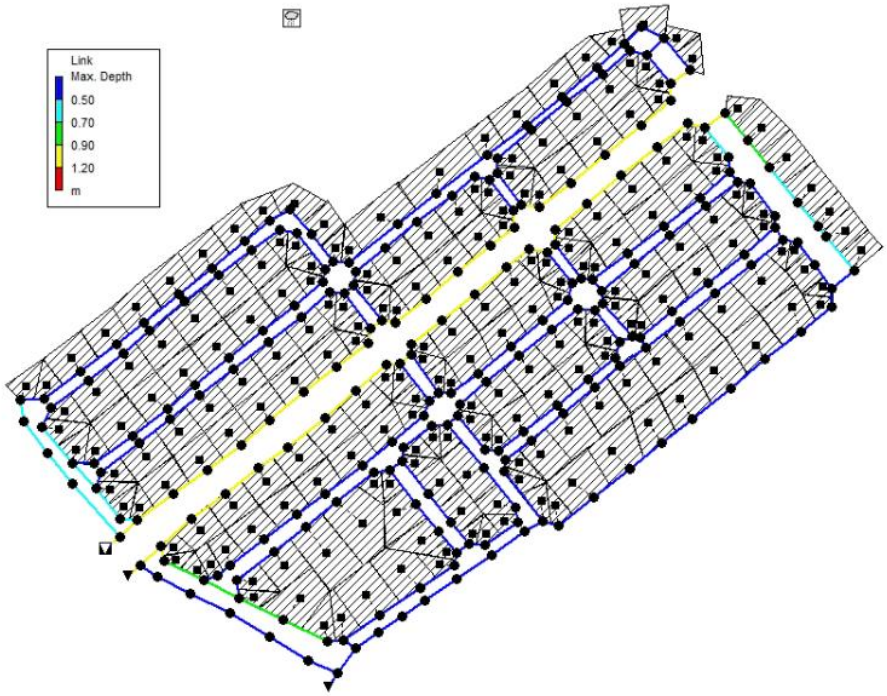

Figure 6. Dimensions of culverts and locations of manholes and discharge gates in the stormwater drainage system. (Note: Triangle symbolizes outfall, Circle symbolizes manhole).

For the culverts responsible for bearing the load, they will be designed with D = 600, 800, and 1000. The culvert with D = 1000 is the main load-bearing culvert directly connecting to the branch culvert system leading to the two main discharge gates of block 5C. The manholes and the bottom elevation of the manholes are also designed to be appropriate for the terrain of the area.

2.3. Setting up the watershed and stormwater drainage

2.3.1. Rainfall reception watershed

In the model, there are a total of 195 drainage areas, with each area linked to a corresponding manhole. The entire urban area, including (planned): 3 villa areas, 1 mixed-use area, 1 social housing area, 2 educational areas, and 3 terraced housing areas. The drainage areas in the SWMM model will be divided according to the planned development. The imperviousness percentage (%Imprev) is based on TCVN 7957:2008 standards [18].

Table 1. Impervious surface parameters.

Surface Water Drainage Characteristics	Impermeable Parameter Values (%)
Roof, Concrete Covering	0.75
Grass, Garden, Park	0.32

2.3.2. Stormwater drainage areas

SWMM is a hydrological-hydraulic model consisting of two simulation blocks, Runoff and Extran, used to determine the relationship between rainfall and runoff, then simulate the hydraulic dynamics of flow in the drainage system. Results from the RUNOFF block (*runoff hydrograph at the rainfall reception manholes*) will serve as inputs for the EXTRAN simulation block. The EXTRAN block of SWMM uses the finite difference method with current numerical schemes to solve the 1-D Saint-Venant equation to simulate hydraulic results in the drainage system [12].

2.4. Data series used in calculation

In urban drainage simulations, in addition to the rainfall runoff system and terrain of the research area, to calculate flood levels and water levels in each drainage branch, data on rainfall amounts and tidal levels at each discharge point must be input into the model. All data on rainfall amounts and water levels are collected from the Provincial Meteorological and Hydrological Station in Can Tho province.

- The rainfall amounts used in model calibration and validation are two rainfall events occurring on April 2, 2023, and July 29, 2023, with total rainfall amounts of 60.8 mm (90 minutes) and 48.8 mm (435 minutes), respectively (Figures 7a, b).

- The initial water level at each discharge point is also declared similarly for the two time points, based on the correlation equation between the water levels at the Can Tho station and Cai Nai presented in the methodology above (Figures 7c, d).

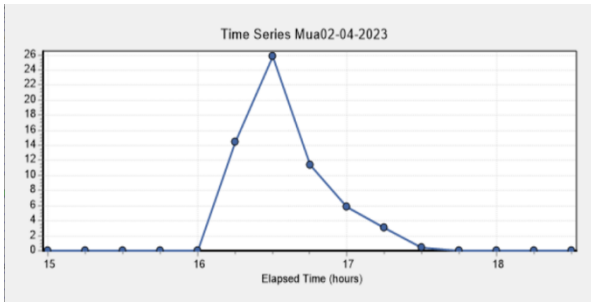

a) Rainfall curve on April 2, 2023

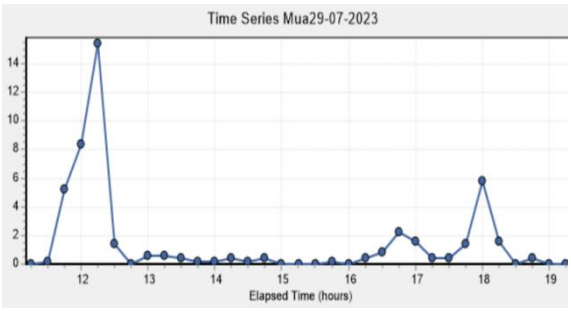

b) Rainfall curve on July 29, 2023

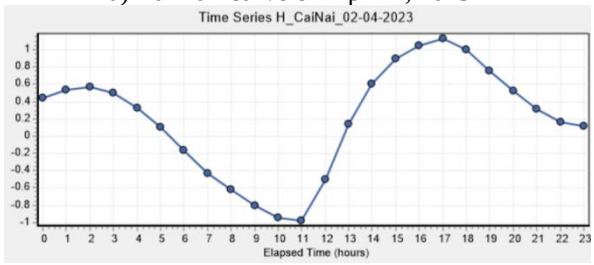

c) 24-hour water level on April 2, 2023

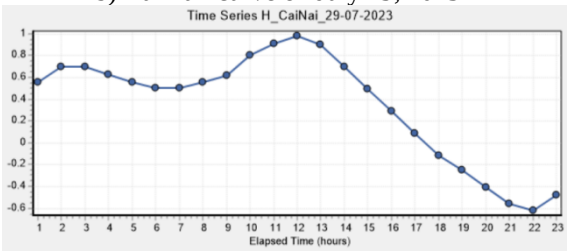

d) 24-hour water level on July 29, 2023

Figure 7. Input hydro-meteorological database for the model.

3. Results and solutions

3.1 Model calibration and validation

3.1.1. Model calibration

To check and calibrate the model, consider the highest flooded areas, then recalibrate with actual flood data and adjust the declared parameters such as permeability coefficient, slope, culvert elevation, manhole depth, etc. Continue to simulate again, if the results meet the requirements, proceed to check the main evaluation area of the study area. Repeat the

calibration steps until we obtain a set of model parameters that closely simulate the actual results.

Table 2. Detailed results of flooding levels at manholes.

Node	Flooded CMS	Volume 106 ltr	Meter Flooding	Node	Flooded CMS	Volume 106 ltr	Meter Flooding
19c_3	0.033	0.003	0.019	9a_5	0.042	0.006	0.045
19d_3	0.041	0.004	0.025	9a_4	0.014	0.006	0.044
19d_2	0.034	0.003	0.026	19a_4	0.022	0.004	0.026
19d_1	0.012	0.003	0.024	19a_5	0.027	0.003	0.026
9a_7	0.049	0.006	0.04	19b_2	0.006	0.002	0.012
9a_6	0.038	0.006	0.044				

Figure 8. Land use status at locations of drains with water level in each manhole.

The simulation results of the flooding situation during the rainfall event on April 2, 2023, were replicated through the SWMM management model to closely match reality. According to Table 2 and Figure 6, the water level at each manhole (overflow water level) fluctuated between 0.01-0.05m; mostly concentrated in the residential areas with high-rise buildings (from node 19d_1 to 19d_3, 9a_4 to 9a_7,…).

However, according to the assessment criteria for flooding from the Ministry of Construction (document 338/BXD-KTQH), a flooding depth of ≤ 0.1 m poses no risk. Based on the simulation results from the model, with values below 0.05m, the study area is evaluated as not being flooded due to heavy rain or tidal surges. This result corresponds to the data collected during the survey on the flooding situation in the area provided by residents and management.

3.1.2. Model validation

The rainfall event used to validate the model occurred on July 29, 2023, with a total rainfall of 48.8 mm lasting for 7 hours. Compared to the rainfall event on April 2 used for calibration, this rainfall event did not cause flooding. The results are presented specifically in the drainage lines to demonstrate that this rainfall did not cause manhole overflow (Figure 9). This validates the drainage lines causing flooding during the rainfall event on April 2.

The rainfall began at 11:30 with a rainfall amount of 0.2mm; water started to appear in the drain at 11:48; peaked at 12:30 and began to recede at 12:45. Thus, with the two rain

events used in model calibration and validation, reliable and close-to-reality results have been achieved. These parameter sets are further used to simulate various Low-Impact Development (LID) scenarios.

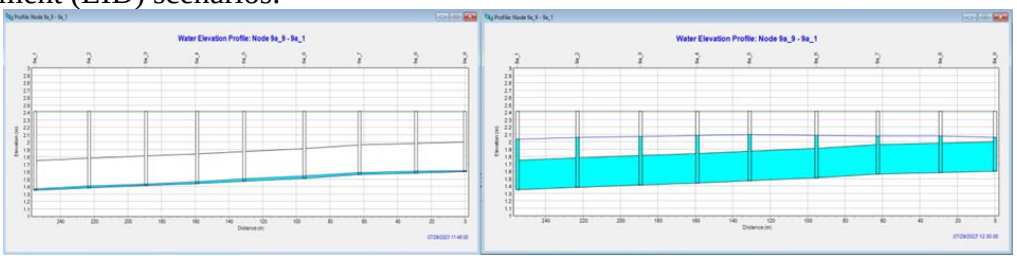

a) Time of water appearance in the conduit

b) Time of maximum water level

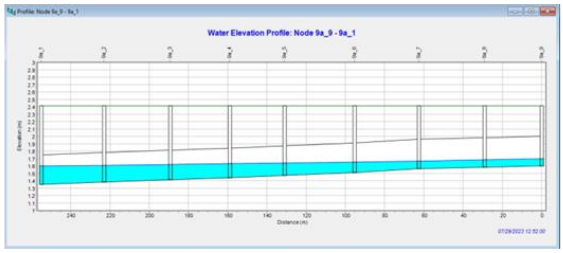

c) Duration of water recession

Figure 9. Water volume in the conduit during the rain event on July 29, 2023.

Furthermore, the urban area of Hung Thanh Ward, Can Tho City, along the Cai Nai River, is a newly planned area, currently undergoing infrastructure development such as housing, villas, residential areas, commercial centers, and multifunctional areas, with many vacant lots (Figure 2). Therefore, it has a good permeability and is not prone to flooding even during heavy rainfall events, unlike some older residential areas in the inner city of Can Tho [21]. The rainfall events selected on April 2nd and July 29th, 2023, are the most recent events collected during the study period and are rainfall events measured in 15-minute intervals at the Can Tho Meteorological Station. Hence, the study can only utilize these two existing rainfall events, which have been identified as having significant intensity and causing flooding in some inner-city areas of Can Tho, for simulation and model calibration.

Regarding tidal flooding, based on the collected real-world data and surveys, we have profiles showing the cross-sectional elevation of the Cai Nai River and the elevation of the bank (ground level) in the residential area (Figure 4), along with a dataset of the highest tide levels over a period of more than 40 years (1980-2023) (Figure 10). Accordingly, the bank elevation in the school area is G = 2.41m, and the maximum height H max up to the current time (2023) is 2.20 m. Based on this real-world data, it can be observed that the research area is currently not susceptible to flooding from rainfall or tidal surges.

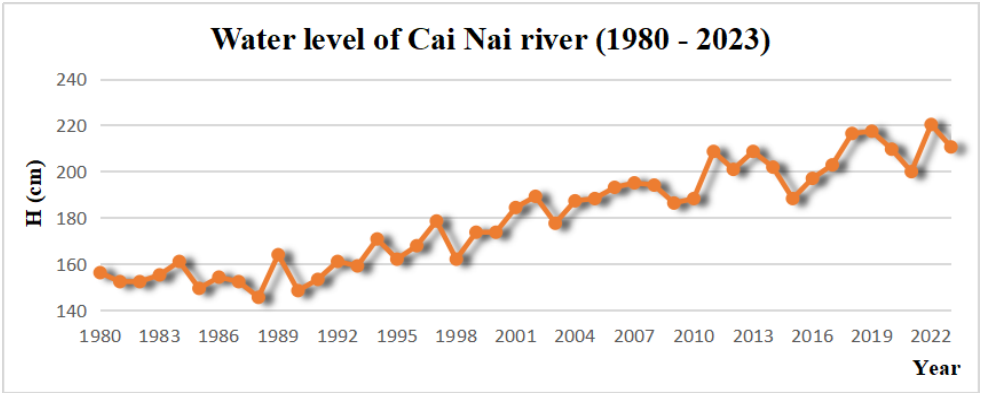

Figure 10. Water level at Cai Nai river from 1980 to 2023.

To avoid repeating the old architectural style and excessive concreteization, the study utilizes the significant rainfall event on April 2nd, 2023, along with the scenario of 100% urbanization of this new residential area to propose effective LID solutions.

3.2 Solutions to minimize urban flooding damage

LID solutions [13–17] include Bio-Retention Cell, Rain Garden, Green roof, Infiltration Trench, Permeable pavement, Rain barrel. Depending on the needs of urban planning for residential areas, integrated urban areas, these solutions are applied appropriately. For green infrastructure, the study chose to increase the watershed's permeability by 30% combined with Permeable pavement solution. This solution is implemented in parking lots, parks, parts of sidewalks, and road shoulders, etc (Figure 12).

Below (Figures 11-13) is the structure of a permeable pavement.

Benefits of Permeable Pavement:

- Effective water drainage: Helps address part of the water drainage issue during heavy rain without the need to increase the drainage capacity.

- Cost savings: Reduces costs for drainage systems while maintaining comfort and convenience.

- Moisture retention: Preserves moisture in the soil and air in the area, creating a favorable environment for plant growth.

- Economic solution: Using interlocking pavers as pavement structure may be a more economical and flexible choice compared to asphalt or concrete solutions.

The study simulated permeable pavement in reducing surface runoff, decreasing the amount of water overflowing into the drains, and increasing the time for water to accumulate in the drainage system.

The results of applying the assumed LID solution - permeable pavement - in the mathematical model show an effective reduction in the volume of runoff generated from rainfall on the surface by up to 30%

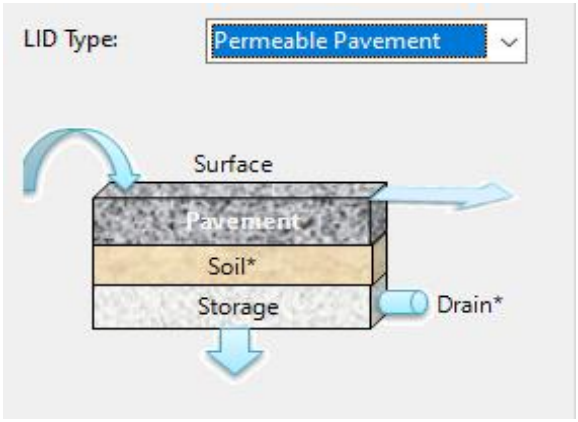

Figure 11. Structure of permeable pavement in flood mitigation support construction.

Figure 12. Example of permeable pavement structure for parking lot.

Figure 13. Some types of permeable pavement.

(Table 3). This solution also enhances the soil's permeability, thereby shortening the time for surface runoff to form in each watershed.

Table 3. Reduction rate of peak flow volume in each watershed.

Solution	Q_{max}	Peak Reduction Q (%)
Urbanization	0.3	-
Permeable pavement	0.2	30

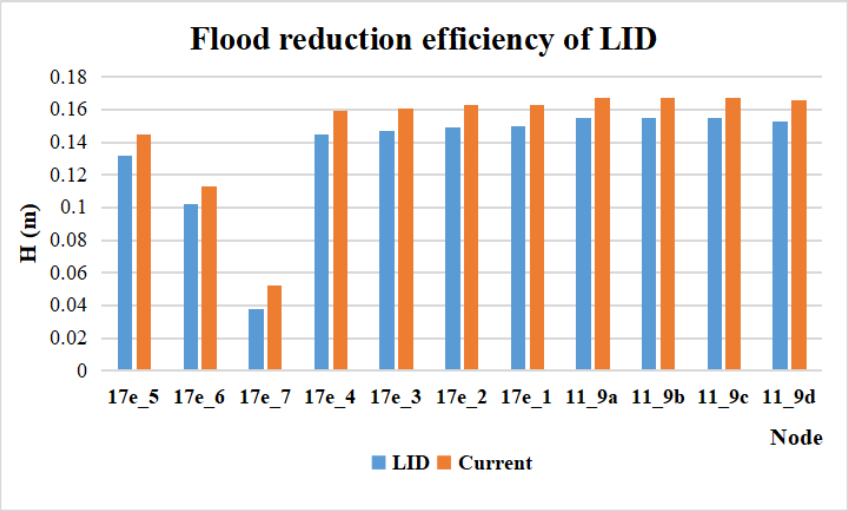

Figure 14. Effectiveness of reducing water levels at manholes.

The effectiveness of LID solutions in reducing flooding is quite promising. However, because the flooding caused by the rain event on April 2, 2023, was assessed to have only a mild impact, the overall effectiveness of this solution in reducing flooding may not be clear. Nevertheless, in general, based on the statistical data in Table 3 and Figure 14, we can observe a significant reduction in the flow volume to each manhole.

4. Conclusion

LID and SWMM in stormwater management offer long-term sustainability, economic efficiency, and provide a foundation for urban development in a positive direction, adapting to climate change. Regarding the assumed LID solutions for watersheds prone to flooding due to heavy rain, they have shown good effectiveness, serving flood mitigation for constructions, especially as these solutions have high sustainability and are suitable for urbanization processes while still ensuring flood prevention. The comparison of total water volume to each manhole between two scenarios before and after urbanization with LID implementation has significantly reduced the flow to each manhole.

However, because the research area is still in the planning stage of urban development and lacks specific designs, the integration of LID solutions to assess enhancement has limited basis for implementation.

The issue of selecting rainfall events causing flooding in this urban area is addressed in the model calibration and validation section. As this is a newly planned urban area in the development phase, with vacant land and good permeability, it does not experience flooding due to rainfall. Regarding tidal flooding, the elevation adjustments ensure no flooding occurs. Therefore, when selecting flood-causing rainfall events to assess the accuracy of the model, the author only chose two existing rainfall events that were evaluated to cause significant flooding in some neighboring areas of Can Tho City.

Author contribution statement: Developing research ideas: N.V.H.; Process data: processing, manuscript writing: N.T.H.; Set up and run the model: N.V.H., N.T.H.; Reviewed and completed the manuscript: N.V.H.

Competing interest statement: The authors declare no conflict of interest.

Reference

1. Technology Transfer Center, Southern Branch, Thuy Loi University. Project for Upgrading and Renovating the Bun Xang Regulating Lake - Can Tho City. 2015.
2. Hai, D.M. The effect of design storm characteristics on low-impact development practices for rainfall run off control. *J. Water Resour. Environ. Eng*. **2020**, *68*, 98–106.
3. Lan, N.T.M.; Dung, D.T.; Quang, C.N.X.; Giang, N.N.H. Assessing the applicability of sustainable urban drainage systems in Binh Chanh district, Ho Chi Minh city. *J. Hydro-Meteorol*. **2021**, *732*, 49–64.
4. Ngan, N.T.; Trung, N.H. Application of GIS and SWMM model to assess urban flooding in Metro Residential area of Ninh Kieu district. *Earth Environ. Sci*. **2023**, *1170*, 1–8.
5. Hieu, N.N.; Tu, T.T.; Hoa, H.V.; Nam, T.H. Evaluating approaches to dispersed flood reduction in urbanized low-lying areas on the periphery of HCMC. *Builder* **2019**, *327-328*, 1–21.
6. Majid, O.A.; Sanayei, H.R.Z.; Heidarzadeh, H.; Mahabadi, N.A. Modeling and investigating the effect of the LID methods on collection network of urban runoff using the SWMM model (case study: Shahrekord city). *Model. Earth Syst. Enviro.* **2020**, *7*, 1–16.
7. Luan, Q.; Fu, X.; Song, C.; Wang, H.; Liu, J.; Wang, Y. Runoff effect evaluation of LID through SWMM in typical mountainous, low-lying urban areas: A case study in China. *Water* **2017**, *9(6)*, 439.
8. Zhang, Z.; Hu, W.; Wang, W.; Zhou, J.; Liu, D.; Qi, X.; Zhao, X. The hydrological effect and uncertainty assessment by runoff indicators based on SWMM for various LID facilities. *J. Hydrol*. **2022**, *613*, 128418.
9. Taji, S.G.; Regulwar, D.G. LID coupled design of drainage model using GIS and SWMM. *J. Hydraul. Eng*. **2021**, *27*, 376–389.
10. Yu, Y.; et al. A new LID spatial allocation optimization system at neighborhood scale: Integrated SWMM with PICEA-g using MATLAB as the platform. *Sci. Total Environ*. **2022**, *831*, 154843.
11. Binh, C.T. Feasibility assessment of sustainable stormwater management system planning for Long Thanh High-Tech Industrial Zone - Dong Nai. 2018.
12. IGIP and WACC-ARCASIA JV. Pilot implementation of Efficient Management Model (BMP) adapted to climate change in the central area of Soc Trang city, Soc Trang province. 2016.
13. Carter, T.; Butler, C. Ecological impacts of replacing traditional roofs with green roofs in two urban areas. *Cities Environ.* **2008**, *1(2)*, 9.
14. Mentens, J.; Raes, D.; Hermy, M. Dirk Raes and Department, Green roofs as a tool for solving the rainwater runoff problem in the urbanized 21st century. *Landscape Urban Plan.* **2006**, *77*, 217–226.
15. De Oliveira, E.W.N.; da Silva, L.P.; Mary, W. Telhados verdes para habitações de interesse social: retenção das águas pluviais e conforto térmico. *Universidade do Estado do Rio de Janeiro*, **2009**, *18*.
16. Hoffmann, B.; et al. Sustainable urban drainage systems. Sustainable Urban Drainage Systems, 2016, pp. 20.
17. Zhang, L.; Ye, Z.; Shibata, S. Assessment of rain garden effects for the management of urban storm runoff in Japan. *Sustainability* **2020**, *12(23)*, 9982.

18. National Standard (TCVN 7957:2008). Drainage - Networks and external structures - Design standards
19. Xu, T.; Jia, H.; Wang, Z.; Xuhui Mao & Changqing Xu. SWMM-based methodology for block-scale LID-BMPs planning based on site-scale multi-objective optimization: A case study in Tianjin. *Front. Environ. Sci. Eng.* **2017**, *11*, 1. https://doi.org/10.1007/s11783-017-0934-6.
20. Huong, N.T.T. Application of SWMM model for planning stormwater drainage to prevent flooding for Phuoc Kien, Phuoc Loc, Long Thoi, Nhon Duc communes - Nha Be district. *J. Sci. Technol. Ton Duc Thang Univ.* **2015**.
21. Can Tho: Heavy off-season rain relieves heat after many hot days. Internet: Heavy off-season rain relieves heat after many hot days. Vietnam+ (VietnamPlus), 2023.
22. Park, J.; Yoo, Y.; Park, Y.; Yoon, H.; Kim, J.; Park, Y.; Jeon, J.H.; Lim, K.J. Analysis of runoff reduction with LID adoption using the SWMM. *J. Korean Soc. Water Qual.* **2008**, *24(6)*, 805–815.
23. Rossman, L.A. Stom water management model user's manual version 5.1. United States Evironment Protection Agency, United States, 2015, pp. 353.

JOURNAL OF
HYDRO-METEOROLOGY

Research Article

Evaluate the correct and the skill of the IFS model for minimum temperature, average temperature, maximum temperature forecasting in short term (24 hours) at 09 regions in Vietnam

Le Thi Thu Ha[1]*, Nguyen Thu Hang[2], Tran Thi Thanh Hai[1], Nguyen Thi Tuyet[3]

[1] Meteorological and Hydrological Forecasting Management Department; leha246@gmail.com; haitran84@gmail.com
[2] National Center for Hydro-Meteorological Forecasting; nthang0676@gmail.com
[3] Ho Chi Minh University of Natural Resource and Environment; nttuyet@hcmunre.edu.vn

*Corresponding author: leha246@gmail.com; Tel.: +84–904290269

Received: 12 February 2024; Accepted: 18 March 2024; Published: 25 March 2024

Abstract: Conceptually, forecast verification is simple, you just need to compare the forecast factors and observed factors. The accuracy of a forecast is a measure of how close to the actual weather the forecast was. The reliability of a forecast is the average agreement between the forecast values and the observed values. The skill of a forecast is performed based on some benchmark forecast, usually by comparing the accuracy of the forecast with the accuracy of the benchmark. The benchmark forecast can be a climatic value. Meanwhile, the correct forecast is bias between the forecast value and the observed value within the allowable range. This study evaluates the correct and forecasting skill of the IFS model (by European Centre for Medium-Range Weather Forecasts) for minimum temperature (T_m), average temperature (T_{ave}), maximum temperature (T_x) forecasting in 24 hours at 09 regions in Viet Nam. The results show that within 24 hours, the IFS model predicts a high bias for the T_m (from 0.2 to 0.9^{o}C) and a low bias for the T_{ave} (from -0.2 to -0.9^{o}C) and T_x (from -1.0 to -2.0^{o}C). The correct in the southern region is higher than in the northern region (average about 10 to 15%). The skill of IFS model is higher than the benchmark (skill for the T_m has exceeded the Benchmark value by 0.4 to 0.6; skill for the T_{ave} has exceeded the Benchmark value by 0.5 to 08), in there, the skill of T_m and T_{ave} is higher than skill of T_x at the most regions, except in the Southern region, the skill of IFS model is lower than the benchmark for T_{ave} and T_x.

Keywords: Accuracy; Reliability; Skills; Forecast Verification.

1. Introduction

According to Guidelines of World Meteorological Organization (WMO) [1], the general purpose of the verification is to ensure that the forecast and warning products are accurate, competent, and reliable from a technical point of view. This is distinct from whether the products are actually meeting user needs. However, technical verification must be based on methods appropriate to the user's needs. There are many studies on verification methods. Allan Murphy, a pioneer in the field of forecast verification, wrote an essay on what makes a forecast "good" [2], a good forecast is a forecast that satisfies the following three criteria: Consistency: the level of forecast changes according to changes in situation; Good quality: the degree of agreement between forecast and observation; Valuable: the extent to which the forecast supports decision making and brings benefits; Also according to the research of [2], forecast quality includes the following nine attributes: Bias;

Correlation; Accuracy; Forecasting skill; Reliability; Resolution; Sharpness; Discrimination and Uncertainty. Simply, forecast verification includes accuracy and skill. Note that, the other attributes of forecast quality also affect the value of the forecast.

According to the research of [3–5] describe methods for assessing the value of the forecasts. Forecast quality is not the same as forecast value. High forecast quality if the forecast and observation are well according to some objective criteria. Forecast value helps the user to make a better decision.

Meanwhile, regarding the verification results, according to the research of [6–9]: the verification results are more reliable when the quantity and quality of verification data are high. The usual approach is to determine the confidence interval for the verification score using approximate, analysis methods; Regarding stratification results, to obtain reliable verification statistics, the verification data should be divided by time and space. For example, according to the study [10], the verification data is divided by season, geographical region, monitoring frequency, etc.

Regarding the standard verification methods, there are many studies for greater detail of the standard verification methods see [11] or one of the excellent the research of [12], [13–15] on forecast verification and statistics. The results see that, with methods for forecast of continuous variables such as temperature, the verification indices as Bias, MAE, MSE and RMSE. These verification indices are simple and useful to explain to users before making decisions. The Bias index indicates the direction of the forecast bias, where the MAE and RMSE indices indicate the average amplitude of the forecast error. Therefore, people often use a combination of these indicators to provide an estimate of reliability.

In Viet Nam, Meteorological and Hydrological Administration has been invested in by the Ministry of Natural Resources and Environment to buy products (images are available on the page website: http://www.ecmwf.int) and numerical data (GRIB code transmitted over the Internet) of the European Centre for Medium-Range Weather Forecasts (ECMWF) to serve operational forecasting since the end of 2011. The data source of the ECMWF is considered plentiful with high reliability. Besides, some studies related to assessing the skills of models, including the IFS model such as studies by [16–18]. The studies mainly evaluated the skill for rainfall forecast and show that: Both skill validations of station-based and spatial-based show low skills of models for high thresholds of 24h accumulated rainfall forecast [18]. The IFS model has best forecast skill in comparison with the other models. However, all given model is under-estimating in forecasting extreme heavy rainfall events [16]; For rainfall quantity forecast, IFS model has skill from 24 hours to 48 hours lead time and less skill at 72 hours lead time. However, IFS model has skill for number of heavy rainfalls [17]. As for temperature, research by [19] shows: With the using of automatic calibration method, the forecast quality of the IFS model is significantly improved. According to the provisions of legal documents on verification the quality of hydro-meteorological forecasting and warning [20], the reliability is understood as determining the allowable error between the forecast value and the observed value. If the forecast value is within the allowable error range that mean correct; if it is outside the allowable error range, that mean not correct. Accordingly, the correct of forecast value is determined within ± 1 level compared to the observed value; Long term will have a wider allowable error range than short term. For meteorological natural disasters such as tropical storms, heavy rainfall, and heat waves, in addition to evaluating the forecast value, also evaluate the time of influence and scope of influence. According to legal documents is also assessed through the "completeness" of newsletter content and "timeliness" of newsletter delivery. For the temperature, within a forecast period from 1 to 3 days, allowable error ranges from -2^{o}C to 2^{o}C.

In general, there are not many detailed studies in Vietnam for temperature forecast factors, most of the studies focus on the standard verification methods, with few studies related to regulations at the legal documents.

This study will initially evaluate the skill of the IFS model for temperature forecasting in short term at all regions in Viet Nam. In addition, to determine whether the model can be applied in operational forecasting, the study will also evaluate the correct of the model following the legal documents.

2. Materials and Methods

2.1. Description of study site

Figure 1 presents a map of the study area, there are 09 regions in Viet Nam: 1) the Northwestern region; 2) the Mid-North region; 3) the North Eastern region; 4) the Red River Dela region; 5) the North Central region; 6) the Mid-Central region; 7) the South Central region; 8) the Central Highland region; 9) the Southern region.

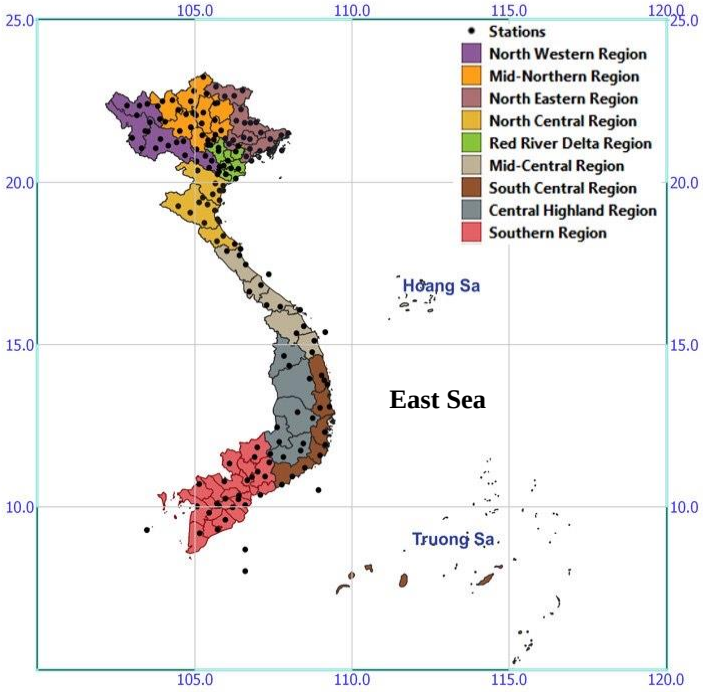

Figure 1. The study area at 09 regions in Viet Nam.

2.2. Data collection

In this study used: Observed data of daily minimum temperature, average temperature, maximum temperature from December 2019 to December 2022 of 184 synoptic stations in Viet Nam and shown in Table 1.

Climatic data from 1981 to 2010 of minimum temperature, average temperature, maximum temperature of 138 synoptic stations in Viet Nam (Table 1).

Table 1. Information about synoptic stations at 9 regions in Viet Nam.

Rg	Code	Station	Rg	Code	Station	Rg	Code	Station	Rg	Code	Station
Northwestern	48/01	Muong Te	Northeastern	48814	Vinh Yen	North Central	48840	Thanh Hoa	Central Highland	48865	Kon Tum
	48/02	Sin Ho		48/52	Tam Dao		48/70	Nhu Xuan		48866	Playcu
	48/03	Tam Duong		48808	Cao Bang		48/72	Tinh Gia		48867	An Khe
	48/06	Than Uyen		48/33	Bao Lac		48/74	Quy Chau		48868	Yaly
	48800	Muong Lay		48/40	Ng. Binh		48844	T. Duong		48872	Ayunpa
	48/09	Tuan Giao		48/43	T. Khanh		48/75	Quy Hop		48876	EaHleo
	48/10	Pha Din		48807	That Khe		48/76	Tay Hieu		48878	Buon Ho
	48811	Dien Bien		48830	Lang Son		48/79	Con Cuong		48/98	M Drak

Rg	Code	Station	Rg	Code	Station	Rg	Code	Station	Rg	Code	Station
Mid-Northern	48/07	Phieng Lanh	Red River Delta	48/46	Mau Son	Mid-Central	48/77	Quynh Luu	Southern	48875	B.M. Thuot
	48/05	Muong La		48/47	Bac Son		48/80	Do Luong		48869	EaKmat
	48806	Son La		48/48	Huu Lung		48/81	Hon Ngu		48885	Lak
	48/16	Song Ma		48/49	Dinh Lap		48845	Vinh		48882	Dac Mil
	48/17	Co Noi		48838	Mong Cai		48/82	Huong Son		48886	Dak Nong
	48/18	Yen Chau		48/50	Quang Ha		48846	Ha Tinh		48880	Da Lat
	48/19	Bac Yen		48837	Tien Yen		48/84	Huong Khe		48881	Lien Khuong
	48/20	Phu Yen		48834	Co To		48/73	Hoanh Son		48884	Bao Loc
	48/25	Moc Chau		48836	Cua Ong		48/86	Ky Anh		48/83	Cat Tien
	48/26	Mai Chau		48833	Bai Chay		48/87	Tuyen Hoa		48883	Phuoc Long
	48/61	Kim Boi		48/60	Uong Bi		48848	Dong Hoi		48895	Dong Phu
	48/63	Chi Ne		48/53	Hiep Hoa		48847	Ba Don		48898	Tay Ninh
	48/64	Lac Son		48/55	Luc Ngan		48/89	Con Co		48/78	Tri An
	48818	Hoa Binh		48/56	Son Dong		48849	Dong Ha		48896	Bien Hoa
	48803	Lao Cai		48809	Bac Giang		48/90	Khe Sanh		48/71	Ta Lai
	48/30	Bac Ha		48/54	Bac Ninh		48852	Hue		48/88	Long Khanh
	48802	Sa Pa		48826	Phu Lien		48/91	A Luoi		48899	Thu Dau Mot
	48/29	Pho Rang		48828	Hon Dau		48/92	Nam Dong		48894	Nha Be
	48/08	Mu.C.Chai		48839	Bach. L.Vi		48855	Da Nang		48903	Vung Tau
	48815	Yen Bai		48/57	Ba Vi		48/93	Tam Ky		48918	Con Dao
	48/14	Van Chan		48817	Son Tay		48/94	Tra My		48919	Huyen Tran
	48/35	Luc Yen		48820	Lang		48/85	Ly Son		48906	Moc Hoa
	48805	Ha Giang		48819	Hoai Duc		48863	Q.Ngai		48912	My Tho
	48/31	Hoang S Phi		48825	Ha Dong		48/95	Ba To		48911	Vinh Long
	48/32	Bac Me		48/59	Chi Linh		48/96	Hoai Nhon		48901	Ben Tre
	48/34	Bac Quang		48827	Hai Duong		48864	An Nhon		48902	Ba Tri
	48/38	Dong Van		48822	Hung Yen		48870	Quy Nhon		48908	Cao Lanh
	48812	T.Quang		48823	Nam Dinh		48/97	Son Hoa		48904	Cang Long
	48/36	Ham Yen		48829	Van Ly	South Central	48873	Tuy Hoa		48909	Chau Doc
	48/37	Chiem Hoa		48821	Phu Ly		48877	Nha Trang		48897	Tra Noc
	48/39	Cho Ra		48832	Nho Quan		48879	Cam Ranh		48910	Can Tho
	48/42	Ngan Son		48824	Ninh Binh		48892	Song T.Tay		48905	Vi Thanh
	48810	Bac Can		48/65	C.Phuong		48890	Phan Rang		48913	Soc Trang
	48831	Thai Nguyen		48835	Thai Binh		48887	Phan Thiet		48907	Rach Gia
	48/44	Dinh Hoa		48842	Hoi Xuan		48888	La Gi		48917	Phu Quoc
	48/23	Minh Dai		48/67	Yen Dinh		48889	Phu Quy		48916	Tho Chu
	48/51	Phu Ho		48/68	Sam Son		48891	Phan Ri		48915	Bac Lieu
	48813	Viet Tri		48/69	Bai Thuong		48861	Dak To		48914	Ca Mau

Forecast data of IFS model with information and shown in Table 2.

Table 2. Information about IFS model.

Resolution	Lead Time	Time Series	Products
0.125°	24 hours to 240 hours	2019 - 2022	Surface: Temperature 2m, Sea Level Pressure, rainfall, wind 10m (For the T_{ave}, calculated through the Temperature 2m, averaging the time periods 00, 06, 12 and 18z. The T_m and T_x are taken as the minimum value and maximum value during the period 00, 06, 12 and 18z of that day) Upper level: Geopotential Height, wind, Relative Vorticity, 1000-500mb (thickness&mslp), 300/200mb (divergence&wind)…

2.2. Methods

Figure 2 presents conceptual framework of the applied methodology in this study, in which the input data are from the IFS model, monitoring data of the stations, climatic data of the stations; Next, we process these data, statistic matrices and the results are verification indices.

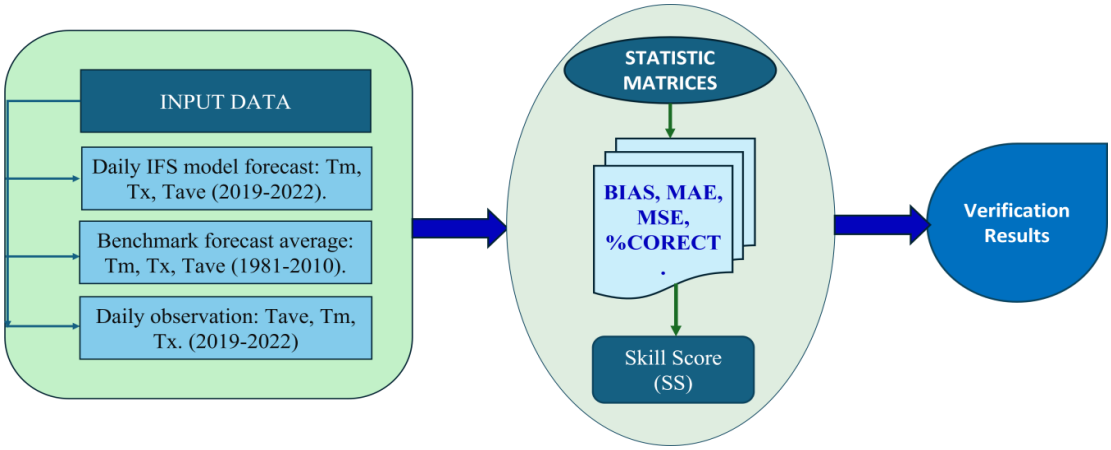

Figure 2. Conceptual framework of the applied methodology in this study.

There are many scientific documents on methods to forecast verification, for example the research of [3, 10]. According to WMO [1], there are two basic variables for forecasting: continuous variables (variables with numeric values) and grouped variables such as rain or no rain or hierarchical by intensity (light rain, moderate rain and heavy rain...). These variables can be predicted by giving specific values or by probabilities. Probabilistic forecasting will be more meaningful than numerical forecasting, in that users can make decisions based on probability and their perception.

The following simple example of a set of twenty maximum temperature forecasts will be used in this section to illustrate the score and shown in Table 3.

Table 3. Example for forecast verification indices.

MAX TEMP (°C)					
Forecast (F)	**Observed (O)**	**F-O**	**ABS(F-O)**	**$(F-O)^2$**	**Within ± 2°C**
17	17	0	0	0	1
24	20	4	4	16	0
28	29	-1	1	1	1
22	25	-3	3	9	0
14	16	-2	2	4	1
16	17	-1	1	1	1
17	17	0	0	0	1
16	16	0	0	0	1
15	14	1	1	1	1
19	18	1	1	1	1
22	19	3	3	9	0
21	17	4	4	16	0
16	18	-2	2	4	1
20	18	2	2	4	1
27	30	-4	4	16	0
21	20	1	1	1	1
15	14	1	1	1	1

	MAX TEMP (ºC)					
	Forecast (F)	**Observed (O)**	**F-O**	**ABS(F-O)**	**$(F-O)^2$**	**Within ± 2ºC**
	22	28	-6	6	36	0
	20	23	-3	3	9	0
	15	18	-3	3	9	0
Average:	19.4	19.8	-0.4	2.1	6.9	60%
			Bias	MAE	MSE	% correct

a) Reliability

Suppose there are N forecasts f_i and corresponding observations o_i for i = 1...N

A gross measure of reliability is the mean bias. It is simply the average of the forecast value minus the average observed value as in equation (1).

$$\text{Bias} = \frac{1}{N}\sum_{i=1}^{N}\left(f_i - O_i\right) \tag{1}$$

For the example in Table 3, N=20, the average predicted value is 19.4°C and the average observed value is 19.8°C, so the average error value is -0,4°C, which means the forecast value is lower than the actual value. This is a simple method to determine reliability.

b) Accuracy

Various accuracy measures are shown in the previous table for this example. In terms of accuracy, the Mean Absolute Error or MAE is in equation (2):

$$\text{MAE} = \frac{1}{N}\sum_{i=1}^{N}(|f_i - o_i|) \tag{2}$$

The Mean-Square Error or MSE is presented in equation (3) and The Root-Mean-Square Error or RMSE is presented in equation (4).

$$\text{MSE} = \frac{1}{N}\sum_{i=1}^{N}(f_i - o_i)^2 \tag{3}$$

$$\text{RMSE} = \sqrt{\text{MSE}} = \sqrt{\frac{1}{N}\sum_{i=1}^{N}(f_i - o_i)^2} \tag{4}$$

According to the above example, a mean absolute error of 2.1°C means that the precision between the mean difference of predicted and observed temperature values is 2.1°C.

However, users are often interested in the largest possible error of the forecast, so will use the formula to calculate RMSE, which will be 2.6°C.

Another measure that is commonly used for weather elements such as temperature, is the "percent correct" of forecasts that are within some allowable range, e.g., within ±2°C or ±3°C. This is shown in the above table by putting a 1 when the forecast was within ±2°C of the observed maximum, and 0 otherwise, then averaging the values. The result for this example is that 60% of the forecasts are within ±2°C.

c) Skill

The skill of a forecast is exercised against some benchmark forecast, usually by comparing the accuracy of the forecast with the accuracy of the benchmark forecast. The benchmark forecast can be a climatic value or a value from an automated product.

For example, the climatic value of temperature during this period is 20°C, accordingly Table 4 gives the following evaluation results compared to the climatic value:

Table 4. Example for benchmark forecast verification indices.

	MAX TEMP (°C)					
	Benchmark Forecast (F)	**Observed (O)**	**F-O**	**ABS(F-O)**	**$(F-O)^2$**	**Within ± 2°C**
	20	17	3	3	9	0
	20	20	0	0	0	1
	20	29	-9	9	81	0
	20	25	-5	5	25	0
	20	16	4	4	16	0
	20	17	3	3	9	0
	20	17	3	3	9	0
	20	16	4	4	16	0
	20	14	6	6	36	0
	20	18	2	2	4	1
	20	19	1	1	1	1
	20	17	3	3	9	0
	20	18	2	2	4	1
	20	18	2	2	4	1
	20	31	-11	11	121	0
	20	20	0	0	0	1
	20	14	6	6	36	0
	20	28	-8	8	64	0
	20	23	-3	3	9	0
	20	18	2	2	4	1
Average:	20.0	19.8	0.3	3.9	22.9	35%
			Bias	MAE	MSE	% correct

MAE_f is the absolute error for the forecast and MAE_b is the absolute error for the benchmark, then the forecast skill is calculated as (5):

$$1-\frac{MAE_f}{MAE_b}=1-\frac{2.1}{3.9}=0.45 \quad (5)$$

Or it can be calculated through the mean squared error of the forecast and the benchmark as (6):

$$1-\frac{MSE_f}{MSE_b}=1-\frac{6.9}{22.9}=0.7 \quad (6)$$

If the accuracy measure being used is the percent correct (of forecasts that are within an acceptable range of the observations), then another skill measure is as (7):

$$\frac{PC_f-PC_b}{100\%-PC_b}=0.38 \quad (7)$$

where the value of 0.38 means that the percent correct for the actual forecasts has gone 0.38 of the distance between the benchmark value of 35% and a perfect score of 100%.

d) Interpolation method

The grid data predicted from the model are interpolated to 184 synoptic station points using the bilinear interpolation method.

e) Regulation about the correct

Table 5 shows the correct used for forecast temperature in Clause 3, Article 12 of Circular No. 41/2017/TT-BTNMT of the Minister of Natural Resources and Environment promulgating technical regulations on assessing the quality of meteorological forecasting.

Table 5. The correct of forecast temperature according to regulation.

Error between forecast value and observed value	**Forecast time from 1 - 3 days**			**Forecast time from 4 - 10 days**		
	< -2°C	**- 2°C÷2°C**	**> 2°C**	**< -3°C**	**- 3°C÷3°C**	**> 3°C**
The reliability	-	+	-	-	+	-

3. Results and discussion

3.1. The correct and the skill of minimum temperature

Using WMO's guidelines, we calculated the BIAS, MAE, MSE, % correct indices of the IFS model from 2019-2022 for the T_m in 24 hours for 184 synoptic stations nationwide, then averaged at 09 regions in Viet Nam, the results are given in Table 6. Table 6 shows that for the 24-hour forecast period, the forecast T_m tends to be higher than the actual temperature from 0.2 to 0.9^{o}C in the most regions, except in the Northwestern region and the Red River Delta region, the forecast T_m tends to be lower than the actual temperature from -0.1 to -0.5^{o}C. The average amplitude of forecast error is largest in the Red River Delta region and smallest in the Southern region with MAE equals 1.4 and MSE equals 3.6^{o}C. With an allowed error range of ± 2^{o}C, the correct reaches from 96 to 98% for the southern provinces such as the Central Highland region, South Central region, and Southern region; the Mid-Northern region, Mid-Central region, and Northwestern region have the correct of 84 to 88%; the Red River Delta region, North Central region, and Northeastern region with the correct of 76 to 82%. This result is quite consistent because the monsoon circulation regime affecting the northern regions is more complex than the southern region, so the temperature variation in the northern regions is higher than the southern regions.

Table 6. The BIAS, MAE, MSE, % correct indices of the IFS model from 2019-2022 for the T_m in 24 hours at 09 regions in Viet Nam.

Region	Forecast (F)	Observed (O)	BIAS	MAE	MSE	%Correct
Northwestern	Average: 19.3	19.3	-0.1	1.0	1.8	88%
Mid-Northern	Average: 20.0	19.8	0.2	1.1	2.1	84%
Northeastern	Average: 20.6	20.4	0.2	1.2	2.6	82%
Red River Delta	Average: 21.4	21.9	-0.5	1.4	3.6	76%
North Central	Average: 22.3	22.2	0.2	1.2	2.7	80%
Mid-Central	Average: 23.7	22.8	0.9	1.1	1.9	86%
South Central	Average: 25.3	24.8	0.5	0.7	0.7	98%
Central Highland	Average: 20.4	20.1	0.2	0.7	0.8	96%
Southern	Average: 24.7	24.7	0.0	0.6	0.6	98%

The BIAS, MAE, MSE, % correct indices between the 30-year climatic average value (Benchmark) and the observed value from 2019-2022 for the T_m in 24 hours period are calculated for 138 synoptic stations, then averaged at 09 regions in Viet Nam, the results are given in Table 7.

Table 7. The BIAS, MAE, MSE, % correct indices of Benchmark from 2019-2022 for the T_m in 24 hours at 09 regions in Viet Nam.

Region	Benchmark (F)	Observed (O)	BIAS	MAE	MSE	%Correct
Northwestern	Average: 18.6	19.3	-0.7	1.8	5.3	66%
Mid-Northern	Average: 19.3	19.8	-0.5	1.9	6.1	64%
Northeastern	Average: 20.0	20.4	-0.4	2.0	7.0	58%
Red River Delta	Average: 21.1	21.9	-0.8	2.1	7.2	56%
North Central	Average: 21.1	22.2	-1.1	2.1	6.7	55%
Mid-Central	Average: 22.0	22.8	-0.7	1.4	2.9	77%
South Central	Average: 24.5	24.8	-0.3	0.7	0.9	96%
Central Highland	Average: 19.4	20.1	-0.8	1.2	2.1	83%
Southern	Average: 24.3	24.7	-0.4	0.8	1.0	96%

The skill of IFS model for T_m through comparison between the accuracy of the model's forecast value and the Benchmark is shown in Figure 3. In most regions, the model's forecast skill for the T_m has exceeded the Benchmark value by 0.4 to 0.6, especially in the Central Highland region, the percent correct for the actual forecasts has gone 0.8 of the

distance between the benchmark value of 76% and a perfect score of 100%. However, the benchmark's MAE and MSE are larger than the model's MAE and MSE, that mean the benchmark's error is larger than the model's error.

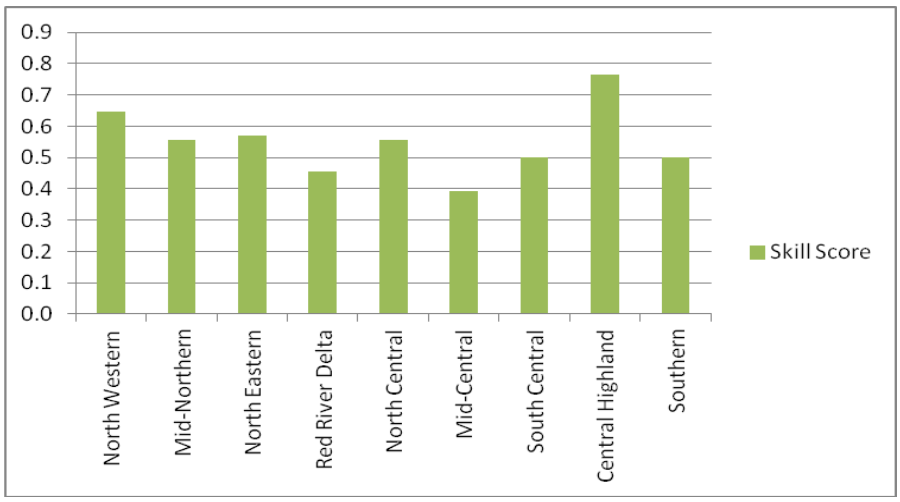

Figure 3. Skill score of IFS model for T_m at 09 regions in Viet Nam.

3.2. The correct and the skill of average temperature

The BIAS, MAE, MSE, % Correct indices of the IFS model from 2019-2022 for the T_{ave} in 24 hours for 184 synoptic stations nationwide, then averaged at 09 regions in Viet Nam, the results are given in Table 8.

Table 8. The BIAS, MAE, MSE, % correct indices of the IFS model from 2019-2022 for the T_{ave} in 24 hours at 09 regions in Viet Nam.

Region	Forecast (F)	Observed (O)	BIAS	MAE	MSE	%Correct
Northwestern	Average: 21.8	22.4	-0.6	1.1	1.7	89%
Mid-Northern	Average: 22.1	22.4	-0.3	1.0	1.6	91%
Northeastern	Average: 22.6	22.9	-0.3	1.0	1.6	91%
Red River Delta	Average: 23.5	24.3	-0.8	1.4	3.0	75%
North Central	Average: 24.3	24.5	-0.2	1.1	1.9	87%
Mid-Central	Average: 25.4	25.3	0.1	0.7	0.9	96%
South Central	Average: 27.2	27.2	-0.1	0.4	0.3	100%
Central Highland	Average: 22.9	23.5	-0.6	0.8	0.8	99%
Southern	Average: 26.6	27.5	-0.9	1.0	1.3	95%

Table 8 shows that for the 24-hour forecast period, the forecast T_{ave} tends to be lower than the actual temperature in most regions. The average amplitude of forecast error is largest in the Red River Delta region and smallest in the South-Central region, with MAE from 0.4 to 1.4^{o}C. With an allowed error range of ± 2^{o}C, the correct reaches from 95 to 100% in the southern provinces such as the Mid-Central region, South Central region, Central Highland region, and Southern region; the Northwestern region, the Mid-Northern region, Northeastern region, and North Central region have the correct of 87 to 91%; the Red River Delta region has the lowest correct of 75%.

Table 9 about the results of Benchmark's BIAS, MAE, MSE, % Correct indices from 2019-2022 for T_{ave} at 09 regions shows that the correct is lower in the northern provinces and very high in the southern provinces, especially the correct in the South-Central region and Southern region reaches from 97 to 98%.

Table 9. The BIAS, MAE, MSE, % correct indices of Benchmark from 2019-2022 for the T_{ave} in 24 hours at 09 regions in Viet Nam.

Region	Benchmark (F)	Observed (O)	BIAS	MAE	MSE	%Correct
Northwestern	Average: 21.8	22.4	-0.6	1.8	5.4	62%
Mid-Northern	Average: 22.1	22.4	-0.3	1.9	5.9	61%
Northeastern	Average: 22.7	22.9	-0.2	2.0	6.4	59%
Red River Delta	Average: 23.5	24.3	-0.8	2.2	7.2	53%
North Central	Average: 23.8	24.5	-0.7	2.0	6.4	56%
Mid-Central	Average: 24.8	25.3	-0.5	1.5	3.6	71%
South Central	Average: 27.0	27.2	-0.2	0.7	0.8	98%
Central Highland	Average: 22.8	23.5	-0.7	1.1	1.8	88%
Southern	Average: 27.1	27.5	-0.4	0.8	1.0	97%

The skill of IFS model for T_{ave} through comparison between the accuracy of the model's forecast value and the Benchmark is shown in Figure 4. At the most regions, the model's forecast skill for the Tave has exceeded the Benchmark value by 0.5 to 08, especially in the Mid-Central region and the South Central region, the percent correct for the actual forecasts has gone 09 to 1. Except in the Southern region, the model's forecast skill for the Tave has lower than the Benchmark. This can be explained by the fact that the temperature regime in the Southern region has little change. Climatic values can be used to predict the average temperature of this region. That like the T_m, the benchmark's MAE and MSE are larger than the model's MAE and MSE for T_{ave}.

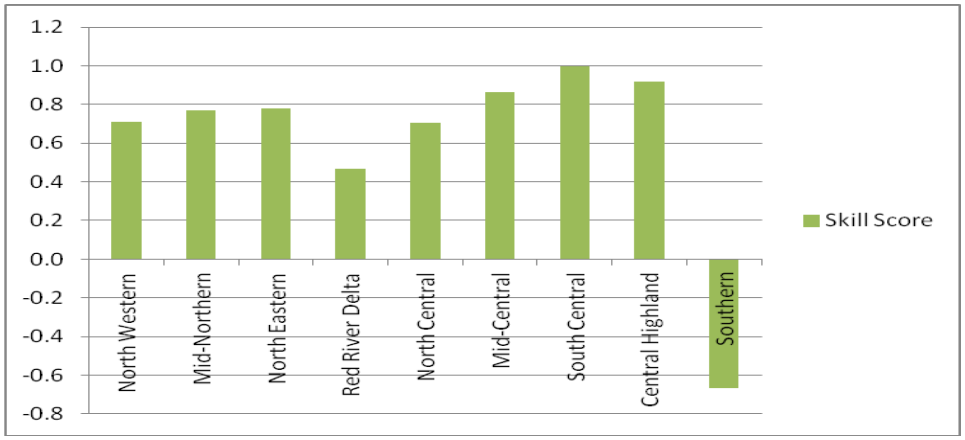

Figure 4. Skill score of IFS model for T_{ave} at 09 regions in Viet Nam.

3.3. The correct and the skill of maximum temperature

With the same method, the results of the BIAS, MAE, MSE, % Correct indices of the IFS model from 2019-2022 for the T_x within 24-hour period at 09 regions in Viet Nam is given by Table 10.

Table 10. The BIAS, MAE, MSE, % correct indices of the IFS model from 2019-2022 for the T_x in 24 hours at 09 regions in Viet Nam.

Region	Forecast (F)	Observed (O)	BIAS	MAE	MSE	%Correct
Northwestern	Average: 26.2	27.7	-1.5	2.4	7.9	45%
Mid-Northern	Average: 25.7	26.7	-1.0	2.1	6.5	53%
Northeastern	Average: 25.7	26.9	-1.2	2.1	6.5	50%
Red River Delta	Average: 26.9	28.0	-1.0	2.3	7.8	50%
North Central	Average: 27.7	28.4	-0.7	1.9	5.8	61%
Mid-Central	Average: 28.4	29.4	-1.0	1.7	4.0	66%
South Central	Average: 30.6	31.1	-0.5	0.9	1.3	91%
Central Highland	Average: 27.9	28.9	-1.1	1.5	3.3	72%
Southern	Average: 30.1	32.1	-2.0	2.1	5.6	51%

Table 10 shows that for the 24-hour forecast period, the forecast T_x tends to be lower than the actual temperature at the most regions, about from 1.5 to 2.0^{o}C. The average amplitude of forecast error is largest in the Northwestern region and the Red River Delta region and smallest in the South-Central region (MAE is approximately 2.4^{o}C, MSE is approximately 8^{o}C in the northern regions, meanwhile MAE and MSE are only approximately 1^{o}C in the South-Central region). With an allowed error range of ± 2^{o}C, the South-Central region has the highest correct of 91%; the North Central region, the Mid-Central region, and the Central Highland region have the correct of 61 to 72%; the other regions have the lower correct of 45 to 53%.

Table 11. The BIAS, MAE, MSE, % correct indices of Benchmark from 2019-2022 for the T_x in 24 hours at 09 regions in Viet Nam.

Region	Benchmark (F)	Observed (O)	BIAS	MAE	MSE	%Correct
Northwestern	Average: 27.4	27.7	-0.3	2.7	11.3	43%
Mid-Northern	Average: 26.6	26.7	-0.1	2.5	9.8	47%
Northeastern	Average: 27.0	26.9	0.1	2.5	9.8	48%
Red River Delta	Average: 27.1	28.0	-0.9	2.8	11.4	38%
North Central	Average: 28.0	28.4	-0.5	2.6	10.4	44%
Mid-Central	Average: 29.1	29.4	-0.3	2.1	7.5	55%
South Central	Average: 30.7	31.1	-0.4	1.0	1.6	89%
Central Highland	Average: 28.4	28.9	-0.5	1.6	3.8	66%
Southern	Average: 31.5	32.1	-0.6	1.2	2.0	85%

Table 11 shows that, for the T_x, Benchmark has quite high correct in the South-Central region and the Southern region with reaches from 85 to 89%. In the remaining regions, the correct is lower, only about 40 to 60%.

The skill of IFS model for T_x is shown in Figure 5, which shows that, skill of T_x is lower than skill of T_m and T_{ave}, only exceeding 0.1 to 0.2 compared to the benchmark value at the most regions. Except in the Southern region, the model's forecast skill for the T_x has lower than the benchmark. Similar to the explanation for average temperature, the reason the model's skill is lower than the benchmark because the temperature regime of the Southern region is largely unchanged, especially in winter, despite the influence of the cold air, but only the wind regime changes, while the T_x in this region has little change. Compared to the model, the average amplitude of benchmark forecast error is larger.

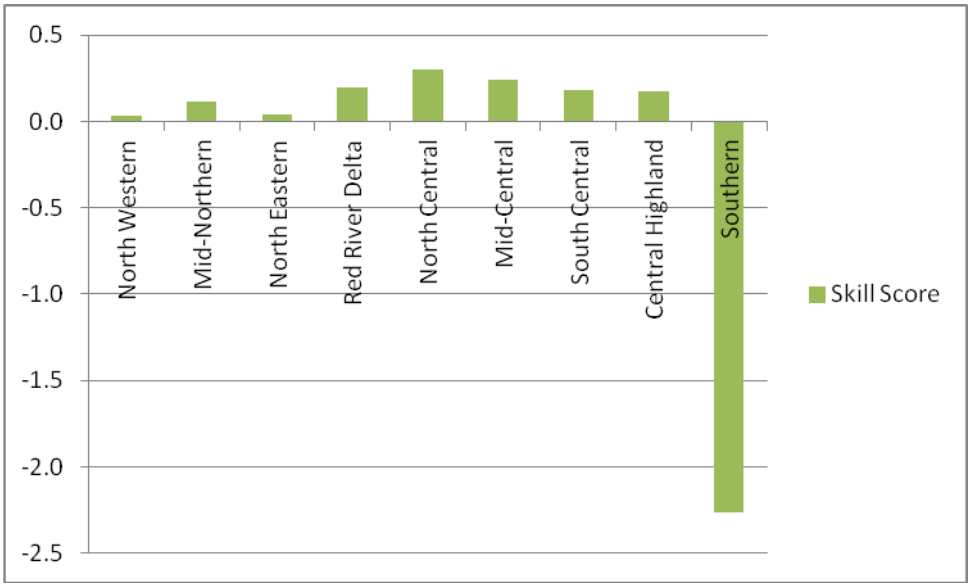

Figure 5. Skill score of IFS model for T_x at 09 regions in Viet Nam.

4. Conclusion

Through the verification of forecast error indices and forecast skill according to WMO guidance and regulations of legal documents on assessing the quality of meteorological forecasting within allowable error range about ± 2^{o}C for temperature, in this study we evaluate the correct and the skill of the IFS model from 2019-2022 for the minimum temperature, average temperature, maximum temperature within the 24-hours forecast period at 09 regions in Viet Nam, the results show:

- Regarding forecast bias: The IFS model tends to forecast the minimum temperature to be higher than the actual one, while the average temperature and maximum temperature to be lower than the actual one at the most regions. The average amplitude of forecast error is highest in the Red River Delta region.

- Regarding the correct: The IFS model forecast the minimum temperature and average temperature with higher correct than the maximum temperature. The correct in the southern region is higher than in the northern region, with the highest correct in the South-Central region, and the lowest correct in the Red River Delta region.

- Regarding the skill: The IFS model has better forecast skill for the minimum temperature and average temperature at the most regions. Except in the Southern region, the model's forecast skill is lower than the benchmark forecast (for average temperature and maximum temperature).

Author contribution statement: Conceived and designed the experiments; Analyzed and interpreted the data; manuscript editing: H.T.T.L; Analysis tools or data; performed the experiments: H.T.N; Wrote the draft manuscript: H.T.T.T; Contributed reagents, materials: T.T.N.

Acknowledgements: This study is supported by the funding of the project titled "Research the scientific basis to develop national technical regulations on assessment of hydro-meteorological forecasting and warning in accordance with regulations of the World Meteorological Organization (WMO) " grant number: TNMT.2023.02.34.

Competing interest statement: The authors declare no conflict of interest.

References

1. WMO. Guidelines on performance assessment of public weather services - No. 1023, 2000.
2. Murphy, A.H. What is a good forecast? An essay on the nature of goodness in weather forecasting. *Wea. Forecasting* **1993**, *8*, 281–293.
3. Murphy, A.H. Forecast verification. Economic value of weather and climate forecasts. Katz, R.W., Murphy, A.H. (Eds). Cambridge Univ. Press, chapter 7, 1997, pp. 19–74.
4. Thornes, J.E.; Stephenson, D.B. How to judge the quality and value of weather forecast products. *Meteorol. Appl.* **2001**, *8*, 307–314.
5. Wilks, D.S. A skill score based on economic value for probability forecasts. *Meteorol. Appl.* **2001**, *8*, 209–219.
6. Seaman, R.; Mason, I.; Woodcock, F. Confidence intervals for some performance measures of yes-no forecasts. *Aust. Met. Mag.* **1996**, *45*, 49–53.
7. Hamill, T.M. Hypothesis tests for evaluating numerical precipitation forecasts. *Wea. Forecasting* **1999**, *14*, 155–167.
8. Kane, T.L.; Brown, B.G. Confidence intervals for some verification measures - a survey of several methods. Proceeding of the 15th Conference on Probability and Statistics in the Atmospheric Sciences, Amer. Met. Soc., 8-11 May 2000, Asheville, North Carolina, 2000.

9. Hamill, T.M.; Juras, J. Measuring forecast skill: is it real skill or is it the varying climatology? *Q. J. Royal Met. Soc.* **2006**, *132*, 2905–2923.
10. Stanski, H.R.; Wilson, L.J.; Burrows, W.R. Survey of common verification methods in meteorology. World Weather Watch Tech. Rept. No. 8, WMO/TD No. 358, WMO, Geneva, 1989, pp. 114.
11. Katz, R.W.; Murphy, A.H. (Eds): Economic value of weather and climate forecasts. Cambridge University Press, Cambridge, 1997.
12. Jolliffe, I.T.; Stephenson, D.B. Forecast Verification: A practitioner's guide in atmospheric science. 2nd Edition. Wiley and Sons Ltd, 2012, pp. 274.
13. Murphy, A.H.; Katz, R.W. Probability, statistics, and decision making in the atmospheric sciences. Westview Press, Boulder, CO, 1985.
14. Murphy, A.H.; Winkler, R.L. A general framework for forecast verification. *Mon. Wea. Rev*. **1987**, *115*, 1330–1338.
15. Nurmi, P. Recommendations on the verification of local weather forecasts (at ECWMF member states). ECMWF Operations Department, 2003.
16. Hoa, V.V. Comparative study skills rain forecast the middle part and central highland of several global models. *VN J. Hydrometeorol.* **2016**, *667*, 1–8.
17. Ba, T.D.; Hoa, V.V.; Tri, D.Q. A verification of short-term rainfall forecast by using ifs model of ECMWF on the northern central region. *VN J. Hydrometeorol.* **2019**, *697*, 33–43.
18. Nga, N.T.; Thanh, C.; Hung, M.K.; Tien, D.D. Verification of quantitative rainfall forecast from IFS and WRF model for the northern region of Viet Nam. *VN J. Hydrometeorol.* **2021**, *730*, 79–92.
19. Minh, L.T.; Lam, H.P. Automatically correction for forecasts city temperature from the ifs model output. *VN J. Hydrometeorol.* **2018**, *693*, 41–47.
20. MoNRE. Circular No. 41/2017/TT-BTNMT dated October 23rd, 2017 of the Minister of Natural Resources and Environment promulgating technical regulations on assessing the quality of meteorological forecasting, 2017.

Table of content